



NBS TECHNICAL NOTE 1009

U.S. DEPARTMENT OF COMMERCE/National Bureau of Standards

Laser Beam Profile Measurements Using Spatial Sampling, Fourier Optics, and Holography

QC
100
.U5753
NO.1009
1979
C.2

NATIONAL BUREAU OF STANDARDS

The National Bureau of Standards¹ was established by an act of Congress March 3, 1901. The Bureau's overall goal is to strengthen and advance the Nation's science and technology and facilitate their effective application for public benefit. To this end, the Bureau conducts research and provides: (1) a basis for the Nation's physical measurement system, (2) scientific and technological services for industry and government, (3) a technical basis for equity in trade, and (4) technical services to promote public safety. The Bureau's technical work is performed by the National Measurement Laboratory, the National Engineering Laboratory, and the Institute for Computer Sciences and Technology.

THE NATIONAL MEASUREMENT LABORATORY provides the national system of physical and chemical and materials measurement; coordinates the system with measurement systems of other nations and furnishes essential services leading to accurate and uniform physical and chemical measurement throughout the Nation's scientific community, industry, and commerce; conducts materials research leading to improved methods of measurement, standards, and data on the properties of materials needed by industry, commerce, educational institutions, and Government; provides advisory and research services to other Government Agencies; develops, produces, and distributes Standard Reference Materials; and provides calibration services. The Laboratory consists of the following centers:

Absolute Physical Quantities² — Radiation Research — Thermodynamics and Molecular Science — Analytical Chemistry — Materials Science.

THE NATIONAL ENGINEERING LABORATORY provides technology and technical services to users in the public and private sectors to address national needs and to solve national problems in the public interest; conducts research in engineering and applied science in support of objectives in these efforts; builds and maintains competence in the necessary disciplines required to carry out this research and technical service; develops engineering data and measurement capabilities; provides engineering measurement traceability services; develops test methods and proposes engineering standards and code changes; develops and proposes new engineering practices; and develops and improves mechanisms to transfer results of its research to the ultimate user. The Laboratory consists of the following centers:

Applied Mathematics — Electronics and Electrical Engineering² — Mechanical Engineering and Process Technology² — Building Technology — Fire Research — Consumer Product Technology — Field Methods.

THE INSTITUTE FOR COMPUTER SCIENCES AND TECHNOLOGY conducts research and provides scientific and technical services to aid Federal Agencies in the selection, acquisition, application, and use of computer technology to improve effectiveness and economy in Government operations in accordance with Public Law 89-306 (40 U.S.C. 759), relevant Executive Orders, and other directives; carries out this mission by managing the Federal Information Processing Standards Program, developing Federal ADP standards guidelines, and managing Federal participation in ADP voluntary standardization activities; provides scientific and technological advisory services and assistance to Federal Agencies; and provides the technical foundation for computer-related policies of the Federal Government. The Institute consists of the following divisions:

Systems and Software — Computer Systems Engineering — Information Technology.

¹Headquarters and Laboratories at Gaithersburg, Maryland, unless otherwise noted; mailing address Washington, D.C. 20234.

²Some divisions within the center are located at Boulder, Colorado, 80303.

MAR 26 1979

1.01 400-0112

GC 100

US 752

no. 1009

1979

C. 2

Laser Beam Profile Measurements Using Spatial Sampling, Fourier Optics, and Holography

Eric G. Johnson, Jr.

Electromagnetic Technology Division
National Engineering Laboratory
National Bureau of Standards
Boulder, Colorado 80303



[†] Technical Note no. 1009

U.S. DEPARTMENT OF COMMERCE, Juanita M. Kreps, Secretary

Sidney Harman, Under Secretary

Jordan J. Baruch, Assistant Secretary for Science and Technology

NATIONAL BUREAU OF STANDARDS, Ernest Ambler, Director

Issued January 1979

NATIONAL BUREAU OF STANDARDS TECHNICAL NOTE 1009
Nat. Bur. Stand. (U.S.), Tech. Note 1009, 96 pages (Jan. 1979)
CODEN: NBTNAE

U.S. GOVERNMENT PRINTING OFFICE
WASHINGTON: 1979

For sale by the Superintendent of Documents, U.S. Government Printing Office, Washington, D.C. 20402

Stock No. 003-003-02019-2 Price 2.75 (Add 25 percent additional for other than U.S. mailing)

CONTENTS

	<u>Page</u>
1. INTRODUCTION.....	1
1.1 What this Introduction Contains.....	2
1.2 Defining Beam Profile.....	2
1.3 Various Methods to Measure Beam Profile.....	3
1.3.1 The Methods Using Fewer Assumptions.....	3
1.3.2 The Focal Plane Method.....	4
1.3.3 The Mirror Scan Method Using Two Pinholes.....	4
1.3.4 The Hartmann Plate Method.....	5
1.3.5 The Holographic Method.....	5
1.4 The Purpose of this Paper.....	6
2. AN OVERVIEW OF THE BASICS USING THE HOLOGRAPHIC METHOD.....	7
2.1 What this Overview Contains.....	7
2.2 The Main Features of the Diffraction Process by a Single Aperture.....	7
2.3 Looking at the Interference Pattern in the Far Field and Fourier Plane for Two Apertures.....	8
2.4 Important Properties of Fourier Optics as Applied to the Holographic Method.....	10
2.5 Important Properties of the Holographic Process.....	10
2.6 Important Properties of the Cross-Correlation Process.....	11
2.7 Assembly of the Above Concepts to Define the Holographic Method.....	12
2.8 Summary of this Overview.....	12
3. HOLOGRAM CONSTRUCTION APPARATUS.....	13
3.1 What this Section Presents.....	13
3.2 A Discussion of the Prototype Apparatus Used to Generate the Hologram.....	13
3.3 The Mathematical Model Used to Understand the Hologram.....	13
3.4 Detailed Instructions for Assembling and Aligning the Apparatus in the Construction of the Hologram.....	22
3.5 Results from Construction of the Hologram.....	27
4. THE CROSS-CORRELATION APPARATUS.....	28
4.1 What this Section Presents.....	28
4.2 A Discussion of the Prototype Apparatus Used to Generate the Cross-Correlation Pattern.....	28
4.3 The Mathematical Model Used to Understand the Cross-Correlation Pattern.....	28
4.3.1 The Model that Contains the Spatial Details of the Irradiance.....	28
4.3.2 The Simplified Model that Ignores Details of the Irradiance--the Calibrated Model.....	31
4.4 Instructions for Assembling and Aligning this Apparatus to Generate the Cross-Correlation Patterns.....	34
4.5 Calibration of this Prototype Apparatus.....	36
4.6 The Cross-Correlation Patterns.....	37
5. MODIFYING THE PROTOTYPE APPARATUS TO GENERATE A MORE EFFECTIVE UNIT.....	56
5.1 What this Section Presents.....	56
5.2 A Scale Change between Original Hologram and a New Sampling Plate Makes a Better Instrument.....	56
5.3 Thoughts about a Cross-Correlation System that Can Make Beam Profile Measurements that Are Orthogonal.....	57
5.4 Features of the Proposed Reflection System.....	59
5.5 A Beam Profile System that Can Be Mass Produced.....	66
6. CONCLUSIONS DRAWN FROM THE PROTOTYPE APPARATUS.....	68
7. ACKNOWLEDGMENTS.....	70
8. REFERENCES.....	71

APPENDICES

	<u>Page</u>
A	IMPORTANT FORMULAS FOR FOURIER OPTICS..... 73
A.1	The Fourier Transform..... 73
A.2	The Imaging Formula..... 75
A.3	The Displacement Formulas..... 75
B.	THE DIFFRACTION DETAILS OF A SQUARE HOLE..... 76
B.1	What this Appendix Presents..... 77
B.2	The Far-Field Diffraction Pattern..... 77
B.3	The Fourier Transform Pattern..... 80
C.	THE DIFFRACTION DETAILS OF A CIRCULAR HOLE..... 82
C.1	What this Appendix Presents..... 82
C.2	The Far-Field Diffraction Pattern..... 82
C.3	The Fourier Transform Pattern..... 84
D.	DEPTH OF FIELD ANALYSIS FOR FOURIER OPTICS..... 85

LIST OF FIGURES

	<u>Page</u>
Figure 1. The hologram generating apparatus - block diagram-----	14
Figure 2. The cross-correlation generating apparatus - block diagram-----	15
Figure 3. The pinhole sampling unit for the prefilter plane-----	16
Figure 4. The coordinates for the prefilter beams-----	19
Figure 5. The coordinates and structure of the spots at the cross-correlation plane-----	19
Figure 6. Two examples of output at the cross-correlation plane - one exit beam at prefilter-----	38
Figure 7. Two examples of output at the cross-correlation plane - two exit beams at prefilter-----	39
Figure 8. Television picture of the cross correlation plane - two exit beams with $\ell_1 = -1, +1$ and $\ell_2 = 0$ at prefilter with approximately equal phase and amplitudes-----	40
Figure 9. Same picture as figure 8 except beams are approximately 180° out of phase-----	41
Figure 10. Television picture with $\ell_1 = +1$ and $\ell_2 = \pm 1$ at prefilter with approximately equal phase and amplitudes-----	42
Figure 11. Same picture as figure 10 except beams are approximately 180° out of phase-----	43
Figure 12. Television picture with $\ell_1 = 0$ and $\ell_2 = \pm 1$ at prefilter. Here beams are in phase-----	44
Figure 13. Television picture with $\ell_1 = -1$ and $\ell_2 = \pm 1$ at prefilter. Here beams are out of phase-----	45
Figure 14. Television picture with $\ell_1 = +1, \ell_2 = -1$ and $\ell_1 = 0, \ell_2 = 0$ -----	46
Figure 15. Television picture with $\ell_1 = -1, \ell_2 = -1$ and $\ell_1 = 0, \ell_2 = 0$ -----	47
Figure 16. Final examples of output at the cross-correlation plane-----	48
Figure 17. Television picture with all nine holes illuminated and the cross correlation output not saturating the vidicon-TV unit-----	51
Figure 18. Television picture showing saturation of vidicon-TV unit-----	51
Figure 19. Television picture showing the cross correlation not properly aligned-----	52
Figure 20. A partial view of the beam profile apparatus-----	53
Figure 21. The remaining view of the beam profile apparatus-----	54
Figure 22. A picture of the object and calibration beam-----	58
Figure 23. An improved beam profile measurement scheme-----	58
Figure 24. The basic beam profile measurement process-----	60
Figure 25. Beam profile measuring apparatus using reflection optics (not to scale)-----	61
Figure 26. Beam sampling pattern in the prefilter plane-----	62
Figure 27. Resulting spot pattern in the cross-correlation plane-----	64
Figure A.1. Relationships between surface "1," "2," and "3" for a simple lens---	74

LASER BEAM PROFILE MEASUREMENTS USING
SPATIAL SAMPLING, FOURIER OPTICS, AND HOLOGRAPHY*

Eric G. Johnson, Jr.

Using appropriate holography, lenses, mirrors, and a two-dimensional array of small holes to sample the electric field of a laser pulse, we demonstrate a technique for beam profile measurements at a preselected observation plane. This method can measure the amplitude and phase of a laser pulse at each preselected sampling point on a transverse observation plane. Subject to constraints, these measurements can provide separated visual images of the temporal pulse shapes for the amplitude and phase at each of the sampled electric fields. This paper describes the basic concepts for beam profile measurements via holography and uses pictures generated by a prototype system for illustration.

This unit may be calibrated by using a cw laser beam of the same wavelength as the carrier or a Q-switched laser pulse. Therefore, a user can make beam profile measurements of a laser pulse in real time. This technique requires appropriate scaling of the lenses and mirrors, and uses a different hologram to allow the unit to work optimally for each wavelength.

We define the potential limits and virtues of the holographic method. In addition, we define limits and virtues of other beam profile techniques such as the two-pinhole scanning method and the Hartmann plate method.

Finally, we indicate possible directions for eventual commercial and scientific exploitation of the holographic method. The technique can be used for near- and far-infrared wavelengths and, with appropriate changes in the optics, for visible wavelengths.

Key Words: Amplitude; beam profile; cross correlation; digital sampling; fourier optics; holography; laser; laser parameters; laser pulse; optical processing; phase; precision measurements; wave front.

1. INTRODUCTION

Using lasers for communication, material processing, and precision measurements is now a significant activity and is expected to become a major element in the national economy. This trend arises from the fact that a laser beam can be highly directional and can permit efficient placement of high-power densities (irradiance) at well-defined locations. A consequence of these two properties is the use of lasers to communicate via optical fibers as well as to weld and evaporate various materials.

Timely development and incorporation of lasers into our society require tools that measure what happens. The prime applications of lasers require knowledge of each beam including the irradiance at every point in space and at every instant of time. Because exact measurements are impossible to attain, we must use mathematical models and many assumptions to define a minimum but sufficient group of measurements so we can infer the values for key parameters of these laser beams. Some parameters of current interest are laser power, energy, pulse shape, and beam profile (wavefront).

Work at the National Bureau of Standards (NBS) has been to generate and use methods to measure accurately power and energy in a continuous wave (cw) or a pulsed laser beam. Existing calorimeters and power meters can measure selected ranges of power and energy in a

* Funded in part by the Combined Calibration Group (CCG) of the Department of Defense under project number 77-109 and 78-109.

laser with an absolute uncertainty of less than one to five percent at discrete wavelengths such as 0.6328, 1.06, and 10.6 μm . NBS's efforts provide a basis for controlling the quality and safety of various lasers during their use in commercial and scientific equipment.

NBS is currently developing measurement systems that can document the time behavior of the power in a laser pulse at a sample rate of one nanosecond or slower for the 10.6 and 1.06 μm wavelengths. This activity is a step toward real-time control of a laser beam.

The development of a beam profile measurement system for pulsed lasers is the subject of this technical note. NBS's prime goal is to generate techniques that can permit simultaneous measurement of the beam profile, both irradiance and phase, in real time. Once we know how a pulse evolves in both time and space, we can use feedback techniques with adaptive optics to improve the form of laser pulses for purposes such as launching them into optical fibers, directing them into fusion devices, controlling their profile for welding, drilling, and blasting on surfaces of microcircuits; and for communicating through a highly scattering medium such as fog, smoke, or rain. Significant development remains to optimize the systems using lasers.

1.1 What this Introduction Contains

Because people in the laser community have asked me why beam profile measurements are of interest, I include a brief discussion about those measurements in subsection 1.2. I then discuss the methods for beam profile measurements and indicate their virtues and limits in subsection 1.3. The technical details of each method are abbreviated because key features appear later in this technical note or are covered adequately in the literature. I report the essential conceptual point about each method without requiring the reader to understand mathematical and experimental details.

My principal intent is to explain and document the holographic method, discussed briefly in subsection 1.3.5. Other methods are explained in subsections 1.3.2 to 1.3.4.

Subsection 1.4 details this paper's purpose because, as I have found in numerous conversations, there is a need for preliminary discussion to familiarize the reader with the vagaries of beam profile measurements.

1.2 Defining Beam Profile

Laser beams are electromagnetic fields. Current evidence indicates they propagate according to Maxwell's equations. Therefore, to completely prescribe the electromagnetic field, the reader needs to know the medium of propagation, usually defined by an index of refraction which can be a function of time and space, a state of polarization, or the amplitude and phase of the electric field as a function of time at a selected two-dimensional surface. Because the transverse dimensions of these beams are large compared with their wavelength, the vector nature of the beam usually can be approximately described by scalar concepts. At some stage in design of a system, polarization must be considered. Since the wavelength is fairly sharply defined, the time dependence of the carrier is usually treated as harmonic. The spatial dependence of the index of refraction usually is assumed to be known for a given apparatus. These approximations mean only the amplitude and phase of the electric field along a selected transverse surface to the beam need be measured to predict all subsequent space and time behavior of the beam.

Even with the above approximations, the complete measurement requires both the amplitude and phase at all points on the chosen transverse surface.* From this information all other amplitudes and phases on other transverse surfaces can be deduced using appropriate solutions to the Helmholtz equation. Because this set of measurements implies a four-fold infinity* of numbers, many more assumptions about the structure of a laser beam in a given apparatus are needed to permit restricted measurements to prescribe the beam.

*If a beam has strong directional character, then the number of measurements can be significantly reduced to some countable or finite number.

This requirement for many (not necessarily unique) assumptions to get useful data can cause ambiguity in the definition of beam profile measurements. Briefly, the above discussion shows there can be no complete set of beam profile measurements; there can only be approximate subsets. This means that the appropriate beam profile measurements are strongly dependent on the lasers being used in a given system and on the goals of that system. For example, if your beams are purely Gaussian everywhere, cylindrically symmetric, and steady in time, only the following five parameters on a given transverse surface need to be measured: (1) the two coordinates for the center of peak irradiance of the profile; (2) the distance from the center to the half-peak irradiance value; (3) the total power in the beam; and (4) the radius of curvature of the phase front.

In conclusion, I define beam profile measurements as amplitude and/or phase measurements on a transverse plane of a beam that collect sufficient information to specify it. For example, the method in subsection 1.3.2 only measures the amplitude. This method can still measure the beam profile provided certain facts about the beam are known. If these facts are not available, then a simple measurement of amplitude will not be sufficient. In this case, a different method for beam profile measurement should be used.

1.3 Various Methods to Measure Beam Profile

There are numerous methods for performing beam profile measurements which can be grouped into three classes. I make no attempt to present all possible methods. All methods can be used for far- and near-infrared visible wavelengths. Each wavelength requires appropriate detectors and optics. For example, mirrors can be used at 10.6 μm .

The first class assumes the beam profile has a known shape such as Gaussian; all that is required is an irradiance scan to deduce the unknown width of the beam. One method of this class uses an aperture of 10 to 100 μm diameter in front of a linear detector to intercept and scan the beam systematically. A second method uses a fine wire whose diameter is comparable to the half-power width of the beam [1]. The detector captures the entire beam, and the wire moves at constant velocity to generate a shadow of the wire on the detector. By using appropriate assumptions about the beam profile and by studying the current pulse from the detector, the width of the beam is deduced. Both methods are quantitative. However, there is no information about the phase front of the beam in the plane of these measurements. That fact requires additional measurements of irradiance at new planes along the optical axis of the laser beam and the application of solutions to the Helmholtz equation. This procedure only works for stable beams.

The second class of measurement methods uses an optical flat or some other beam dividing device to generate an interference pattern across the beam profile [2]. These methods are quantitative if the original beam irradiance is uniform; hence, the output pattern is determined by the phase front. If the irradiance of the original beam has nonuniformities, then the interference pattern becomes modified. To get quantitative results, it is necessary to make additional assumptions about or measurements of the structure of the irradiance to determine its effect on the interference pattern. Using appropriate scan methods, making measurements at two surfaces, and applying the appropriate solution to the Helmholtz equation can permit this technique to become quantitative even if the irradiance is nonuniform.

The third class of methods is discussed in more detail in subsections 1.4.1 to 1.4.5 because it is less dependent on specific features of a beam profile. This means these methods can be part of a general measurement instrument. Because these methods have more physical and conceptual complexity than those in the other classes, the previous methods should be used when appropriate.

1.3.1 The Methods Using Fewer Assumptions

The four methods described in subsections 1.4.2 to 1.4.5 make fewer simplifying assumptions about the actual phase front and the irradiance than do the previous methods. Each has a different limit for valid use. Those limits are described in the following subsections. In all cases, the appropriate method to use with a given laser system depends on desired results. Further, there is a brief discussion of calibration techniques for each method.

1.3.2 The Focal Plane Method

This method accepts that only the irradiance distribution at the far field of a laser beam has importance [3]. Consequently, the beam passes through a lens or reflects off a mirror with appropriate radii of curvature to generate the far-field pattern at the focal plane. To measure the irradiance pattern, the detectors in the focal plane can be a vidicon with TV scan speed, a two-dimensional array of detectors, or a single detector with appropriate moving mirrors and pinholes.

This method's limits are set by the linearity of the vidicon unit, the speed of the scanning processes, the spatial resolution of the detector array, and the selection of the appropriate lens or mirror to match key spatial details in the far-field irradiance pattern with the spatial resolution of the detector system.

A direct calibration of a system using the focal plane method is complex, which is one very important constraint of the method. If we could have a uniform, high irradiance beam of significant cross section with a known plane wavefront, then a straightforward scan technique could be developed using this beam to calibrate the focal plane system. However, generation of such large area plane-waves at an adequate irradiance level can be difficult. In principle, a known source could be used to develop the calibration of the system. One likely possibility is a point source. To be sure the calibration of the system is adequate requires a detailed two-dimensional scan by both a single point source and a pair of closely spaced point sources that have their far fields well developed before their beams enter the system. Scans by both source configurations should be done at different optical distances from the focal plane to calibrate the curvatures of their phase fronts.

The above calibration works as long as the detectors are linear over the entire range. If they are not, a beam splitter can be used to scale the unknown beam to the irradiance levels of the calibration system, so that the focal-plane system can work as a calibrated unit.

The principal value of the focal plane method is its measurement capability for the details of the far-field irradiance pattern. As discussed in reference [3], any residual radius of curvature in the near-field phase front can cause an apparent distortion of the irradiance pattern in the focal plane. To minimize this problem for detectors in this plane and to be sure the irradiance pattern is not significantly modified by the residual radius of curvature, we require the focal length of the lens to be such that the depth of field is large compared to the dimensions of the detectors. Under these conditions, an accidental curvature causes no significant errors in measurement of the irradiance pattern.

1.3.3 The Mirror Scan Method Using Two Pinholes

This method uses a moving mirror to direct the beam in a systematic two-dimensional scan across a fixed pair of pinholes followed by a beam splitter [4,5]. The device has two detectors. One measures the total irradiance through the two pinholes in one beam of the beam splitter. A moving spatial filter intercepts the second beam's interference pattern, and the filtered radiation is focused either by a lens or by a spherical mirror into a second detector. The time dependence of the output from the two detectors, coordinated with the motions of the mirror and the filter, generates two electrical signals containing details of the amplitude and phase of the beam profile.

The scan speed of the mirror limits the rate of change of the beam profile that can be followed. The usual speed is about 0.01 second per frame, i.e., about the TV scan rate. As long as the beam changes at a rate that is slower than this scan, the measurement made by the device is well defined and has high precision. If the beam profile changes at a speed comparable to or faster than this scan, then the output fails to map the input.

An apparent limitation arises from the spatial resolution of a TV scan. A telescope can overcome it by changing the scale of the beam before the scan takes place, thereby enabling the TV output to contain the details of interest.

This unit can be calibrated by using the one- and two-point sources described in the previous section. With this method a few discrete positioning changes of the sources are used rather than the detailed two-dimensional scan prescribed for the focal plane method.

The two-pinhole method has potential for high precision. Its limitations are the extreme expense of the instrument, the scan speed, and the apparent lack of stability of the calibration.

1.3.4 The Hartmann Plate Method

This method bypasses the TV scan limit suffered by the previous systems [6,7,8]. The basic device is a plate with holes that intersect and diffract the laser beam. These holes are placed in a pattern to make the desired spatial sampling of the beam profile. The amplitude and phase at each sampled point are extracted by a system of detectors. The detector structure at each hole stands on the optical axis at the closest point where the diffraction pattern is a well-developed Airy disk. Each disk has a center of irradiance which depends on the phase gradient relative to the plane defined by the hole. Further, the total power in each Airy disk is proportional to the irradiance at the sampling hole. To find the center of irradiance requires either a two-dimensional array of detectors for each hole or an X and Y position sensing (helipot) system [9, 10]. With appropriate electronics at each sampled hole, it is thus possible to measure both the phase and amplitude of a laser beam.

The space required for each Airy pattern to prevent significant overlap limits the spatial resolution. A diverging lens or mirror can improve this.

A second limitation is the time constant of the electronics. A detector array can have a response time of one nanosecond. The helipot appears to have a response time slower than one microsecond. This fact distorts the output relative to the input at high speeds.

The speed and accuracy with which the phase information can be extracted from the electronics defines the final limit. To deduce the phase requires a detailed unfolding of the time and spatial response structures of the detection system. As long as this unfolding is not complex, the system can perform accurate phase measurements. The detector array permits the best accuracy in phase measurement. The price is a system with numerous channels of output that must be processed with parallel electronics or stored on a multi-channel data system.

Unlike the previous methods, the Hartmann method does not need point sources for calibration. The distances between sampling holes may make possible a calibration by a uniform irradiance and a uniform phase front at each pair of neighboring holes in the plate. Unlike the point source technique described in the focal plane method, this calibration can be done at power levels comparable to those in the laser beam of interest. This implies a less severe constraint on the actual linearity of the detectors.

1.3.5 The Holographic Method

This subsection presents the essential operations of the holographic method which uses elements from all three previous methods. This method minimizes the limitation of the electronic response time; hence, laser pulses can be better measured in real time. Obviously, there is always a final limitation to the response time for any system due to the time constants in the detectors.

The holographic method makes a beam profile measurement in the following sequence. First, a Hartmann plate with a periodic pattern of holes intercepts and samples the beam. Second, a series of lenses or mirrors generates the Fourier transform of the pattern from the plate at the focal plane. Third, the transformed pattern is passed through a hologram located at the focal plane. The hologram was previously generated by a beam profile of approximately known amplitude and phase characteristics. Fourth, the filtered beam exiting from the hologram is transformed by a second lens or mirror system to get the cross correlation. Under proper conditions, using the appropriate hologram* and proper sperturing of the sampled laser beams, the resulting pattern in this correlation plane now has spots with intensities showing only amplitude information about each sampled hole and spots with

is generated at the speed of light and represents an optical processing sequence. All electronics are delayed to the last step. This fact minimizes the unfolding effects of finite response time in detectors. Since the hole pattern is stationary in this plane the size of each detector can be small, which substantially decreases the detector's time constant.

The physical complexity of this system is greater than the previous systems. However, the calibration process has been simplified greatly, and it appears that the precision will eventually be higher than for previous methods. The number of calibration beams can be greatly reduced. Even fewer calibration values are necessary compared with the Hartmann plate method. Details of the calibration process are presented in subsections 4.3.2 and 4.5.

The relative phase between neighboring beams is determined only to a modulus of $2\pi n$ radians, where n is some arbitrary integer. This fact means the range of allowed variation in the phase front between sampled holes must be restricted to obtain unambiguous beam profile data. For highly directional laser beams, this is not critical. For beams of high divergence, the holographic method may have little value. Some other method is probably more appropriate. Usually rapid variations in the phase front from a plane wave indicates that the spatial coherence properties are not important. The beam does not have strong directionality. This poor directional character may imply a spatially incoherent source could work as well or better.

The sampling pattern of the Hartmann plate limits the spatial resolution of the measurement of the beam profile. Appropriate use of beam expanders in front of the Hartmann plate can minimize the impact of this technical limit.

The ultimate limitations of the holographic method are set by the total number of detectors used to measure the time behavior of the beam profile and by the physical size of each sampling hole. Each sampling hole needs about 2.25 channels; thus, 100 sampling holes imply at least 200 detectors.

The above completes the general discussion on the beam profile methods; we pass to the next subsection and make a detailed study of the holographic method.

1.4 The Purpose of this Paper

At this point the reader should have a sense of what beam profile measurements are as well as how and why they are done. The reader may not yet have detailed understanding of how wave propagation works, what are Fourier optics, and how beam sampling permits phase and amplitude measurements with high precision. To provide necessary background, appendix A details the Fourier optics notions, and appendices B and C describe diffraction patterns of square and circular holes in the Fourier optics approximation. These results are then summarized and used in section 2 to show how ideally-shaped laser beams can be used for precision measurements.

After we complete the technical overview in section 2, we describe in sections 3 and 4 the prototype system constructed during 1977 at NBS (Boulder, Colorado) to demonstrate the holographic method. In section 3, we describe both the derivations of the mathematical models for the method and the alignment process for the apparatus. Section 4 describes the apparatus that generated the cross-correlation patterns. Because the alignment process requires an understanding of the concept of depth of field, I include appendix D which explains the idea in a form different from that usually found in the literature.

Because the original system is a prototype and the basic holographic method is new, many things were learned during this study. Section 5 describes what was learned and suggests improvements to the basic system.

*This hologram can be generated so that it works for far-and near-infrared. This paper is a demonstration of the concepts using visible light. Subsection 5.4 describes the reflection system that can be used for 10.6 μm .

Finally, section 6 draws conclusions from the evaluation of the prototype unit and from analysis of questions raised by various people in the laser community.

2. AN OVERVIEW OF THE BASICS USED IN THE HOLOGRAPHIC METHOD

Subsection 1.4.5 describes briefly the holographic method using terms defined in various books and papers on holography and Fourier optics. Section 2 explains in more detail the meaning of those terms and techniques so that subsequent sections can use freely those notions to define the holographic method.

2.1 What this Overview Contains

To understand the holographic method requires a thorough comprehension of the diffraction of coherent light by a single aperture. If an aperture is small compared to the spatial details in the original beam, then the subsequent structure of radiation out of this aperture is known from the theory and previous experiments. To make precision measurements of beam profile, only the details of the Fourier plane and the near field of the diffraction pattern are needed. The extremely complex intermediate field structure can be ignored. Subsection 2.2 gathers the relevant information about the single aperture that is necessary for the precision measurements.

Because a single aperture generates insufficient information about an arbitrary laser beam profile, we must use multiple apertures in a sampling plane and understand the resulting Fourier plane pattern, and we need to know how to use the pattern to make precise and proper measurements of an arbitrary beam profile. To help explain the use of multiple apertures, we discuss in subsection 2.3 the diffraction by two apertures under far-field and Fourier plane conditions.

The analysis of multiple beam sampling for the actual holographic method is discussed in subsections 3.3 and 4.3.

Three concepts in the holographic method may be difficult to understand: Fourier optics, holograms, and cross correlation. To be sure the reader has a clear picture of what is important about each, subsection 2.4 addresses Fourier optics, 2.5 describes the holograms, and 2.6 discusses cross correlation.

Subsection 2.7 assembles the above ideas to expand the discussion in subsection 1.3.5 about the properties of the holographic method.

In subsection 2.8, I summarize the holographic method and indicate what this paper presents in the remaining sections using the terminology developed in section 2 and the appendices A, B, C, and D.

2.2 The Main Features of the Diffraction Process by a Single Aperture

The key reason for using apertures to sample a laser beam profile is to gather precise information about two important beam parameters, the average intensity and phase across each aperture. The apertures suppress the effects of the gradients in the irradiance and the phase across each aperture. By using the Fourier plane as a critical measurement surface, we can perform precise measurements on the average intensity and phase with a minimum generation of error caused by phase and irradiance gradients and by variations in the exact form of the apertures.

Because the beam is sampled just at selected coordinates, we have precise information only on selected features of a laser beam. Therefore, to have meaningful beam profile data requires that information is unambiguous and consistent with subsequent use of the beam.* In short, the measurement technique for beam profile must be appropriate. For example, if

*The beam measured here would usually be one generated from the main laser beam by a grating or a wedge-beam splitter.

only the intensity distribution of a laser beam's far field is important but the effects of the propagation process are unimportant, then aperturing the laser beam for profile measurements can be a mistake. In this case, it makes more sense to generate the Fourier plane of the laser beam without an aperture in front of the optics, and then to aperture the irradiance pattern in the Fourier plane for the selected beam profile information. However, to control or know this irradiance pattern for near, intermediate or far field in real time, details on the phase front in the near field of the laser beam are needed. In this case, the far-field measurements are insufficient and not appropriate. There are circumstances when it is not possible to measure the focal plane irradiance because the distribution is too small and the available space is limited; therefore, near-field phase and amplitude measurements are necessary to infer the far-field irradiance pattern.

Returning specifically to diffraction details by a selected aperture, we develop the far-field and the Fourier plane patterns for two shapes, namely a square and circle, in appendices B and C. In both, the information about the average irradiance and phase multiplies the field pattern generated by the unknown laser beam illuminating these apertures (see equations B.6 and C.5). Note that the patterns are different for the square and circular apertures. Further, to get accurate results, the variation in position off the optical axis for the peak irradiance caused by the gradient in the phase ($b_{1\ell}$ and $c_{1\ell}$ are not zero) must be unimportant. To become insensitive to the shape of the aperture requires measurements that correct for this influence. The holographic method reduces sensitivity by using a significant fraction of the field pattern in the Fourier plane and by comparing that pattern with an appropriate pattern stored on a filter in that plane. By this process, the differences between the two patterns are minimized and their similarities are maximized. We see these details in sections 4.3, 5.4, and 5.5.

Shrinking an aperture to such a size that gradients in the phase are insignificant is easy. Unfortunately, the amount of laser power through each aperture is so greatly reduced that this can impose a stringent demand on the allowed detectors. One potential solution to this problem would be to use a laser amplifier at each aperture that would preserve the details of the average irradiance and phase striking the aperture to eliminate completely the gradient effects and yet generate sufficient gain to compensate for the small sampling area. At present, there are no such amplifiers; therefore, we compensate by using larger apertures and then restricting the allowed gradients across a given aperture. Of course, in high power or energy lasers the size of the apertures can be smaller than those needed for low power or energy lasers.

Incidentally, the constraint that the gradient of the phase across an aperture be less than some value is opposite to the conditions for optimum operations of the Hartmann plate method. In this case, it is necessary for the phase gradient be greater than some prescribed value so that variations in the phase front beyond a trivial plane wave can be detected. I do not show constraints applied to the holographic method in the later subsections; they strongly depend on the actual apparatus. Sections 3.3 and 4.3 give the correct mathematics for the square aperture case. In final analysis, when a precision apparatus is built, the precise dynamic range of each parameter at each aperture is measured. At this time we make approximations and computer simulations of ideal systems.

2.3 Looking at the Interference Pattern in the Far Field and Fourier Plane for Two Apertures

The far-field pattern for two square apertures ℓ_1 and ℓ_2 can be directly written from the results in eq. (B.6) as (see note below*):

Note "" means to multiply in this and subsequent expressions except when used for complex conjugation. The difference is obvious in each expression.

$$U_2(x_2, y_2) = [A_0 a^2 e^{ikz} / (i\lambda z)]$$

$$* \left[\begin{array}{l} e^{id_{\ell 1}} \exp \left\{ \frac{ik}{2z} [(x_2 - g_{\ell 1})^2 + (y_2 - h_{\ell 1})^2] \right\} \\ * \operatorname{sinc} \left[\left(\frac{(x_2 - g_{\ell 1})}{\lambda z} + \frac{b_{\ell 1}}{2\pi} \right) a \right] \operatorname{sinc} \left[\left(\frac{(y_2 - h_{\ell 1})}{\lambda z} + \frac{c_{\ell 1}}{2\pi} \right) a \right] \\ + e^{id_{\ell 2}} \exp \left\{ \frac{ik}{2z} [(x_2 - g_{\ell 2})^2 + (y_2 - h_{\ell 2})^2] \right\} \\ * \operatorname{sinc} \left[\left(\frac{(x_2 - g_{\ell 2})}{\lambda z} + \frac{b_{\ell 2}}{2\pi} \right) a \right] \operatorname{sinc} \left[\left(\frac{(y_2 - h_{\ell 2})}{\lambda z} + \frac{c_{\ell 2}}{2\pi} \right) a \right] \end{array} \right] \quad (2.3.1)$$

To qualitatively understand this equation, we simplify it by assuming λz is large enough and the aperture diameter a is small enough, and we only consider $x_2, y_2 \sim 0$. In this case, the above expression simplifies to:

$$U_2(x_2, y_2) = \frac{A_0 a^2 e^{ikz}}{i\lambda z} * \left[\begin{array}{l} e^{id_{\ell 1}} \exp \frac{ik}{2z} [(x_2 - g_{\ell 1})^2 + (y_2 - h_{\ell 1})^2] \\ + e^{id_{\ell 2}} \exp \left\{ \frac{ik}{2z} [(x_2 - g_{\ell 2})^2 + (y_2 - h_{\ell 2})^2] \right\} \end{array} \right] \quad (2.3.2)$$

Next we presume the irradiances on the two apertures are identical; thus $d_{2\ell 1} = d_{2\ell 2}$.

With these simplifications, the irradiance pattern in the far field for two apertures becomes:

$$I[x_2, y_2] = 2I_f * \left[\begin{array}{l} 1 + \cos \left\{ d_{1\ell 1} - d_{1\ell 2} + \frac{k}{2z} \left(\begin{array}{l} (x_2 - g_{\ell 1})^2 - (x_2 - g_{\ell 2})^2 \\ + (y_2 - h_{\ell 1})^2 - (y_2 - h_{\ell 2})^2 \end{array} \right) \right\} \end{array} \right], \quad (2.3.3)$$

where $I_f \equiv \left(\frac{a^2}{\lambda z} \right)^2 A_0^2 \exp(-2d_{2\ell 1})$. This 100% modulation pattern contains detailed information about the relative phase between two apertures, namely $d_{1\ell 1} - d_{2\ell 2}$, as well as the irradiance illuminating both apertures, namely the value fixed by $d_{2\ell 1}$.

By appropriate study of the details of the far-field irradiance pattern without all the above simplifications, you can get the relative phase between the two apertures as well as the individual irradiances, namely those values fixed by $d_{2\ell 1}$ and $d_{2\ell 2}$. Unfortunately

measurement of those details can be complex. That is why constraints are imposed on the system so we can make accurate beam profile measurements.

The Fourier plane pattern $U_f(x_2, Y_2)$, for two square apertures ℓ_1 and ℓ_2 can be directly written from the results (B.24) as:

$$U_f(x_2, y_2) = \frac{A_o a^2}{i\lambda f} \exp [i(2kf+(n-1)tk)] \left[\begin{array}{l} e^{i[d_{\ell_1} - \frac{k}{f}(x_2 g_{\ell_1} + y_2 h_{\ell_1})]} \operatorname{sinc} \left[\left(\frac{x_2}{\lambda f} + \frac{b_{\ell_1}}{2\pi} \right) a \right] \operatorname{sinc} \left[\left(\frac{y_2}{\lambda f} + \frac{c_{\ell_1}}{2\pi} \right) a \right] \\ * \\ e^{i[d_{\ell_2} - \frac{k}{f}(x_2 g_{\ell_2} + y_2 h_{\ell_2})]} \operatorname{sinc} \left[\left(\frac{x_2}{\lambda f} + \frac{b_{\ell_2}}{2\pi} \right) a \right] \operatorname{sinc} \left[\left(\frac{y_2}{\lambda f} + \frac{c_{\ell_2}}{2\pi} \right) a \right] \end{array} \right] \quad (2.3.4)$$

Again to illustrate the key features of this pattern, if a is small enough and f is large enough, then the sinc functions are equal to one. If we further assume the irradiance at each aperture is the same, then the resulting irradiance in the Fourier plane becomes:

$$I(x_2, y_2) = 2I_f \left(1 + \cos \left\{ d_{1\ell_1} - d_{1\ell_2} - \frac{k}{f} [x_2(g_{\ell_1} - g_{\ell_2}) + y_2(h_{\ell_1} - h_{\ell_2})] \right\} \right) \quad (2.3.5)$$

where

$$I_f = A_o^2 \left(\frac{a}{\lambda f} \right)^2 \exp (-2d_{2\ell_1}) .$$

We see that the irradiance pattern for both the far field and Fourier plane are similar. The only difference is the phase shift constant,

$\frac{k}{2z} [g_{\ell_1}^2 - g_{\ell_2}^2 + h_{\ell_1}^2 - h_{\ell_2}^2]$, which is present in the far-field expression.

2.4 Important Properties of Fourier Optics as Applied to the Holographic Method

Appendices A and D describe key features of Fourier optics [11,12]. Fourier optics is the holographic method because you generate the Fourier transform of an arbitrary beam profile. Further, this technique allows linear filtering of that transform for another Fourier transform.

Why is the transform important? As already discussed, precision measurements require numerous apertures to extract needed irradiances and phases. As shown in subsection A.3, the Fourier plane has the position details for each aperture buried in the phase term. Thus, the linear filter used to generate the required cross correlations acts uniformly and simultaneously on each electric field from all the apertures. This fact allows optical computing rather than electronic computing; consequently, the measurement rate is faster and probably more accurate.

2.5 Important Properties of the Holographic Process

Holography has two points of importance, both due to the use of a reference beam in conjunction with an unknown object beam. First, using a plane wave as a reference allows a photographic plate to record both phase and irradiance information of the object beam. Second, because the reference beam has its phase front at an angle to the object beam, the density recorded in the plate can generate spatially separated laser beams one of which contains the desired cross-correlation information.

To understand the above points, we discuss briefly the holographic process. We symbolize the incident radiation as:

$$U(x,y) = e^{ik_2z} [O(x,y) + R(x,y)e^{ik_1x}],$$

where $O(x,y)$ represents the electric field for the object beam; $R(x,y)e^{ik_1x}$ represents the reference beam; k_1 labels the vector component along the x axis for the propagation of the reference beam; and k_2 labels the vector component along the z axis for the propagation of both the reference and object beams. The latter has no propagation along the x axis.

The photographic emulsion records an irradiance pattern, namely:

$$I(x,y) = U(x,y) U^*(x,y) . \quad (\text{See note below*})$$

If the irradiance of the reference beam is four or more times the irradiance of the object beam [11, pages 45-60], then the recorded transmittance, t , on the film can be considered to have the form:

$$t(x,y) = f[R(x,y)R^*(x,y)] + \alpha_1 [R(x,y)O^*(x,y)e^{ik_1x}] + \alpha_1 [R^*(x,y)O(x,y)e^{-ik_1x}] + \text{neglected terms}.$$

The function f is the average transmittance and the α_1 is the derivative of this function biased at the average transmittance. The neglected terms are higher derivatives, the biasing effects of OO^* and the nonlinearities of the holographic process. We presume the film has a linear response region. This describes the first feature of the holographic process.

When the transmittance $t(x,y)$ intercepts and filters a laser beam, the exit radiation pattern is given as:

$$E(x,y) \equiv S(x,y) t(x,y) .$$

$S(x,y)$ is the incident electric field before it strikes the photographic emulsion, and $E(x,y)$ is the exiting electric field. Notice there are three beams exiting from this emulsion.

First, the beam, $\alpha_1 S(x,y)O^*(x,y)R(x,y)$, diffracts to propagate with a vector component along the x axis of $+k_1$. Second, the beam $\alpha_1 S(x,y)O(x,y)R^*(x,y)$, diffracts to propagate with a vector component along the x axis of $-k_1$. Third, the beam $S(x,y) [R(x,y)R^*(x,y)]$, contains no diffraction or beam bending; therefore, this beam continues along the original direction of the incident beam, $S(x,y)$.

2.6 Important Properties of the Cross-Correlation Process

As already mentioned in subsections 2.4 and 2.5, the cross-correlation process involves spatial filtering [13]. After the filtering, the appropriate beam,

$C = S(x,y)O^*(x,y)R(x,y)\alpha_1$, becomes transformed. This step converts the C into a series of spots.

Note: The $U^(x,y)$ means complex conjugate of $U(x,y)$.

These spots are distorted images of the original illuminated apertures. The distortion comes from three sources: the aperturing by the filter, the pattern structure of the filter, and the aperturing by the final Fourier transform lens. The number of spots can increase substantially over the original number of apertures used to sample the unknown laser beam. Each spot can have contributions of both irradiance and phase from each sampled beam. The subsequent sections describe filters and approaches to control the form of these contributions.

In conclusion, in the cross-correlation process the filter acts as a grating and beam splitter to direct known fractions of radiation from one aperture to selected spots in the cross-correlation plane. By this diffraction process, the phase and irradiance at each aperture can be referenced in real time to the phases and irradiances of other apertures. This situation permits application of a differential measurement technique comparable to that used in electronic bridges. Because these comparisons are made at localized points, there is substantial reduction both in the response time of detectors and on their effect on the precision of phase and irradiance measurements. This condition is a prime reason for making the detection process in the cross-correlation plane rather than in the Fourier or far field of the original apertures.

2.7 Assembly of the Above Concepts to Define the Holographic Method

I suggest the reader return to subsection 1.3.5 and reread the second paragraph using the understanding generated by discussions in subsections 2.1 to 2.6. Once this is completed, the reader will have a clear overall picture of the holographic method and will be ready to study the details of this method.

2.8 Summary of this Overview

We have seen that developing an understanding of propagating laser beams is important. There is extensive interplay between the ideal understanding of the sampling process, as shown by the discussion of aperturing a laser beam, and the corresponding technical implications of Fourier transform, filtering, and holography [11,12,14]. This interplay generates options for optical processing [13]. By avoiding conversion of the beam profile information as carried by sampled beams, until the last possible moment, we increase our speed for precise measurements. This allows us to use feedback at speeds not currently available and implies a significant technical advance.

3. HOLOGRAM CONSTRUCTION APPARATUS

This section has three goals. First, we describe the front part of the beam profile apparatus built at NBS in 1977. Second, we construct the mathematical model simulating this apparatus. Third, because we want to accelerate transfer of these concepts, we discuss actual equipment.

3.1 What this Section Presents

There are four subsections in this section. Subsection 3.2 defines the structure of the prototype apparatus that generated the hologram used for the cross-correlation process. Subsection 3.3 uses this prototype to fix the necessary mathematics for the simulation describing how the apparatus generates the hologram and how the front end of the cross-correlation process works. Subsection 3.4 specifies the assembly and alignment of the prototype apparatus, and subsection 3.5 lists conclusions relevant to the unit.

3.2 A Discussion of the Prototype Apparatus Used to Generate the Hologram

Using concepts of holography [1] and spatial filtering [13,14,15,16,17], we define the prototype apparatus using the block diagrams in figures 1 and 2 to identify each basic optical component. Each component is discussed in the order in which the laser beam goes through that component.

We generate the reference and object beams by using a beamsplitter to create two beams from the single beam exiting the laser. Because it is convenient for prototyping to study beam profiles with cross sections near 10 mm, we use a beam expander to expand original laser beam from its nominal 1 mm to a 10 mm diameter.

Following the reference beam, a beam expander creates a slowly diverging beam with an approximately Gaussian profile. The beam diameter at the half-power point is 25 mm when the reference beam intersects the film within the liquid gate.

Following the object beam, the attenuator in the path of this beam reduces its power to a convenient level for the hologram. The beam expander generates a Gaussian-like beam with a beam diameter near 10 mm and a plane phase front. This beam is now intersected by the prefilter which samples with nine apertures (see fig. 3). The exiting beams from the prefilter pass through a Fourier transform lens and an image magnification lens to intersect simultaneously the reference beam and the film.

We construct the hologram by exposing the film to the two beams and by developing the exposed film.

3.3 The Mathematical Model Used to Understand the Hologram

We examine each beam in figure 1 with the mathematics defined in the appendices to derive the resulting irradiance pattern recorded by the film. During this process, necessary notation is defined and symbolic abbreviations of the complex details are generated to clarify the essential structure of the process for generating the hologram.

We begin with the reference beam at a position one focal length in front of the first lens of the beam expander. At first, we assume the beam profile is arbitrary, namely

$$U_1(x_1, y_1, z_1), \quad (3.3.1)$$

where z_1 is the distance between the above focal point and the position where the laser beam is split to generate the reference beam.

NOTE: The optical axis is defined operationally as the center of intensity for a cylindrically symmetric laser beam passing through the various optics.

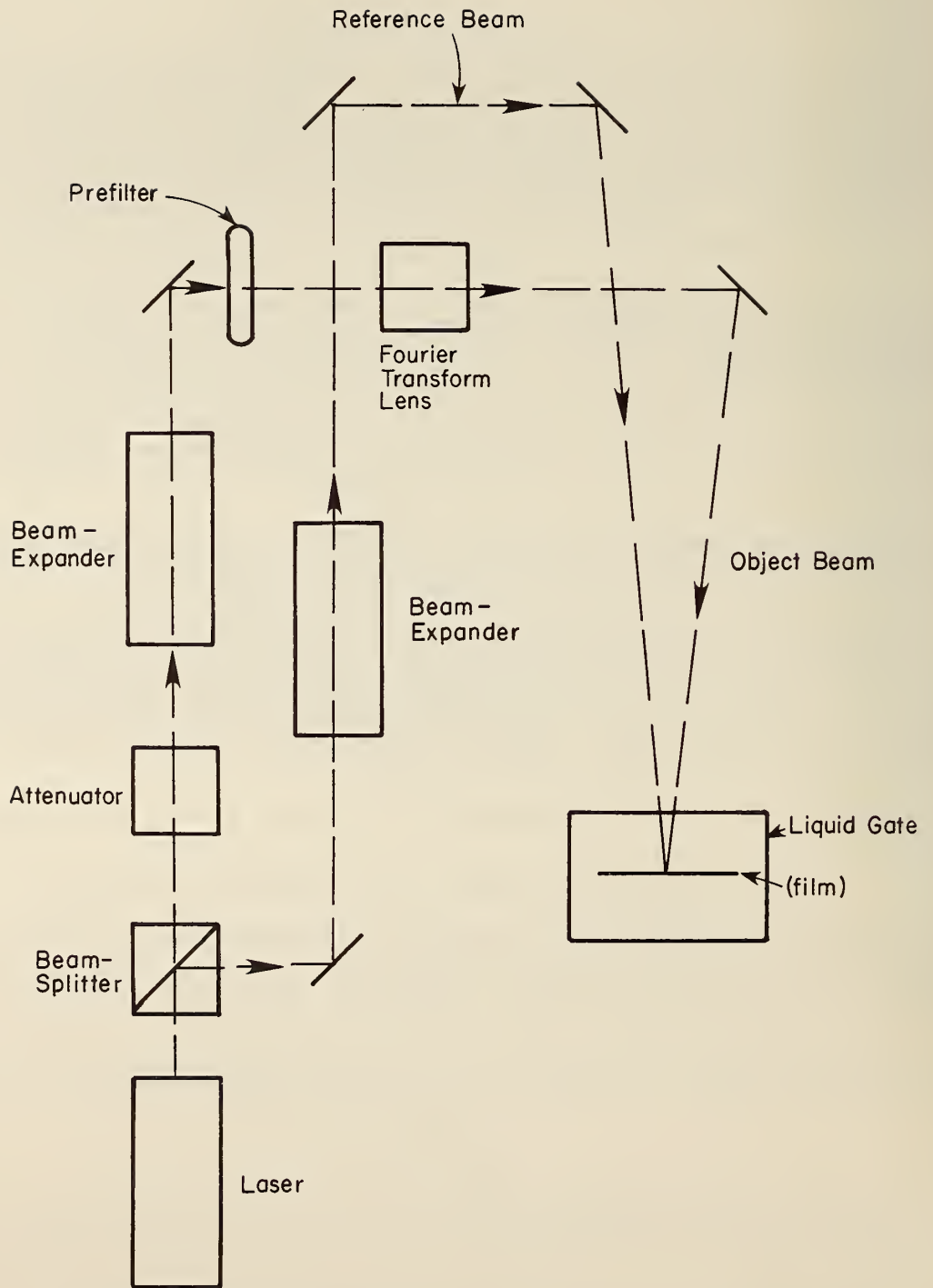


Figure 1. The hologram generating apparatus - block diagram.

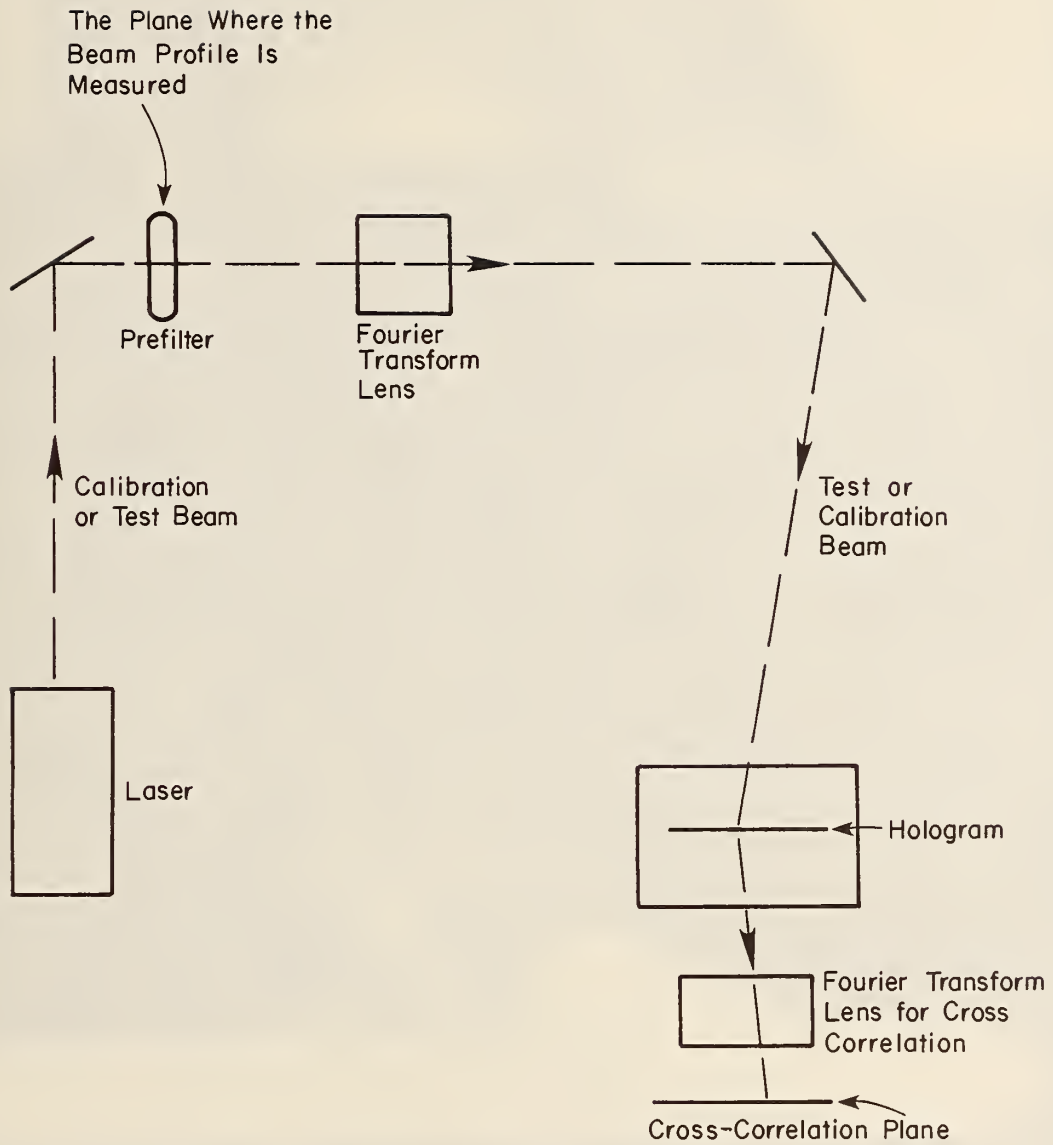


Figure 2. The cross-correlation generating apparatus - block diagram.

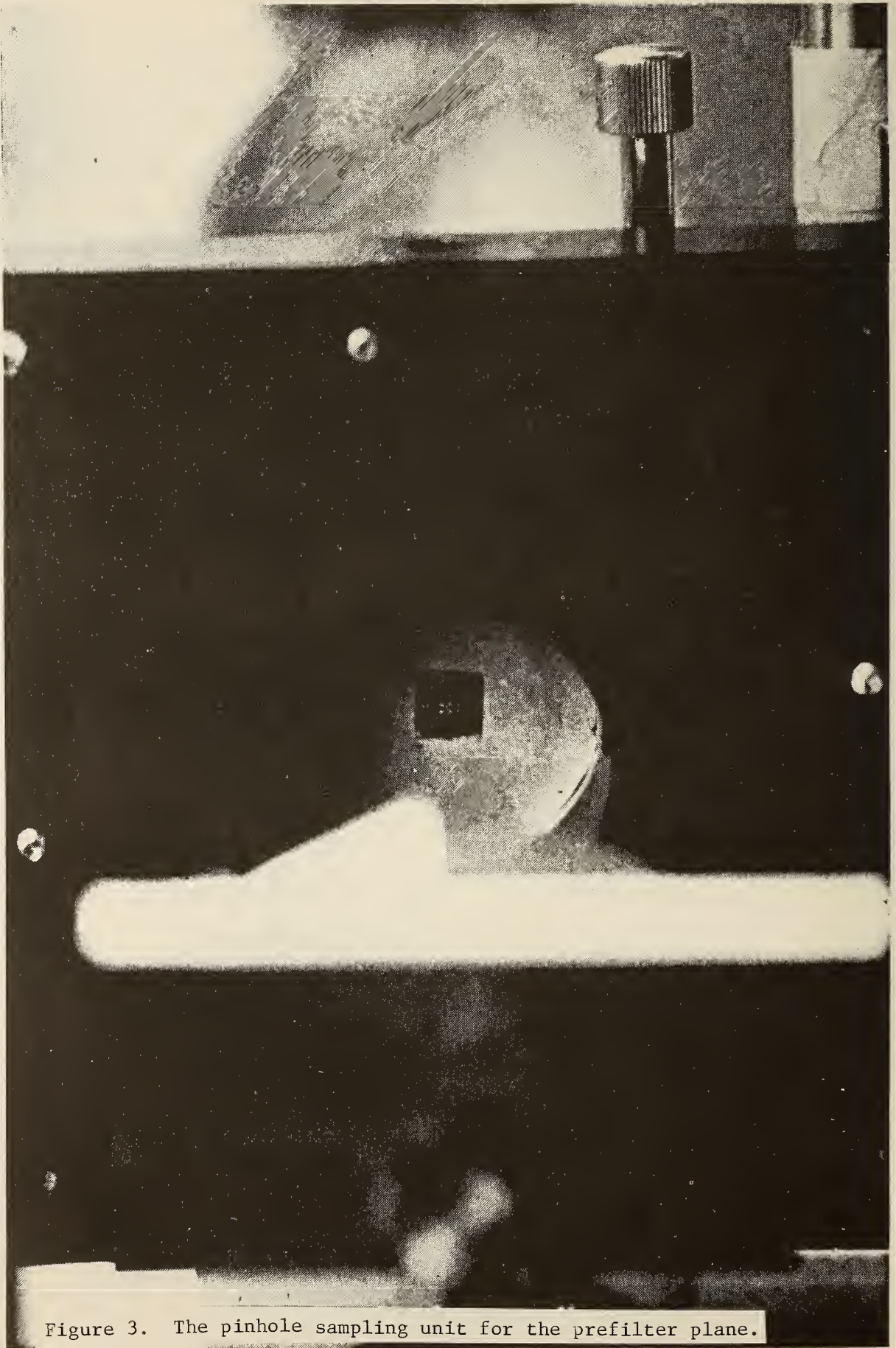


Figure 3. The pinhole sampling unit for the prefilter plane.

The first lens has an equivalent focal length, f_2 . The field at the Fourier plane of this lens as shown by figure A.1 and eqs. (A.4) and (A.5) is:

$$U_2(x_2, y_2; z_2) = \frac{A_2 e^{i\phi_2}}{i\lambda f_2} \int dx_1 dy_1 U_1(x_1, y_1; z_1) h_1(1, 2; f_2), \quad (3.3.2)$$

where the phase shift is $\phi_2 = k[2f_2 + (n_2-1)t_2]$; the distance along the optic axis (see note below) is $z_2 = z_1 + 2f_2$; the attenuation factor and additional phase shift are contained in A_2 ; and the transform function is $h_1(1, 2; f_2) \equiv \exp[-i(u_2 x_1 + v_2 y_1) 2\pi]$. The spatial frequencies are defined as $u_2 \equiv x_2/\lambda f_2$ and $v_2 \equiv y_2/\lambda f_2$. The apparent thickness of the lens is t_2 , and the effective index of refraction is n_2 . The spatial filter at z_2 changes the exit beam U_2 to:

$$U_2^a(x_2, y_2; z_2) \equiv U_2(x_2, y_2; z_2) \text{circ}(r_2/a_1). \quad (3.3.3)$$

The cylindrical coordinates center around the optical axis as $r_2 = (x_2^2 + y_2^2)^{1/2}$, and a_1 is the diameter of the filter. The circ function is defined in appendix C.

The second lens has a focal length, f_3 . It is placed so that a magnified image of the filtered field U_2^a is formed at the film. Using eq. (A.7), the reference beam at the film is given as:

$$R_H(x_3, y_3; z_3) = \frac{1}{M_2} h[x_3, y_3; s_3] U_2^a\left(-\frac{x_3}{M_2}, \frac{y_3}{M_2}; z_2\right) * e^{i\phi_3} A_3 \quad (3.3.4)$$

where the magnification is $M_2 \equiv d_4/d_3$; the effective radius of curvature is $s_3 \equiv d_4/(1 + 1/M_2)$; the phase shift is $\phi_3 \equiv k[d_3 + d_4 + (n_3-1)t_3]$; the optical distance from this second lens to the focal plane of the first lens is d_3 ; and the optical distance from the second lens to the film is d_4 . The imaging condition is satisfied, namely $1/d_3 + 1/d_4 = 1/f_3$. The additional attenuation and phase shifts due to mirrors and the second lens are contained in A_3 . The optical path length is $z_3 = d_4 + d_3 + z_2$.

We now examine the evolution of the object beam. There are two stages showing its development in front of and behind the prefilter.

Because the actions of the attenuator and beam expander are arbitrary, we address the development of the object beam behind the prefilter and delay the discussion of the object beam in front of the prefilter until the end of this subsection.

As already assumed in Appendix B, we presume that the beam shape across each square aperture in the prefilter can be adequately represented as:

$$U_\ell(x_6, y_6; z_6) = \Pi[(x_6 - \ell_1 b)/a] \Pi[(y_6 - \ell_2 b)/a] * A_0 * \exp \left\{ i[b_\ell(x_6 - \ell_1 b) + c_\ell(y_6 - \ell_2 b) + d_\ell] \right\}, \quad (3.3.5)$$

where z_6 is the optical path distance from the beam splitter; x_6, y_6 are the transverse coordinates at the prefilter; b is the distance between the apertures in either x_6 or y_6 directions; a is the edge dimension of each aperture; $g_\ell \equiv \ell_1 b$ labels the x_6 coordinate of the ℓ aperture (see figure 4); $h_\ell \equiv \ell_2 b$ labels the y_6 coordinate of the ℓ aperture; and b_ℓ, c_ℓ, d_ℓ are the parameters for the beam profile across the ℓ aperture. We abbreviate the (ℓ_1, ℓ_2) label as " ℓ ". Only when it becomes necessary to give a detailed label will we expand the notation.

The beam form exiting the prefilter is a simple superposition of the terms in eq. (3.3.5); thus

$$U_p \equiv \sum_{\ell} U_{\ell}(x_6, y_6; z_6) \quad . \quad (3.3.6)$$

The prototype in figure 3 has nine such apertures.

After exiting the prefilter, the object beam goes through a Fourier transform lens arrangement. We can write out the beam profile at the Fourier plane as:

$$U_B[x_7, y_7; z_7] \equiv \frac{a^2 A_o e^{i\Phi_7}}{i\lambda f_7} B_7 \sum_{\ell} \text{sinc}[(u_7 + \frac{b_\ell}{2\pi})a] \text{sinc}[(v_7 + \frac{c_\ell}{2\pi})a] \\ * \exp \left\{ i[d_\ell - 2\pi(u_7 g_\ell + v_7 h_\ell)] \right\} \quad (3.3.7)$$

The phase shift is $\Phi_7 = k[2f_7 + (n_7 - 1)t_7]$; the focal length of the Fourier transform lens is f_7 ; the index of refraction is n_7 ; and the thickness of the lens is t_7 . The optical path distance at the Fourier plane is $z_7 \equiv z_6 + 2f_7$. The spatial frequencies are $u_7 \equiv x_7/\lambda f_7$ and $v_7 \equiv y_7/\lambda f_7$. The additional attenuation and phase shift due to the mirrors and lens are contained in B_7 .

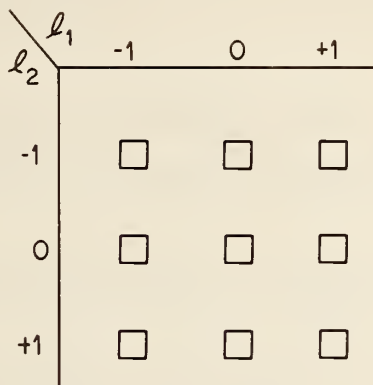
Because the dimensions of the Fourier transform are too small for effective use of the film, we have an image lens which magnifies the pattern [use eq. (A.7)]. Thus, at the film where the hologram is generated, the object beam is now:

$$U_H(x_8, y_8; z_8) = \frac{B_8 e^{i\Phi_8}}{M_8} h[x_8, y_8; s_8] U_8\left(-\frac{x_8}{M_8}, \frac{y_8}{M_8}; z_7\right) \quad . \quad (3.3.8)$$

The magnification is $M_8 = d_8/d_7$; the next optical path location is $z_8 = z_7 + d_8 + d_7$; the radius of curvature is $s_8 = [d_8/(1 + 1/M_8)]$; and the extra phase shift is $\Phi_8 = k[d_8 + d_7 + (n_8 - 1)z_8]$. The additional attenuation and phase shift corrections due to the lens and mirrors are contained in B_8 . This factor also includes the reflections at the liquid gate.

Before we explain the details of the beam at the film plane, we discuss the conditions that allow us to ignore the b_ℓ, c_ℓ terms in eq. (3.3.8). Essentially, a convenient condition for negligible b_ℓ, c_ℓ is that the modification of the sinc function around the first zero

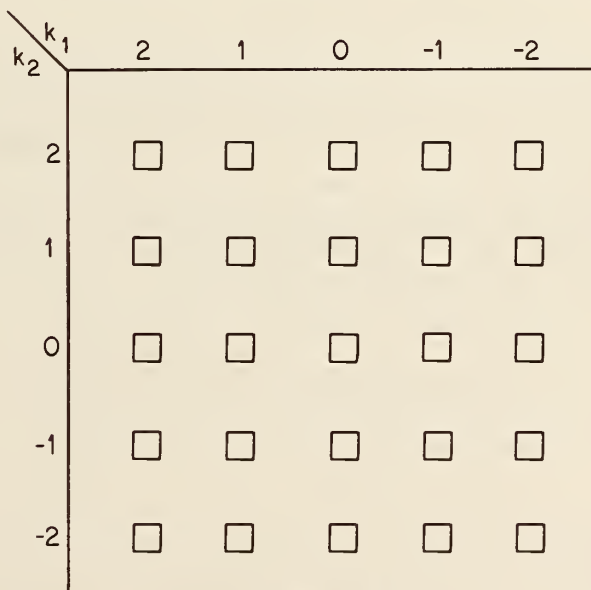
Prefilter



l_1, l_2 labels the spatial position of the laser beams.

Figure 4. The coordinates for the prefilter beams.

Cross Correlation Plane can show a 5 by 5 pattern of spots



k_1, k_2 labels the spatial position of spots in the Cross-Correlation Plane.

Figure 5. The coordinates and structure of the spots at the cross-correlation plane.

be unimportant. This means the magnitude of the gradients, namely $|b_\lambda|$, $|c_\lambda|$, must be such that either is less than

$$(.01) \frac{2\pi}{a} . \quad (3.3.9)$$

Thus, the smaller the edge of the sampling aperture is, namely a , the greater the allowed gradients are. This situation is equivalent to having a large depth of field in the beam profile instrument. For our subsequent discussion, we presume this condition is satisfied and drop the b_λ and c_λ terms in the sinc functions.

Clearly, these constraints finally fix the allowed rate of change of the beam profile between different apertures and show up as a limit to the range of the d_λ terms in the final model used to represent the beam.

The next approximation is to ignore the angle between the reference and object beams (see figure 1). The x_8, y_8 and x_3, y_3 define planes different from the film plane and each other. A rigorous theory generates numerous corrections to deduce the true beam profile recorded in the film plane. Under the conditions that both beams have significant depth of field, then most corrections are insensitive to this angle. Only the plane wave phase term shows any importance and any distortions in the theory will be unimportant.

We show this by extracting temporarily this phase term and writing the reference and object terms as:

$$R(x_3, y_3; z_3) = e^{ikz_3} R_a \quad \text{and}$$

$$O(x_8, y_8, z_8) = e^{ikz_8} O_a;$$

where R_a and O_a are the rest of the details in each beam. Here $y_3 = y_8$, if we assume that the various x coordinates are in the plane defined in figure 1. Then $x_3 = x_9 \cos \theta$ and $x_8 = x_9 \sin \theta$, if we assume the normal to the film bisects the reference and object beams. The z_3 and z_8 become modified to $z_3 = z_9 \cos \theta - x_9 \sin \theta$ and $z_8 = z_9 \cos \theta + x_9 \sin \theta$. We absorb the $z_9 \cos \theta$ factor in R_a and O_a , and note that $\cos \theta = .995$ or is about one when the angle θ is less than 0.1 radian. Thus, we write:

$$x_3 = x_8 = x_9$$

and

$$R_N = p^* R_H^* \quad \text{and} \quad O_N = p O_H \quad (3.3.10)$$

where

$$p \equiv \exp[ikx_9 \sin(\theta)] \quad (3.3.11)$$

The irradiance recorded on the film for a cw laser with no incoherence between the two beams is broken into terms

$$I = I_O + I_1 (p^*)^2 + I_1^* (p)^2 \quad (3.3.12)$$

where the biasing term is $I_O = R_H^* R_H^* + O_H^* O_H^*$; the cross-correlation term is $I_1 = R_H^* O_H^*$; and the virtual image term is I_1^* . The terms p^2 and $(p^*)^2$ cause a sine wave modulation of the intensity pattern and act as a diffraction grating when the hologram is irradiated.

The film exposure has the transmittance as $t(x,y) \equiv t[I]$ just as is shown in equation (2.3.3). (Note there is a time of exposure that has been suppressed in this discussion.) For convenience, we note the form is:

$$t(I) \equiv f(I_0) + \alpha_1(I_1(p^*))^2 + I_1^*(p)^2 \quad . \quad (3.3.13)$$

We have generated the hologram and are now ready to discuss the evolution of the object beam in front of the prefilter.

For the hologram generated to demonstrate the method, we choose an approximately uniform irradiance pattern with zero phase difference between the apertures (other patterns may be used). Since our purpose requires the cross-correlation structure give equal weight to each aperture, we use the plane wave with uniform irradiance.

To generate the desired beam profile with appropriate mathematical terms, we model the attenuator and the beam expander for the object beam.

First, assume the beam profile at the beam splitter for the object beam is:

$$U(x,y;0) \quad . \quad (3.3.14)$$

If we accept that the attenuator is at z_4 , and we use eq. (A.1) to deduce the profile at z_4 , then the profile is:

$$U_A(x_4, y_4; z_4) \equiv \frac{e^{i\phi_4} B_4}{i\lambda z_4} \int dx dy U(x,y;0) h(x_4-x, y_4-y; z_4) \quad . \quad (3.3.15)$$

Here the phase shift is $\phi_4 = kz_4$, and the effects of the attenuator are contained in coefficient B_4 . Technically, the attenuator also can produce beam distortion. For this discussion, we presume there is none.

Now we assume the position, z_4 , is located at one focal length in front of the first lens of the beam expander. This implies that a beam profile at the focal plane after the object beam exits the first lens is the Fourier transform of eq. (3.3.15) as prescribed in eqs. (A.4) and (A.5). To make this beam profile as close to a known profile as possible, we insert a pinhole filter in this plane, namely at $z_5 = z_4 + 2f_4$.

The f_4 is the equivalent focal length of the first lens. If the first lens has a small focal length and we choose arbitrarily a circular filter with a diameter equal to ten wavelengths, then when $w = d_2$ or $d_1 = f_5$ in eq. (A.3), the exiting beam profile from the second lens system at the prefilter becomes:

$$U_p(x_6, y_6; z_6) = \frac{1}{i\lambda f_5} \int dx_5 dy_5 U(x_5, y_5; z_5) h[x_5, y_5; s_5] \\ * \exp \left[\frac{ik}{f_5} (x_5 x_6 + y_5 y_6) \right] * e^{i\phi_6} \quad . \quad (3.3.16)$$

The phase shift $\phi_6 \equiv k(f_5 + d_2 + (n_5 - 1)t_5)$; the radius of curvatures are $s_5 = f_5/(1 - d_2/f_5)$; the focal length of the second lens is f_5 ; the index of refraction is n_5 ; and the equivalent thickness of the lens is t_5 . The distance between the second lens and the prefilter is d_2 .

Applying the conditions that the filter at plane x_5, y_5 has all x_5, y_5 within the 5λ and that the distance $d_2 \equiv mf_5$, thus $s_5 = f_5/(1-m)$, we find the worst phase error in $h[x_5, y_5; s_5]$ is:

$$\frac{k a_5^2}{2 s_5} = \frac{25\lambda\pi(1-m)}{f_5} . \quad (3.3.17)$$

If $f_5 = 30$ mm, $\lambda = 1$ μ m and m is less than 11, then this phase error is less than

$$\frac{75 * 10^{-6}}{30 * 10^{-3}} * 10 \text{ or } 0.02 \text{ radians.}$$

In this case, we set $h = 1$ and assume that the beam profile at prefilter is a Fourier transform of the pattern at the pinhole. If we now assume that the latter pattern is uniform and constant over the aperture, then the prefilter pattern is an Airy disk pattern with a plane wave front. The amplitude variation is deduced from eq. (C.5) and is

$$A \equiv A_o \left(1 - \frac{\pi^2}{8} \left(\frac{a_5^2 r^2}{(d_2 \lambda)^2} \right) \right) \quad (3.3.18)$$

near the center of the beam. Given $a_5 = 5\lambda$ and $d_2 = 10 f_5$, this amplitude becomes

$$A = A_o \left[1 - \frac{10}{8} \left(\frac{25}{100} \left(\frac{r^2}{f_5} \right)^2 \right) \right].$$

If we require less than 1% amplitude error, then

$$\left(\frac{r}{f_5} \right)^2 < .04 \text{ or } r \leq 6 \text{ mm for the } f_5 = 30 \text{ mm.}$$

We now see that the sampling of the object beam in the prefilter plane in a circle of 6 mm radius will show less than 1% error in the uniformity of amplitude and less than 2% error for the irradiance.

Concluding this subsection, we note three points. First, by appropriate choice of beam expander, pinhole, and distance between expander and prefilter, we can make arbitrarily accurate plane waves over selected cross sections with limited ranges of irradiance for the object beam. Second, by similar use of a beam expander and its filter, we make the reference beam have a uniform irradiance and a spherical wave front over a controlled cross section of the film. This means we can construct a high accuracy cross-correlation pattern in the hologram. Third, there is a technical limit to this procedure. Thus, the larger the desired sampling region is, the harder it is to get the precision hologram. However, the computer-generated structures alluded to in subsections 5.2 or 5.4 allow us to generate an appropriate substitute for the hologram constructed by laser beams.

3.4 Detailed Instructions for Assembling and Aligning the Apparatus in the Construction of the Desired Hologram

In our prototype apparatus we used an HeNe laser with a 7 mW output at 0.6328 μ m and with a linear polarization. This laser was chosen because we wanted to have sufficient power for the cross-correlation process and because we wanted to do this evaluation of concepts at a visible laser wavelength.

The choice of a fixed electric-field direction eliminates the need to consider polarization effects. The electric field remains fixed throughout the apparatus if the field points only along either the parallel or the perpendicular direction to a plane defined by the various laser beams within the apparatus. Our apparatus used the perpendicular direction for the electric field.

We used a large metal table with a flat surface to hold various optical components and to fix their relative positions against vibrations caused by moving, rotating, and vibrating equipment; moving people; minor earth tremors; etc. In this prototype, the metal table weighs about 250 kg and has a machined flat surface 0.9 by 1.4 m. Because the room is at ground level, this table has no special shock mounting. All the components shown in figure 1 are on the surface of the table except the laser. It was mounted on a secondary table because there was insufficient space on the main table. It would be better to mount the laser on the main table; however, as long as the reference and object beams are formed and recombined on this table and the time scale for generating the hologram is short enough, the vibrations do not affect significantly the quality of the hologram. This fact is proven by the quality of the resulting cross correlations.

Figure 1 shows numerous plane mirrors used to deflect both beams around the table. These mirrors keep the reference and object beams confined within the table boundaries and allow the beams to cross at the liquid gate.

During construction of a hologram, we split the laser beam into a reference and object beam and kept their electric fields perpendicular to the surface of the table. The beam splitter causes about 50% of the laser power to go into each beam. This beam splitter uses a dielectric film to create the two beams. We need comparable power in each beam to get a proper hologram.

In this prototype apparatus there are no antireflection coatings on the various optical components. The many reflected beams from the various optical surfaces have significant power and can cause serious measurement problems. One way to avoid these beams is to use reflection optics. Unfortunately, this step is not a cure all; there are measurement problems in both types of optics because each interaction of a laser beam with an optical component can change its profile in an unknown way. For example, a plane mirror is not truly plane; therefore, the wavefront is distorted by the irregularities of the mirror. Careful scaling and choice of optical components can reduce these problems to desired tolerances. The other way to avoid these beams is to use antireflection coatings which make the optics expensive.

Continuing to follow the primary laser beam, we now follow the evolution of the reference beam from the splitter to the liquid gate. The reference beam is about 1 mm in diameter at the half irradiance points after the beam exits from the splitter. To avoid resolution problems in the photographic emulsions at the hologram plane and to generate an almost plane wave at this plane for this reference beam, we insert a pair of lenses and a pinhole to make a beam expander.

The initial lens in the beam expander through which the reference beam passes is a "20x" (8 mm focal length) microscope objective. Bubbles and other imperfections in this lens create interference rings in a coherent beam. Precision work requires that these rings be eliminated. Most of the power in the reference beam is concentrated at a plane near the focal plane of the microscope objective. When we passed the beam through an 18 μm pinhole located in this plane, the prototype apparatus removed the rings and also many non- TEM_{00} modes present in the original laser beam and thereby left mainly a TEM_{00} mode (see reference [18] for discussion of laser modes). The filter process is not perfect; consequently, the recorded reference beam introduces error in the hologram. Fortunately, the sampling process at the prefilter plane makes it unnecessary for the structure of the beam used to make the hologram a pure TEM_{00} mode. Subsection 3.3 assumes a different beam instead of the TEM_{00} mode. The exact form of the beam depends on the various components in an apparatus.

Finally, we complete the beam expander using a lens with a focal length of 72 mm and a diameter of 60 mm which changes the curvature of the reference beam so that it exits from the beam expander with a half-power diameter of about 9 mm and shows a slowly diverging wavefront.

At the liquid gate, the reference beam is about 25 mm in diameter at the half-irradiance points. The optical path distance between the beam expander and the liquid gate

is about 2.5 m. This distance insures that at the liquid gate the depth of field, as defined in appendix B, for the reference beam is substantial; therefore, there is no sensitive adjustment necessary in the beam expander or in the mirrors except to make sure the TEM₀₀ mode is present and both the reference and object beams overlap at the film plane. The choice of lenses in the beam expander was determined by readily available optics which had minimal defects.

The preceding discussion defines the reference beam. We now turn to the evolution of the object beam.

At first we need to consider what happens to the unwanted reflected beams from the many optical components in the object beam because they could induce measurement problems and be a safety hazard. Briefly, each spurious beam should be stopped and absorbed. In the interest of brevity, this paper does not describe where each of these beams is located. If a reader wishes to construct some version of this apparatus, he should test his apparatus with visible laser beams to confirm that the spurious beams cannot cause problems or hazards.

Continuing with the object beam out of the beam splitter, we see in figure 1 that this beam goes through an attenuator. This unit contains a half-wave plate and a polarizer. The former is inclined at the brewster angle to eliminate or reduce, substantially, interference between the various transmitted beams. This plate rotates the polarization plane of the object beam by a controlled amount which depends on the orientation of the plate [19]. The polarizer is oriented to pass radiation (1000 to 1) with the electric field perpendicular to the metal table. We use the attenuator to adjust the peak power density of the object beam to be one fourth the irradiance of the reference beam at the film plane. The literature suggests that this ratio of irradiance makes the cross-correlation process efficient and minimizes potential distortions in the hologram [20]. Because this prototype only demonstrates and checks key elements in the cross-correlation process, it is premature to design for optimum operation; therefore, we accepted suggestions in the literature and based many decisions on incomplete information. The section discussing problems and conclusions suggests how this prototype may be improved and what should be considered to make an optimum design.

Continuing with the object beam, we employ a beam expander like the one used for the reference beam. In this prototype apparatus, the translation mounts in this expander do not allow as precise adjustment and mechanical stability as in the beam expander for the reference beam. As a consequence, the pinhole here is 25 μm in diameter rather than 18 μm in diameter. Again, subsection 3.3 considers a different strategy for the filter in the beam expander. For this prototype, the discussion in this subsection is sufficient. For more precise details, consider the issues discussed in subsection 3.3.

The best translation equipment used within this apparatus has 10 μm resolution. An improved version of this apparatus should use translation equipment which can be adjusted and remain stable to better than 1 μm ; otherwise, the apparatus will not remain calibrated for significant periods.

During the initial construction phase, it is necessary to adjust the optical path lengths of both the reference and object beams between the beam splitter and liquid gate so that their lengths are equal to ± 1 cm accuracy. One convenient method having this accuracy for a three-meter path length uses a Ronchi ruling in front of the beam splitter, temporarily removes the beam expanders, and observes the diffraction pattern in the film plane. When the spatial separation between the two first-order diffraction maxima from each beam are equal then their path lengths are equal. After the paths are equalized, the beam expanders are reinserted and the ruling is removed. This adjustment is not critical; it is only necessary to be within the coherence length of the two beams. The next step verifies the adequacy of the adjustments.

Also during the initial construction phase of this apparatus, we confirmed that the metal table is stable. One method uses a magnified image of the interference pattern between the object and the reference beam at the film plane. One way to obtain a magnified image is to use a lens behind the liquid gate near the cross-correlation position (fig. 2) to form an

image of the film plane on a distant, painted metal surface of the wall of the laboratory. An image of the interference pattern of the two beams can be seen if the apparatus is stable. The metal surface creates a flat image plane; a paper surface will not work. Because the spatial frequency of the pattern is high, a magnifying lens is used to see the interference pattern. If no pattern is visible, then the apparatus has insufficient stability for making holograms.

In our prototype apparatus, we had a very quiet laboratory on the ground floor and used a very heavy table. Therefore, the pattern was sharp even though the path length between beam splitter and film plane was about 3 meters.

Continuing the placement of optics into the object beam, we note the following conditions on the liquid gate:

(1) The angle between the reference and object beams should be near 5° to allow maximum resolution [21,22] in the photographic plate and to permit a reasonable separation between the cross correlation [11, page 194] and image beam leaving from the film (see fig. 2). This angle is approximate and not critical.

(2) It is desirable to make the normal to the film plane bisect the angle between the two-beams. This adjustment maximizes the depth of field for the resulting hologram and permits its efficient use as either a cross correlation or an image beam generator. Again this adjustment is not critical.

(3) The liquid gate is filled with water^{*} during all adjustments. (To prevent algae from growing in the water, add 10-20 ppm of CuSO_4 .) IR and UV wavelengths may require different liquid gates and liquids.

The placement of the optical components for the object beam is almost complete. We have two remaining components, the Fourier transform lens and the prefilter. Both units require critical adjustment and clear understanding of their functions, which requires a detailed study of Fourier optics [11,13,14,15,16]. (Appendices A and D of this paper present selected aspects of Fourier optics.)

In this prototype apparatus, we use a single element convex lens with a focal length of 305 mm and a diameter of 89 mm to perform the Fourier transform process. Because the transverse dimensions of the Fourier transform are not large enough for efficient use of the film, we use a second lens with a focal length of 52 mm and a diameter of 35 mm to magnify the Fourier transform and to place that image at the film plane. To be efficient, we make the spatial frequencies for the Fourier transform of the prefilter plane several orders of magnitude lower than the cutoff of the film. This process will keep the potential accuracy for a phase measurement as high as possible. Detailed analysis is necessary to establish the optimum level of magnification. That has not been done here. To align this Fourier transform unit, the following steps are taken:

(1) First, select the location of the prefilter plane, then locate the Fourier transform plane two focal lengths (610 mm) further along the object beam using a variable aperture at the transform plane. This aperture, which must be capable of ranging from 1 mm to 10 mm in diameter, will be used to fix precisely the Fourier plane at the film plane.

(2) To center the variable aperture, remove the beam expander for the object beam and stop the aperture at the Fourier transform plane to 1 mm in diameter and center on the unexpanded laser beam. Note where the center of this beam strikes the film plane and adjust the appropriate mirror to make this position also the center of the expanded reference beam.

(3) Replace the beam expander into the object beam and adjust the expander so that the beam that passes through the aperture at the Fourier transform plane centers at the previous position on the film plane.

(4) Insert the magnifying lens behind the Fourier transform plane to construct as sharp an image as possible of the aperture on the film plane. To make the spatial

*NOTE: A choice of convenience. There may be better liquids.

adjustment of this lens as precise as possible, open up the aperture to the full 10 mm diameter which decreases the depth of field at the film plane (see appendix D). (This lens is not shown in figures 1 or 2).

This report does not discuss the technique for placement of the various translation and rotation mounts because these details are dependent on the type of mount. It is more convenient if a mount adjusts independently of other mounts. Assembly of an optical component requires careful thought about the form of the necessary translations and rotations, which simplify adjustment of the beam profile system. Ideally, the most critical adjustment should be independent of the other adjustments.

(5) Stop down the aperture to 1 mm in diameter at the Fourier plane and insert the Fourier transform lens. Adjust this lens until the spot is centered in the aperture and is as sharp as possible on the film plane. There is substantial depth of field for the adjustment of the object beam along its axis. Adjust the mount so that the translation along the optical axis keeps the spot centered in the aperture over the entire range of adjustments of that mount.

(6) The final adjustment is the accurate positioning of the Fourier transform lens along the optical axis. Temporarily place a mirror in the prefilter mount to reflect the object beam back into the beam expander. Adjust this prefilter so that all adjustments keep the optical axis of the reflected beam parallel to the optical axis of the incident beam. This adjustment can be made accurately by noticing the lack of motion by the reflected spot at an aperture just in front of the laser's exit port. (Here the 25 μm filter is not present in the beam expander.)

When the prefilter unit is adjusted properly, we can make a precise transverse motion of a filter made of two 100 μm pinholes separated by 1 mm mounted in the prefilter unit. By temporarily blocking the reference beam and looking at the image of the film plane for the object beam as formed on the wall of the laboratory, we see an Airy disk superimposed on a series of parallel dark and bright interference lines. When the prefilter unit is moved transversely to the optical axis, the interference fringes will shrink or stretch unless the Fourier transform plane is coincident to the film plane. This condition can be attained by alternately adjusting the position of the Fourier transform lens along the optical axis and testing whether or not the interference pattern remains constant.

Following the above procedures guarantees an accurately placed Fourier transform unit. The following sequence describes how to place the prefilter unit.

(1) Replace the two-pinhole filter with one-pinhole filter. Make sure both filters lie in the same transverse plane. Add a mirror behind the Fourier transform lens to reflect the laser beam back to the prefilter plane. Adjust the position of the pinhole along the optical axis so the speckles reflected from the prefilter plane are as large as possible [23].

(2) Remove the mirror and replace the pinhole filter with the prefilter pattern shown in figure 3, being very careful to locate the new prefilter in the same plane as the previous filters. The prefilter unit is now adjusted properly along the optical axis.

(3) The transverse positions are determined by the part of the incident object beam to be recorded on the hologram. In the prototype apparatus, the prefilter samples the center of the object beam, where the beam is more nearly a pure TEM_{00} mode than at the edges.

(4) Adjust the beam expander to provide a flat wavefront at the prefilter plane. For example, use a mirror placed just in front of the prefilter plane to generate a reflected beam and adjust the beam expander to get the largest speckle reflected from the pinhole within the beam expander.

This discussion completes the adjustments of the object and reference beams. We complete construction of the hologram. Using a silicon power meter, we measured 3.6 μW at the film plane for the reference beam and 0.8 μW for the object beam. These values imply an approximate peak irradiance of 400 $\mu\text{W}/\text{cm}^2$. To get efficient phase holograms requires an

optical density of 2 which corresponds to a total energy density of $80 \mu\text{J}/\text{cm}^2$. We therefore used a shutter speed of 0.2 s.

3.5 Results from Construction of the Hologram

The original intent in this evaluation was to generate a phase transmission hologram because it is more efficient for cross-correlation measurements [11, page 148]; therefore, all holograms produced by this apparatus used the 0.2 s exposure. Technical problems developed in making adequate phase holograms. Since the prime goal of the prototype was to demonstrate the concepts of correlation process, the final hologram was not bleached. The cross correlations shown in subsection 4.6 are from the resulting amplitude hologram. The procedures for developing the plate followed the instructions in references [21,24]. The entire development process left the plate in place. This is the prime reason for using a liquid gate.

After we constructed the hologram and understood the subsequent production of cross correlations, we concluded that the liquid gate is unnecessary and even undesirable. It is necessary only to replace the film plate within 0.1 mm, and to steer the object beam with precision so that the resulting hologram and the object beam used in the cross-correlation process are properly matched. In addition, all potential phase error effects in the hologram used without a liquid gate, such as shrinkage, can be minimized by using an appropriate calibration procedure provided there are no significant humidity effects. In this case, the emulsion must be shielded and sealed by a glass cover.

Information about photographic chemical development is not included because we did not determine the best approach. The reader must get those details from the literature. When it becomes important to increase the accuracy of the beam profile measuring apparatus, then extensive evaluation for appropriate holograms becomes useful. At present, the best choice is an educated guess.

4. THE CROSS-CORRELATION APPARATUS

This section has three goals similar to those in section 3. First, we describe the cross-correlation part of the beam profile apparatus built at NBS in 1977. Second, we construct the two mathematical models simulating this apparatus. Third, because I want to accelerate transfer of these concepts, I discuss actual equipment.

4.1 What this Section Presents

There are five subsections in this section. First, subsection 4.2 defines the structure of the prototype apparatus that generates cross correlations between the illuminated nine-hole prefilter and its hologram. Second, subsection 4.3 uses the unit to fix the mathematics for simulating the cross-correlation process. Third, subsection 4.4 specifies assembly and alignment of the prototype apparatus for optimum correlation. Fourth, subsection 4.5 describes how to calibrate this apparatus. Fifth, to aid intuitive understanding of cross correlation, subsection 4.6 shows both TV pictures and conceptual sketches of observed correlations. The conclusions drawn from this section are discussed in section 6.

4.2 A Discussion of the Prototype Apparatus Used to Generate the Cross-Correlation Pattern

Presuming the reader is now aware of holographic aspects of this apparatus, we define the cross-correlation features using block diagrams in figure 2 to identify each basic component. This subsection explains the function and action of each component. Each component is selected by the order in which the laser beam goes through.

We direct the test or calibration laser beam through the prefilter. In our test apparatus, we use this same beam to generate the hologram, except that we remove the beam splitter. In a beam profile measuring apparatus, it is not necessary to put a beam expander in front of the prefilter. We ignore that operation in the discussion of the prototype unit. For this discussion we presume the input beam has at least a 10 mm diameter.

The illuminated apertures in the prefilter provide the required radiation sources for the Fourier transform lens system. To make the cross correlation work, we use exactly the same setup as we used to generate the hologram. Thus, the position of the apparatus from the prefilter through the hologram is unchanged. We add the Fourier transform lens behind the hologram to form images in the cross-correlation plane from the beams generated by radiation passing through the prefilter-hologram sequence.

To make these images in this plane easy to see and understand, a magnifying lens is used in conjunction with a TV camera and video receiver to show the different irradiance patterns in that plane on a CRT.

4.3 The Mathematical Model Used to Understand the Cross-Correlation Pattern

In subsection 3.3 we generated the first level of mathematics for the prototype system. Here we proceed to the final levels.

In subsection 4.3.1 we derive the expressions that show the expected spot pattern at the cross-correlation plane. To show that the resulting cross correlation can be made insensitive to the details of the spot shape requires numerous assumptions and approximations which are shown here.

A convenient model for operational use of the prototype is the prime goal of subsection 4.3.2 and is therefore generated here. In addition, this subsection shows the analysis of a simple beam profile measuring unit with two apertures at the prefilter. This discussion covers the entire cycle of measurements--namely the calibration of the unit and also the use of the unit for real time beam profile measurements.

4.3.1 The Model that Contains the Spatial Details of the Irradiance

Here we want the form of the test beam at the hologram. The test or calibration beam exiting from the prefilter is represented in eq. (3.3.5). Only the b_ℓ , c_ℓ , and d_ℓ change to

new values, say β_ℓ , ζ_ℓ , and η_ℓ respectively. Following the arguments in subsection 3.3, after eq. (3.3.5) through eq. (3.3.9), we find that the test beam can be symbolized as:

$$U_t(x_8, y_8; z_8) = \frac{B_8 e^{i\phi_8}}{M_8} h(x_8, y_8; s_8) U_{t_1}\left(-\frac{x_8}{M_8}, -\frac{y_8}{M_8}; z_7\right), \quad (4.3.1)$$

where

$$U_{t_1}(x_7, y_7; z_7) = \frac{a^2 A_o e^{i\phi_7}}{i\lambda f_2} B_7 \int_{-\ell}^{\ell} \text{sinc}\left[\left(u_7 + \frac{\beta_\ell}{2\pi}\right)a\right] \text{sinc}\left[\left(v_7 + \frac{\zeta_\ell}{2\pi}\right)a\right] \\ * \exp\left\{i\left[\eta_\ell 2\pi(u_7 g_\ell + v_7 h_\ell)\right]\right\}. \quad (4.3.2)$$

This U_t beam can be restructured according to the discussion near eqs. (3.3.10) and (3.3.11) as:

$$U_{T_2} = p U_t, \quad (4.3.3)$$

to reflect the fact that the test beam is at an angle, θ , to the hologram's normal.

Next, using the transmission in eq. (3.3.13), we denote the exit beams from the hologram after illumination by the test beam U_t as:

$$U^{(ex)}(x_8, y_8; z_8) = p U_t f(I_o) + \alpha_1 p^* I_1^* U_t + \alpha_1 (p)^3 I_1^* U_1. \quad (4.3.4)$$

As indicated by the presence of p , the first term in this expression shows the beam propagates along the direction of the original test beam. In contrast, the second term shows a beam propagating coaxially to the original reference beam. The final term shows that this beam deflects from the mean normal of the test beam by an angle 2θ . The first and last beams are ignored in the cross-correlation process; therefore, we drop those beams and reduce the eq. (4.3.4) to:

$$U_c(x_8, y_8; z_8) = \alpha_1 R_H U_H^* U_t. \quad (4.3.5)$$

We have identified the proper beam. Also we have absorbed the p^* term into R_H and recovered the form shown in eq. (3.3.4).

To complete the cross-correlation process, we use the lens in figure 2 to Fourier transform U_c into:

$$U_9(x_9, y_9; z_9) = \frac{e^{i\phi_9}}{i\lambda f_9} \int dx_8 dy_8 U_c(x_8, y_8) \\ * \exp\left[i2\pi(u_9 x_8 + v_9 y_8)\right]. \quad (4.3.6)$$

This expression can be rewritten with extraneous details suppressed; thus U_0 is:

$$U_9 = A \sum_{\ell} \sum_j H_{\ell,j}[x_9, y_9] e^{i(\eta_{\ell} - d_j^*)}, \quad (4.3.7)$$

where

$$\begin{aligned} H_{\ell,j}[x_9, y_9] \equiv & \int dx_8 dy_8 \operatorname{sinc} \left[a \left(-\frac{x_8}{\lambda f_7 M_8} + \frac{\beta_{\ell}}{2\pi} \right) \right] \operatorname{sinc} \left[a \left(-\frac{x_8}{\lambda f_7 M_8} + \frac{b_j^*}{2\pi} \right) \right] \\ & * \operatorname{sinc} \left[a \left(-\frac{y_8}{\lambda f_7 M_8} + \frac{\zeta_{\ell}}{2\pi} \right) \right] \operatorname{sinc} \left[a \left(-\frac{y_8}{\lambda f_7 M_8} + \frac{c_j^*}{2\pi} \right) \right] \alpha_1 R_H(x_8, y_8) \\ & * \exp \left\{ -2\pi i \left[(g_{\ell} g_j) \left(\frac{x_8}{M_8 \lambda f_7} \right) + (h_{\ell} h_j) \left(-\frac{y_8}{M_8 \lambda f_7} \right) + u_9 x_8 + v_9 y_8 \right] \right\}, \end{aligned} \quad (4.3.8)$$

and where

$$A \equiv \frac{a^4 A_0^2 B_7^* B_8^* B_8^* e^{i\phi_9}}{M_8^2 (\lambda f_7)^2 i \lambda f_9}. \quad (4.3.9)$$

Using the discussion in subsection 3.3 near eq. (3.3.9), we assume β_{ℓ} , b_{ℓ} , ζ_{ℓ} , c_{ℓ} can all be neglected. In this case, we can define $s_8 \equiv a/\lambda f_7 M_8$,

$$H(x_8, y_8) \equiv \alpha_1 R_H \operatorname{sinc}^2[x_8 s_8] \operatorname{sinc}^2[y_8 s_8] \quad (4.3.10)$$

and its Fourier transform as:

$$K(x_9, y_9) = \int dx_8 dy_8 H(x_8, y_8) \exp \left\{ -2\pi i (u_9 x_8 + v_9 y_8) \right\}. \quad (4.3.11)$$

We now rewrite $H_{\ell,j}$ as:

$$H_{\ell,j} = W[x_9 - s_9(\ell_1 - j_1), y_9 - s_9(\ell_2 - j_2)], \quad (4.3.12)$$

where we have defined $s_9 = f_9 b / (f_7 M_8)$, and made explicit the individual components of the vectors, $\vec{\ell}$ and \vec{j} . With appropriate choice of a Kronecker delta function we simulate the positions of the spots in the cross-correlation plane (see figure 5). We rewrite the electric field pattern as:

$$\begin{aligned} U_9(x_9, y_9) &= A \sum_{\ell, j} e^{i(\eta_{\ell} - d_j^*)} W[x_9 - s_9(\ell_1 - j_1), y_9 - s_9(\ell_2 - j_2)] \\ & * \sum_{\vec{k}} \delta_{\ell_1}^{k_1} \delta_{\ell_2 - j_2}^{k_2} \\ &= A \sum_{\vec{k}} W[\vec{x} - s_9 \vec{k}] \sum_{\ell, j} \delta_{\vec{\ell} - \vec{j}}^{\vec{k}} e^{i(\eta_{\ell} - d_j^*)}. \end{aligned} \quad (4.3.13)$$

The vectors are defined as $\vec{x} \equiv (x_9, y_9)$; $\vec{k} = (k_1, k_2)$; $\vec{\ell} = (\ell_1, \ell_2)$; and $\vec{j} = (j_1, j_2)$. We define the detected electric field at the k spot as:

$$D_k(\vec{x} - \vec{k} s_9) = A B_k W(\vec{x} - \vec{k} s_9) \quad (4.3.14)$$

where the B_k is defined in component form as:

$$B_k \equiv \sum_{\ell_1, j_1} \sum_{\ell_2, j_2} \delta_{\ell_1 - j_1}^{k_1} \delta_{\ell_2 - j_2}^{k_2} e^{i(\eta_{\ell_1, \ell_2} - d_{j_1, j_2}^*)} \quad (4.3.15)$$

The power captured by the detector is:

$$P_k = G_k B_k B_k^* \quad (4.3.16)$$

where

$$G_k \equiv \int dx_9 dy_9 A A^* W W^* \quad (\text{Detector})$$

Note that G_k depends on a^8 [see eq. (4.3.9)]; therefore, an increase of 10% in a implies an increase of approximately 100% in power received. Further, the detectors have a conversion term, G_{2k} , that gives the information in volts. We simulate this fact by:

$$V_k = G_{2k} P_k, \quad (4.3.17)$$

where we ignore the problems of finite response time.

This completes the generalized discussion of subsection 4.3.1. Subsection 4.6 shows many possible patterns that reflect the approximations pertinent to eq. (4.3.17).

4.3.2 The Simplified Model that Ignores Details in the Irradiance--the Calibrated Model

We restructure eq. (4.3.15) through (4.3.17) to a more convenient form for the calibration model. Let:

$$A_{\ell_1, \ell_2} \equiv \sqrt{G_1} e^{-d_{2\ell_1, \ell_2}}, \quad (4.3.18)$$

$$\theta_{\ell_1, \ell_2} \equiv d_{1\ell_1, \ell_2} \quad (4.3.19)$$

$$E_{\ell_1, \ell_2} \equiv e^{-\eta_{2\ell_1, \ell_2}}, \quad \text{and} \quad (4.3.20)$$

$$\phi_{\ell_1, \ell_2} \equiv \eta_{1\ell_1, \ell_2}. \quad (4.3.21)$$

The voltage at the kth detector is:

$$V_k = G_{2k} E_k E_k^* , \quad (4.3.22)$$

where the effective electric field on the kth detector at the cross-correlation plane is:

$$\epsilon_k = \sum_{\ell_1, \ell_2} A_{\ell_1-k_1, \ell_2-k_2} E_{\ell_1, \ell_2} e^{i[\phi_{\ell_1, \ell_2} - \theta_{\ell_1-k_1, \ell_2-k_2}]} . \quad (4.3.23)$$

Here $A_{\ell_1, \ell_2} = 0$ when either ℓ_1 or ℓ_2 exceed the range of apertures in the prefilter.

Subsection 4.6 shows that this happens for the prototype unit when either $|\ell_1| \geq 2$ or $|\ell_2| \geq 2$. Incidentally, the range of the cross-correlation index has:

$$|k_1| \leq 2 \quad \text{and} \quad |k_2| \leq 2$$

for the prototype unit.

To illustrate this calibration model, we assume that instead of a three-by-three pattern, we have only two apertures in the prefilter. Therefore, we drop the ℓ_2, k_2 label and let $\ell \equiv \ell_1$ and $k \equiv k_1$. To obtain a correct count in the notation, we set $\ell = \pm 1$ and $k = \pm 2, 0$. The prefilter has the pattern:

$$\ell = +1 \quad -1 \quad .$$

The cross-correlation pattern is:

$$k = -2 \quad 0 \quad +2 \quad .$$

In this case, the electric field at the cross correlation has

$$\begin{aligned} \epsilon_{+2} &= A_1 E_{-1} e^{i(\phi_1 - \theta_{-1})} ; \quad k = +2 ; \\ \epsilon_0 &= A_1 E_1 e^{i(\phi_1 - \theta_1)} + A_{-1} E_{-1} e^{i(\phi_{-1} - \theta_{-1})} ; \quad k = 0 ; \end{aligned}$$

and

$$\epsilon_{-2} = A_{-1} E_1 e^{i(\phi_{-1} - \theta_1)} ; \quad k = -2 . \quad (4.3.24)$$

The output voltage signal for each detector is:

$$\begin{aligned}
 V_2 &= G_{2,2} (A_1 E_{-1})^2 ; \quad k = +2 ; \\
 V_{-2} &= G_{2,-2} (A_{-1} E_1)^2 ; \quad k = -2 ; \text{ and} \\
 V_0 &= G_{2,0} \left[\begin{aligned} &(A_1 E_1)^2 + (A_{-1} E_{-1})^2 \\ &+ 2[A_1 A_{-1} E_1 E_{-1}] \cos Q \end{aligned} \right] ; \quad k = 0 ;
 \end{aligned} \tag{4.3.25}$$

where the phase term is defined as:

$$Q \equiv \phi_1 - \phi_{-1} + \theta_{-1} - \theta_1 . \tag{4.3.26}$$

To make the calibration process as simple as possible, we define:

$$\begin{aligned}
 S_1 &\equiv (E_{-1})^2, \quad F_1 \equiv (A_1)^2 G_{2,2}, \quad \Gamma_1 \equiv G_{2,0}/G_{2,2}, \\
 S_2 &\equiv (E_1)^2, \quad F_2 \equiv (A_{-1})^2 G_{2,-2}, \quad \Gamma_2 \equiv G_{2,0}/G_{2,-2}, \\
 \Delta &\equiv \theta_1 - \theta_{-1}, \text{ and } \delta \equiv \phi_1 - \phi_{-1}.
 \end{aligned} \tag{4.3.27}$$

With this notation, the voltage equations become:

$$\begin{aligned}
 V_2 &= F_1 S_1, \\
 V_{-2} &= F_2 S_2, \quad \text{and} \\
 V_0 &= F_1 S_2 \Gamma_1 + F_2 S_1 \Gamma_2 + 2 \cos(\delta - \theta) (V_2 V_{-2} \Gamma_1 \Gamma_2)^{1/2}.
 \end{aligned} \tag{4.3.28}$$

The S_1 and S_2 are the total power out of each aperture at the prefilter. The above equations assume that the three detectors respond linearly to the received power in the cross-correlation plane.

To perform the calibration process, we use a uniform irradiance beam at the prefilter with a plane wave front. We must vary the relative phase between the two apertures. See subsection 4.5 for a discussion of how this can be done. Also, we must control the total power illuminating the prefilter. We measure the power directly at the prefilter with a calibrated power meter. The calibration process has three steps.

1. Block the second aperture and measure the exit power of the first aperture as well as the response of the three detectors at the cross-correlation plane. The method requires either a substitution technique or a beam splitter with monitor in front of the prefilter and beam steering unit. Results expected are a test of linearity, dynamic range allowed by linearity, and the deduction of F , and $\Gamma_2 F_2$.

2. Block the first aperture and unblock the second. Repeat the above sequence. Results expected are a test of linearity, dynamic range allowed by linearity, and the deduction of F_2 and $F_1\Gamma_1$.
3. Unblock both apertures and set the power at midrange first. Then swing the phase front over a range of phase values. The results here are the allowed dynamic range of θ in calibration model, and the deduction of δ . Repeat this process for the lowest and largest values of input power. Again obtain the dynamic range of θ in the calibration model and also deduce the δ .

Given F_1 , F_2 , Γ_1 , Γ_2 , and δ , we now can measure unknown beams. The three detectors give V_1 , V_2 , and V_o as a function of time. From this data we deduce the power at each aperture, S_1 and S_2 , as well as the relative phase θ as a function of time. The relationships are:

$$\begin{aligned}
 S_1 &= V_1/F_1, \\
 S_2 &= V_2/F_2, \quad \text{and} \\
 \cos Q &= \frac{V_o - V_2 F_1 \Gamma_1 / F_2 - V_1 F_2 \Gamma_2 / F_1}{2[V_1 V_2 \Gamma_1 \Gamma_2]^{1/2}}; \tag{4.3.29}
 \end{aligned}$$

where the positive number Q relates to the relative phase by a many-to-one formula. The sign of Q and the integer n are both unknown and, hence, arbitrary. The formula is:

$$\theta = \delta \pm Q + 2n\pi \tag{4.3.30}$$

If we scale the three detectors so that $F = F_1 = F_2$ and $\Gamma_1 = \Gamma_2 = 1$, then we have a simpler form for the three expressions; namely, $S_1 = V_1/F$, $S_2 = V_2/F$, and $\cos Q = (V_o - V_2 - V_1)/2(V_1 V_2)^{1/2}$. We see that phase measurements are most accurate when V_1 is near V_2 .

4.4 Instructions for Assembling and Aligning this Apparatus to Generate the Cross-Correlation Patterns

In this subsection, we presume that an appropriate hologram has been constructed by the method discussed in subsection 3.4. We now follow the block diagram structure of figure 2. All units in the object beam behind the beam splitter are the same as in figure 1. On the other hand, the optics and mirrors that manipulate the reference beam can be completely removed if new holograms are not needed. In this prototype apparatus, we simply remove the beam splitter to allow the full 7 mW of laser power to strike the prefilter. The same prefilter, discussed earlier and shown in figure 3, acts on this calibration beam.

To complete the cross-correlation process, we add two lenses in the cross-correlation plane. Unlike the process for constructing a hologram, the placement of lenses for the cross correlation behind the hologram is not critical. We used a plano convex lens, which has a 120 mm focal length and a 100 mm diameter, one focal length of optical path length behind the hologram. The water and glass shorten the apparent distance of travel of the laser beam, due to the larger indices of refraction. This scale change must be approximately accounted for.

A comment on the placement of the simple convex lenses in the prototype apparatus is in order. Always place the (most flat) surface (longest radius of curvature) of a lens facing the wave with the least curvature and make the optical axis go through the center of the lens. This procedure will minimize the various aberrations of the lens both in the production of a hologram and in the cross-correlation process. Place the side of the microscope objectives without the screw thread toward the wavefront with the greatest curvature--i.e., the apparent point source of focus. This placement minimizes aberrations of these lenses.

We complete construction of the cross-correlation unit by placing a 20x microscope objective with x, y, and z translation mounts so that the lens magnifies and forms a real image of the cross-correlation plane seen behind the 120 mm lens on the surface of the detection unit. In this prototype case, a vidicon-TV detector unit was used because it was the only system conveniently available within NBS, Boulder, that could detect an array of spots with laser power less than 10 nW. Subsection 4.6 of this paper shows examples of the various cross correlations and illustrates the consequences of the cross-correlation process.

The final discussion in this subsection describes alignment of the apparatus when it is in the cross-correlation configuration.

First, it is unnecessary for the cross-correlation apparatus to have been aligned previously during construction of a hologram. If a transmission hologram that is computer generated is used instead of one generated by the method described in subsection 3.4, then the alignment described previously has not been done. The alignment procedure in subsection 4.4 assumes that the apparatus has no previous alignment history. In the interest of brevity, those alignments within this section which are already described in subsection 3.4 are simply cross-referenced to that description.

Second, to make the cross-correlation process work with maximum accuracy and sensitivity, it is necessary (1) to match the transverse dimensions of the Fourier transform of the prefilter to the transverse dimension of the hologram and (2) to match the spherical phase structure of the calibration beam to that within the hologram. The latter requirement means that either the hologram must contain the same spherical phase structure or additional lenses must be added to remove any spherical phase-front discrepancy between the hologram and the Fourier transform unit. Properly matching these items maximizes the potential dynamic range for the cross-correlation process. How rapidly this range changes under mismatched conditions is a complex function of the hologram and of the laser beam being compared with the hologram [see eq (4.3.8)].

Third, we assume the placement of the lens for the Fourier transform for the proper scaling of the image and proper placement of the prefilter is accomplished, as discussed in subsection 3.4.

Fourth, we assume the approximate placement of the cross-correlation unit and vidicon-TV unit has been done according to subsection 3.4.

Fifth, we assume all subsequent adjustments fine tune the positions of the various units in the basic cross-correlation apparatus, as shown in figure 2. All the remaining adjustments make the cross correlation exhibit as strong a response as possible. To accomplish this end, the calibration beam is similar to the object beam recorded in the hologram. In our apparatus we made a plane wave front with a nearly TEM_{00} intensity profile at the prefilter plane by using the technique discussed in subsection 3.4. Our calibration beam is similar to the object beam.

Given the above beam, each translation of a lens, filter, or hologram is moved individually to make the strength of the cross-correlation pattern as intense and compact as possible (see subsection 4.6 for the illustration of the structure of the pattern).

Once all adjustments have been performed, the apparatus is aligned properly and can be calibrated with a linear detector unit and a sufficiently stable cross-correlation apparatus. In this prototype, the vidicon-TV unit had a nonlinear response to irradiance, and

the beam expander for the object and calibration beams was not sufficiently stable mechanically to allow accurate calibration. Furthermore, as discussed in subsection 5.2, the present spacing of sampling holes of the prefilter relative to the spacing of the sampling holes in the hologram is not optimum for quantitative measurements; therefore, this paper does not attempt to discuss in any detail a calibration procedure of the prototype. That process will be discussed in a subsequent paper when an improved apparatus has been constructed to have the necessary mechanical stability.

4.5 Calibration of this Prototype Apparatus

Although we report no numerical details here, the reader may wish to construct and use an apparatus similar to this prototype. Therefore, this subsection indicates a possible calibration process.

We must calibrate because:

- (a) Someone can move a lens, mirror, etc.
- (b) The laser source can change or be a different wavelength.
- (c) Algae may be growing in the liquid gate.
- (d) The theory is not complete.
- (e) The various dimensions of the parts are not accurately known, etc.

To calibrate requires a mathematical model showing expected behavior. Try the simple model defined in subsection 4.3.2. A basic calibration process could be:

(a) Use a cw laser of the same wavelength that you intend to use for your pulse systems.

(b) Make sure the beam has almost uniform intensity and has its wavefront normal to the prefilter plane over at least two neighboring apertures in the prefilter.

(c) Have some means to translate the above beam so that all neighboring pairs of apertures can be sequentially illuminated with uniform irradiance and zero relative phase.

(d) Have some means to tilt the above beam off the normal so that the relative phases can be changed in a controlled way. Appropriate transverse displacement of the lenses and filter in the beam expander for the calibration beam can accomplish both the beam tilt and its transverse translations. For larger dynamical ranges it may be necessary to insert beam steering devices.

(e) Allow one aperture at a time to radiate. By varying the intensity of the input and measuring the output at all 25 spots, you can develop the data to fix the A_{ℓ_1, ℓ_2} set. Use a small angle wedge (beam splitter) and a calibrated meter to monitor the absolute power in the incident calibration beam. Use a second calibrated power meter just behind the prefilter to determine the transfer ratio of power striking the monitor meter and exiting from each aperture in the prefilter. Confirm that the process is linear under all the conditions defined in (e) and (f). Capture the entire reflected and transmitted beam in these measurements of laser power.

(f) Allow each pair of apertures to radiate in turn. By varying both intensities and relative phases and measuring the corresponding output at all 25 cross-correlation values, you can develop the necessary data to fix the values and to determine the allowed dynamic ranges of A_{ℓ_1, ℓ_2} , θ_{ℓ_1, ℓ_2} for the simple model defined in subsection 4.3.2.

(g) Given the above calibration values, the apparatus can now be used to generate 25 time series signals of an incoming pulse. From that data the nine E_{ℓ_1, ℓ_2} and ϕ_{ℓ_1, ℓ_2} can be deduced.

(h) We make two final comments on the calibration process. First, only eight θ_{ℓ_1, ℓ_2} and eight ϕ_{ℓ_1, ℓ_2} can be fixed; the remaining phases are arbitrarily fixed by some

convention. Second, the ultimate calibration accuracy depends on knowledge of both the relative phase and the irradiance applied to a given pair of apertures in the prefilter. Appropriate design of the control for beam steering can provide the needed information on relative phase. By using least squares and self-consistency in the results, you can deduce the appropriate calibrations and develop absolute ratio measurements.

4.6 The Cross-Correlation Patterns

This subsection contains many figures which show qualitatively the output of the prototype device as defined in subsection 4.2. Because the beam expander for the calibration beam was dimensionally unstable and the responsivity of the vidicon-TV unit was nonlinear, a quantitative evaluation of the cross-correlation process was not useful.

Once the problems discussed in subsections 4.5 and 4.6 are solved during the construction of a high precision and stable unit, the quantitative evaluation of the holographic technique becomes appropriate. Even though this paper is qualitative, the reader can estimate the promise of the holographic technique.

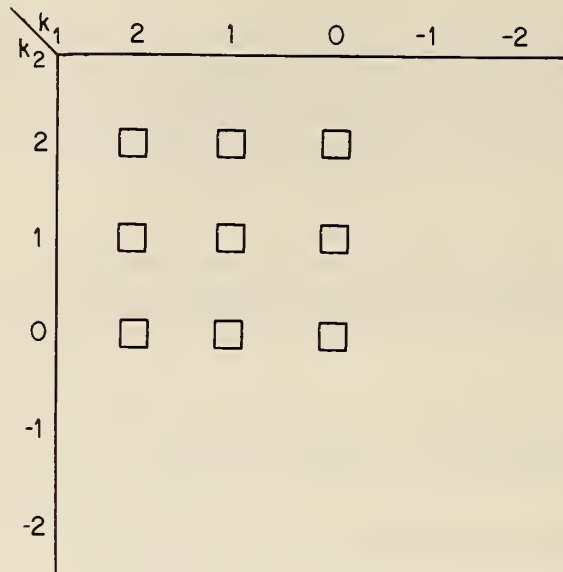
Figure 4 sketches the defined coordinates for the prefilter unit which is a 5 x 5 cm glass plate with a photographic emulsion. Each hole is square with edge dimensions of 0.539 mm; the distance between holes is 1.001 mm. The accuracy of these dimensions is ± 0.001 mm. These dimensions are chosen to get a maximum signal out at the cross-correlation plane with insignificant overlap of the spots in that plane. Subsequent figures show that this choice is qualitatively proper. For high precision quantitative results, this ratio may not be adequate, and the size of the holes may need to be reduced.

Figure 5 sketches the cross-correlation pattern when all nine holes are illuminated at the prefilter. Figures 17, 18, and 19 show the TV pictures of that pattern. These figures are discussed later in this subsection. Figure 6 sketches two cases when a single hole in the prefilter is allowed to pass the laser radiation. Figure 7 sketches what happens when two holes pass the laser radiation.

Given the above sketches, we proceed to actual pictures of the cross-correlation plane. Figures 8 through 15 show cross correlations for various intensity and phase relationships. Their captions should be adequate to explain qualitatively what happens. The fine structure in these spots is a consequence of spatial filtering by the hologram which passed only the center order of the Fourier transform for a square hole [11]. If the beam profile apparatus passes all orders accurately and the holes are small enough, then the intensity profile for each spot in the cross-correlation plane is triangular for a line scan through the center of a spot. Each TV picture in this report has a bright line parallel to the vertical axis passing through some of the spots. A graph on the side of the TV scan shows the intensity profile of those spots along that line scan. The reader can see that this profile is not triangular. This result is expected, given the size of the initial hole and the aperturing by the hologram. These results show how insensitive this apparatus is to defects in the optics and indicate its promise as a precision system for beam profile measurements.

Figure 16 sketches what can happen when all nine beams pass the prefilter with equal intensity.

Case a : Only hole at prefilter with $\ell_1 = -1$, $\ell_2 = -1$ has laser power



Case b : Only hole at prefilter with $\ell_1 = +1$, $\ell_2 = +1$ has laser power

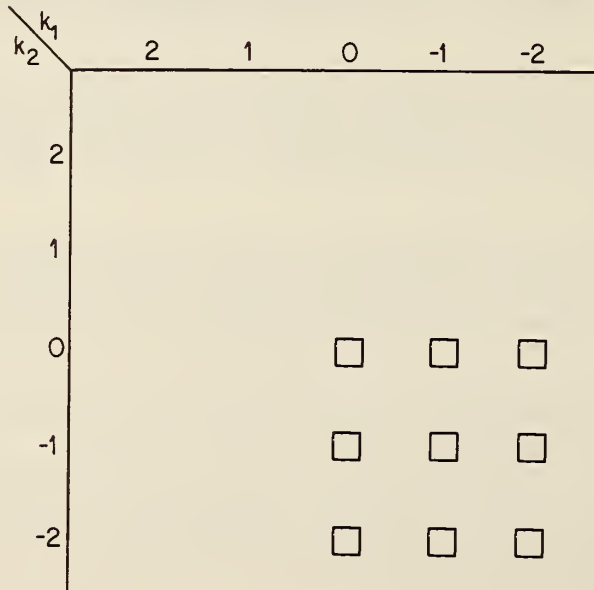
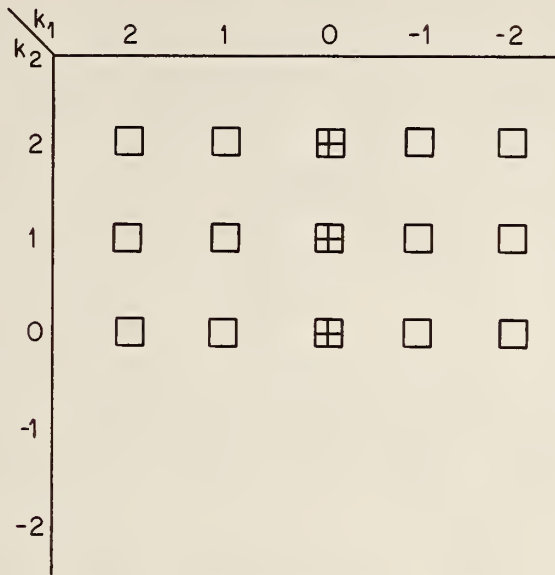


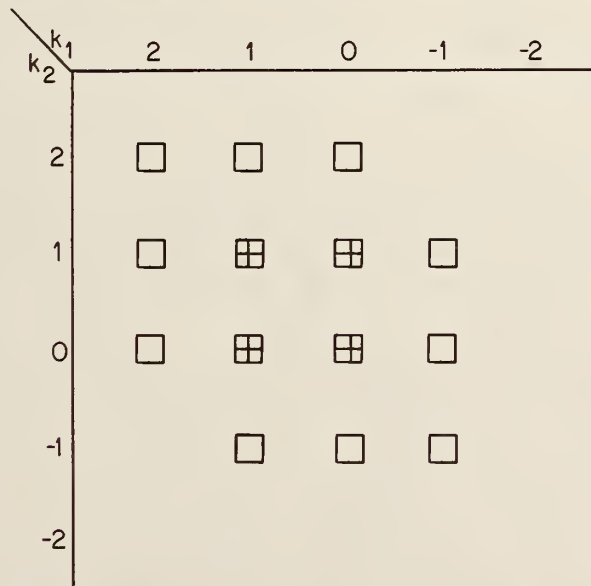
Figure 6. Two examples of output at the cross-correlation plane - one exit beam at prefilter.

Case c: Two beams pass prefilter, namely $\ell_2 = -1$; $\ell_1 = -1$ and $+1$



Spots at $k_1 = 0$ has relative phase information between the two beams from the prefilter.

Case d: Two beams pass prefilter, namely $\ell_1 = -1$, $\ell_2 = -1$; $\ell_1 = 0$, $\ell_2 = 0$



Here four spots which have $k_1 = 1, 0$; $k_2 = 1, 0$ give relative phase information between the two beams from the prefilter.

Figure 7. Two examples of output at the cross-correlation plane - two exit beams at prefilter.

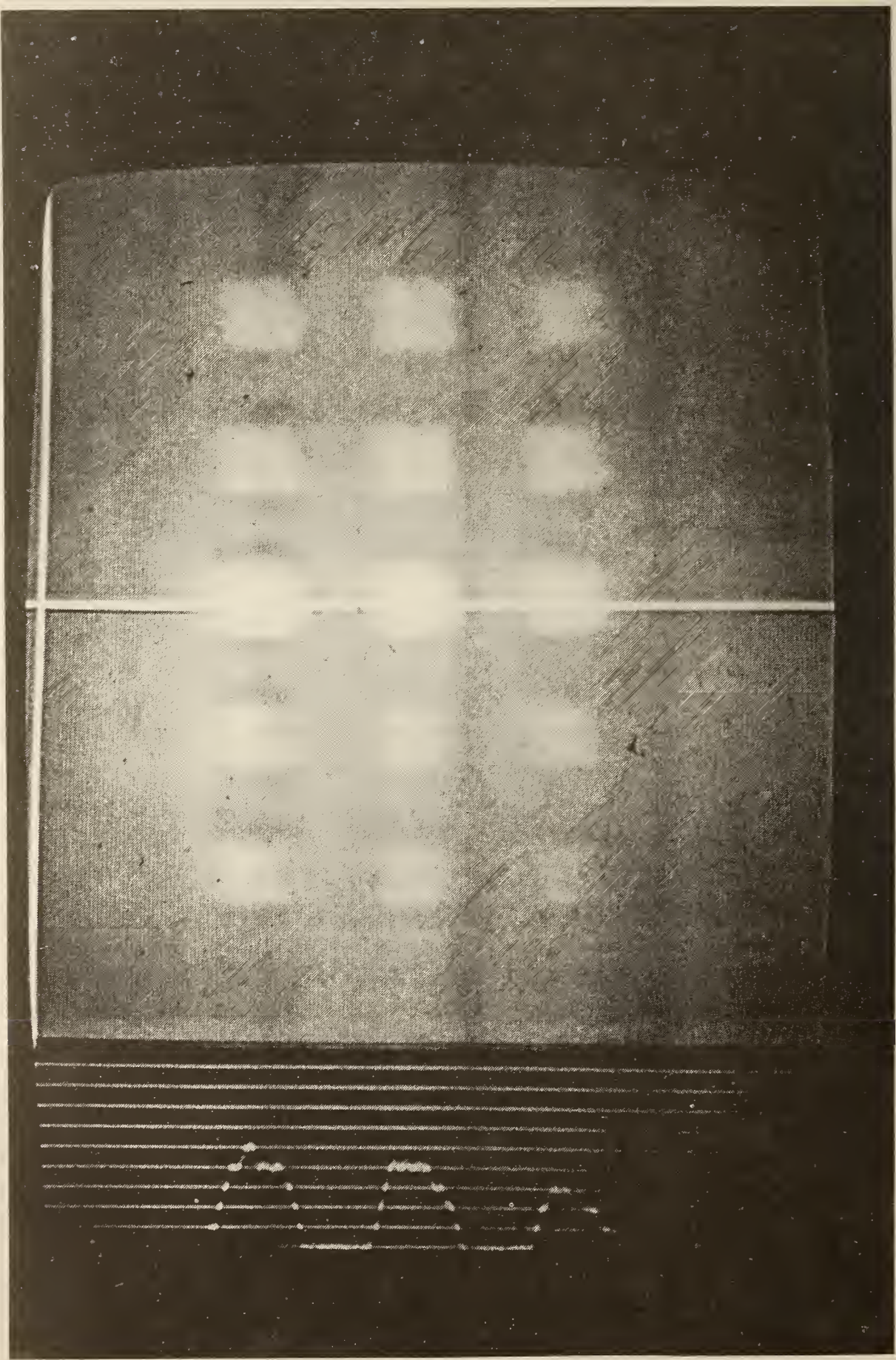


Figure 8. Television picture of the cross correlation plane - two exit beams with $l_1 = -1, +1$ and $l_2 = 0$ at prefilter

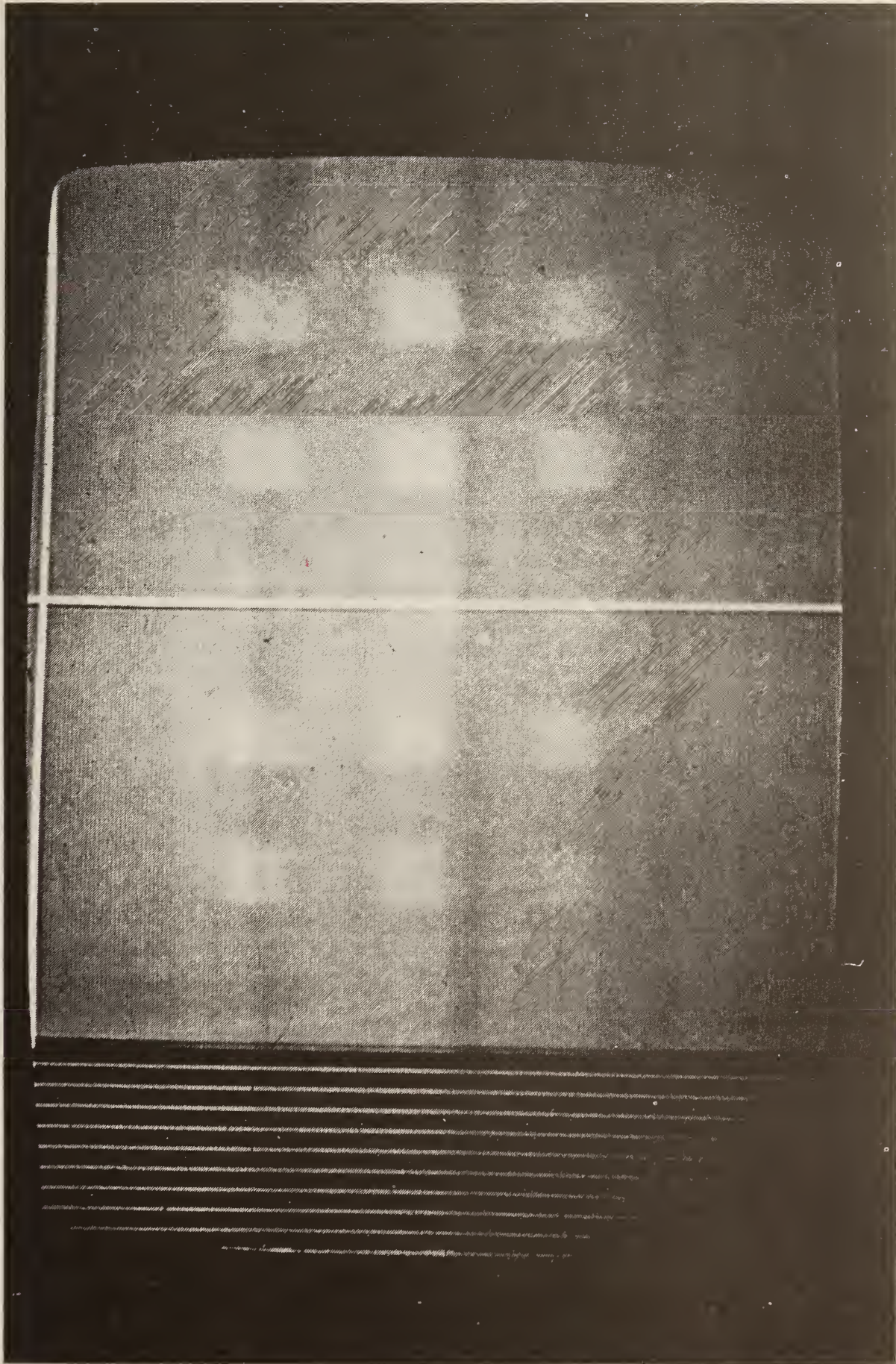


Figure 9. Same picture as figure 8 except beams are approximately 180° out of phase.

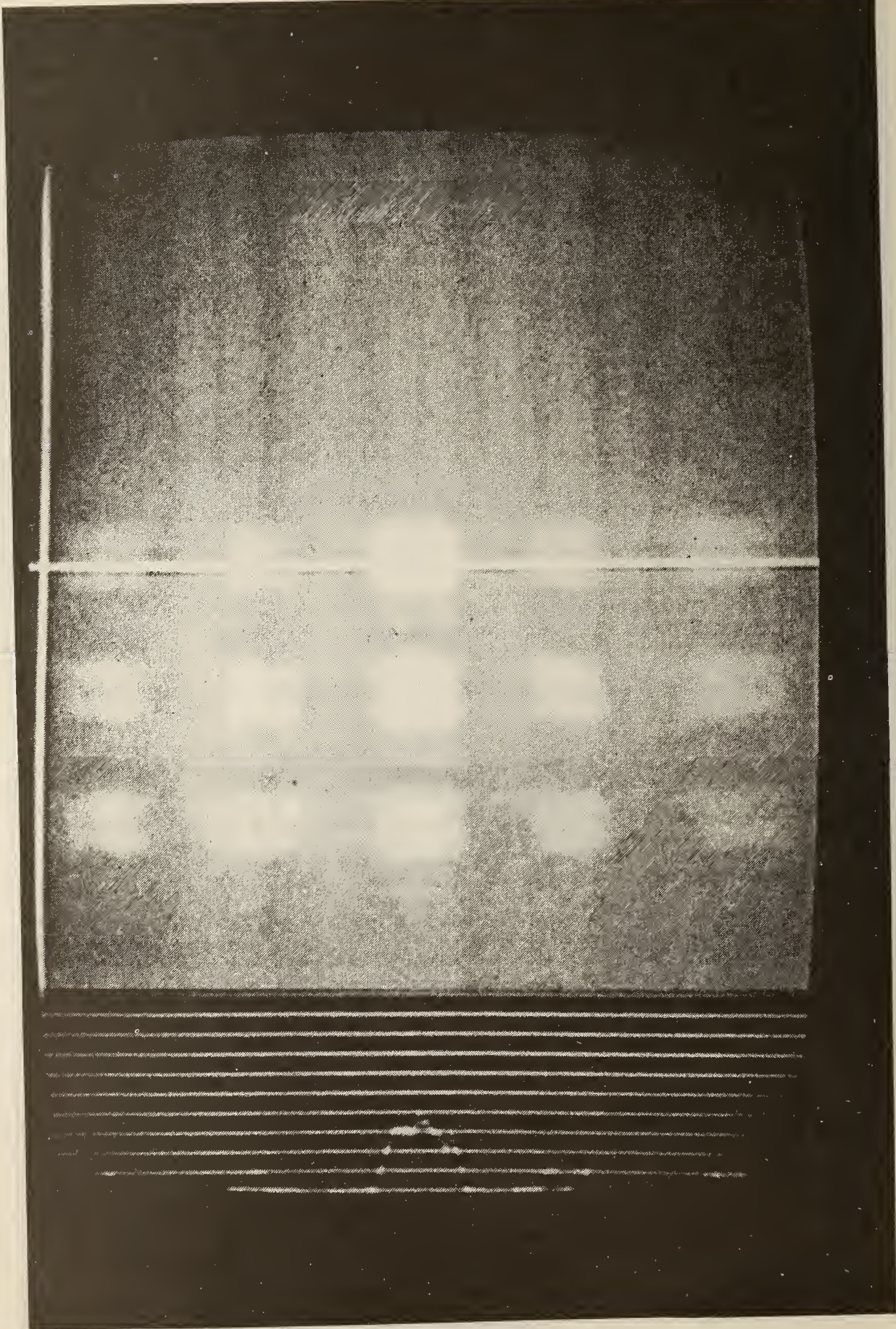


Figure 10. Television picture with $\phi_1 = +1$ and $\phi_2 = \pm 1$ at prefilter with approximately equal phase and amplitudes.

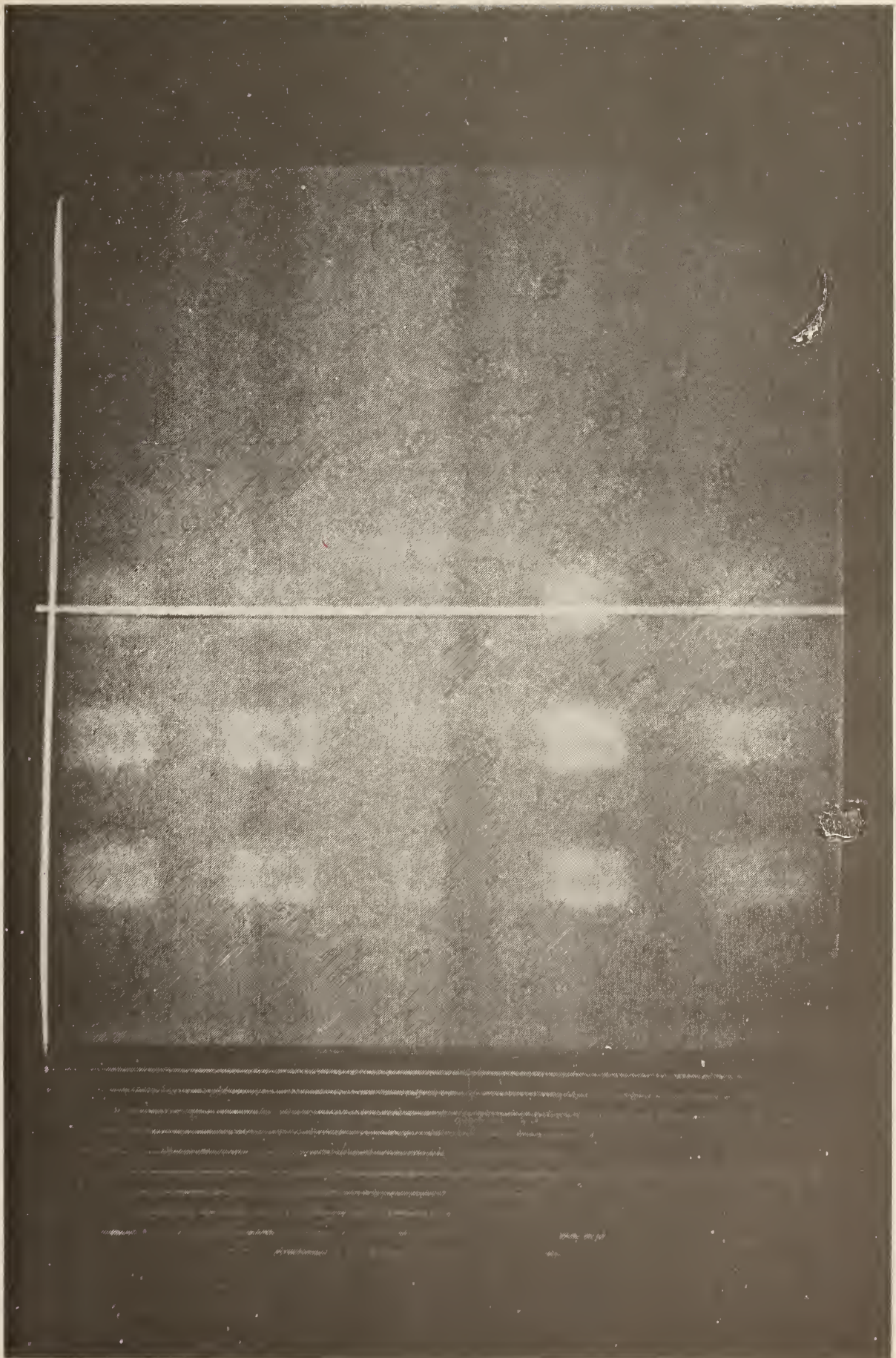


Figure 11. Same picture as figure 10 except beams are approximately 180° out of phase.

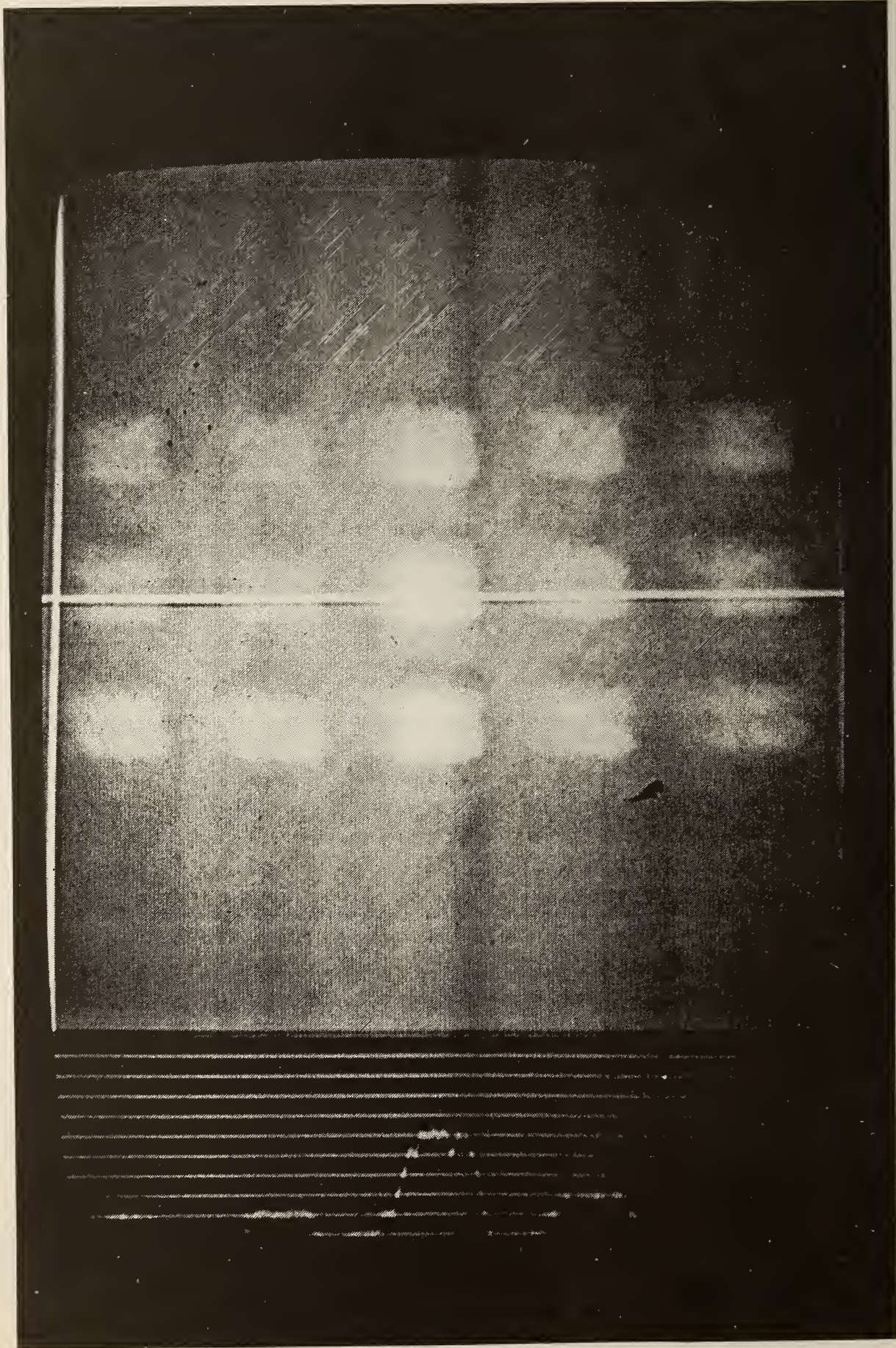


Figure 12. Television picture with $\lambda_1 = 0$ and $\lambda_2 = \pm 1$ at prefilter. Here beams are in phase.

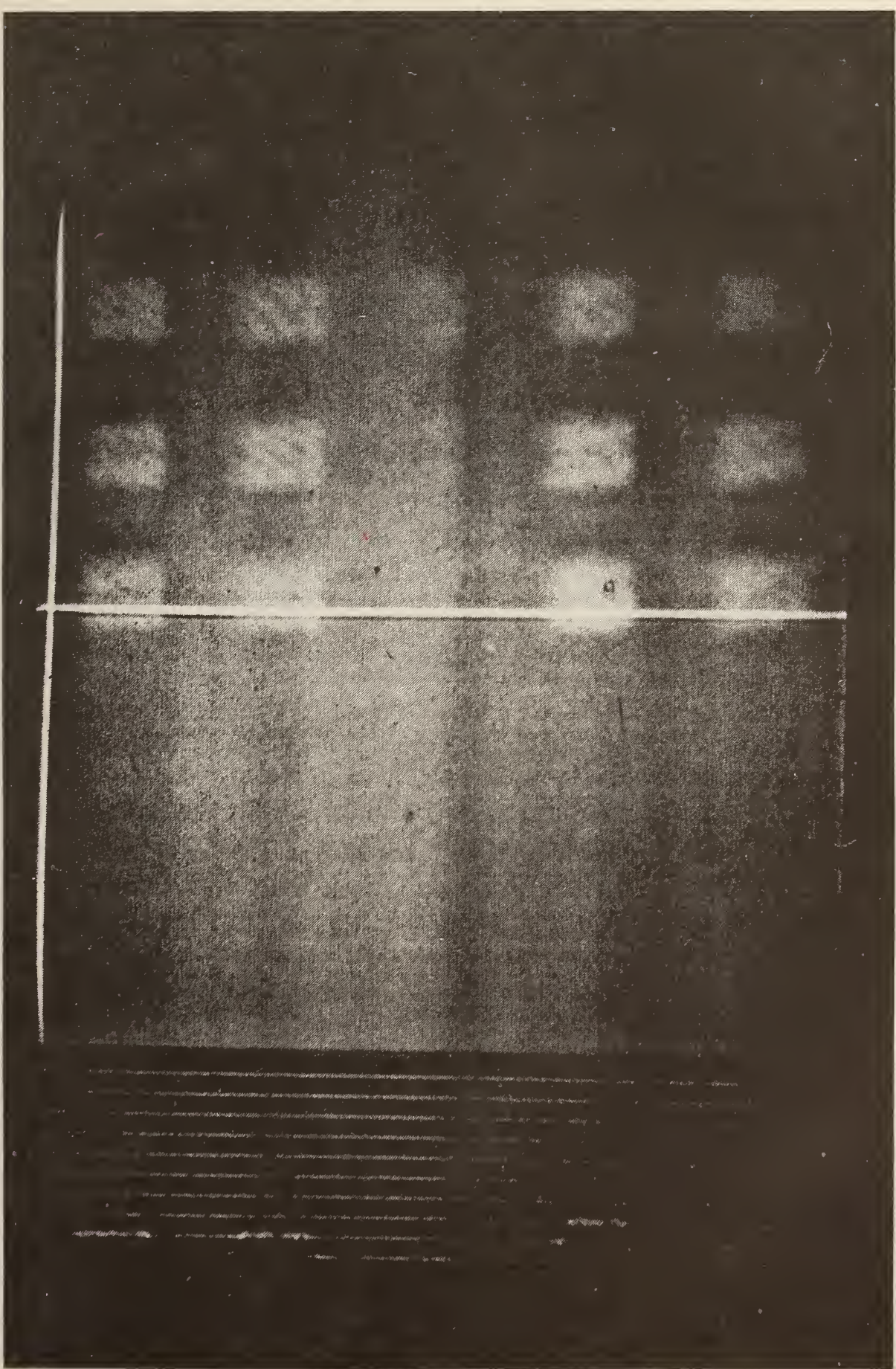


Figure 13. Television picture with $\delta_1 = -1$ and $\delta_2 = \pm 1$ at prefilter. Here beams are out of phase.

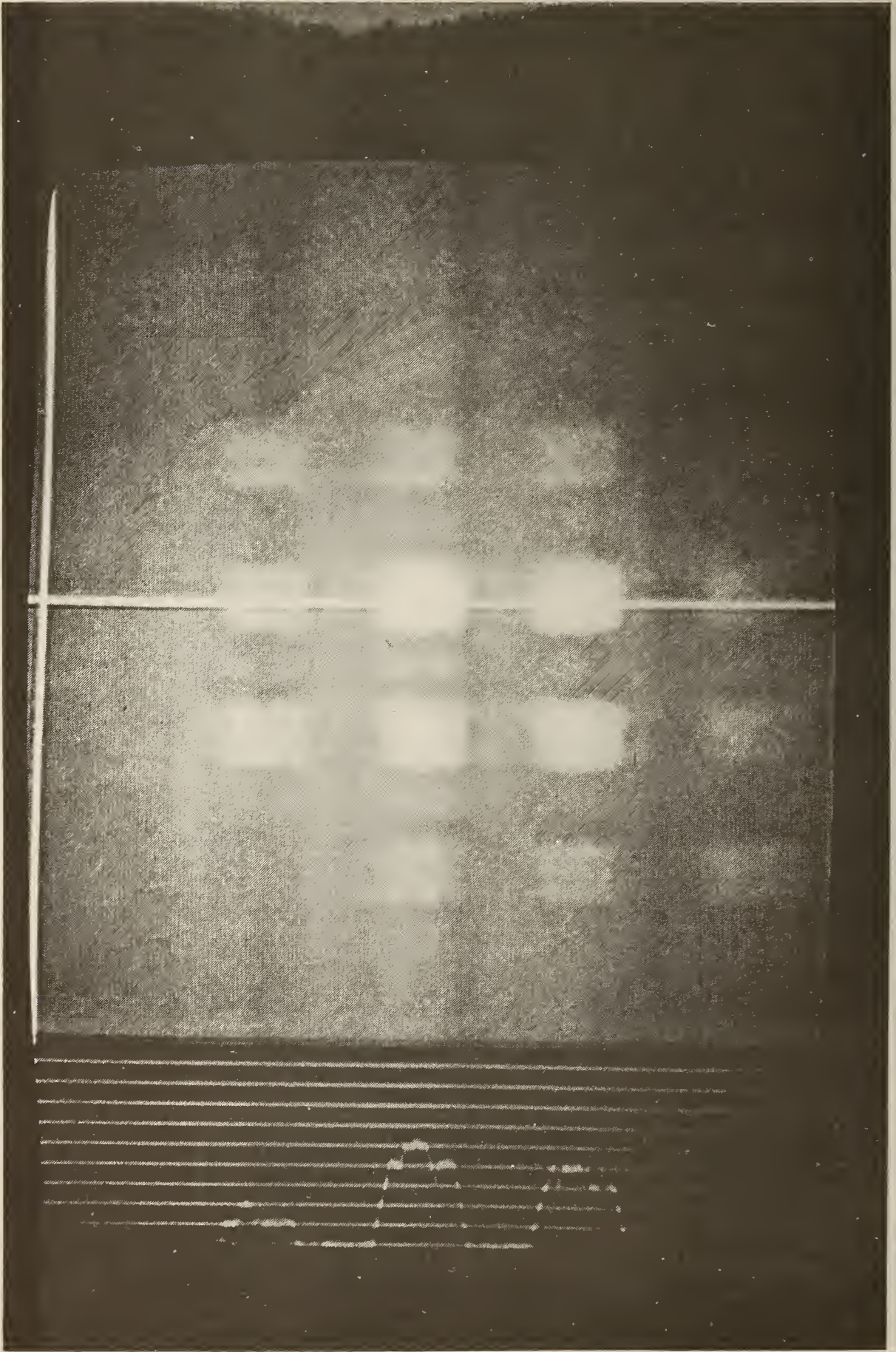


Figure 14. Television picture with $l_1 = +1$, $l_2 = -1$ and $l_1 = 0$, $l_2 = 0$.

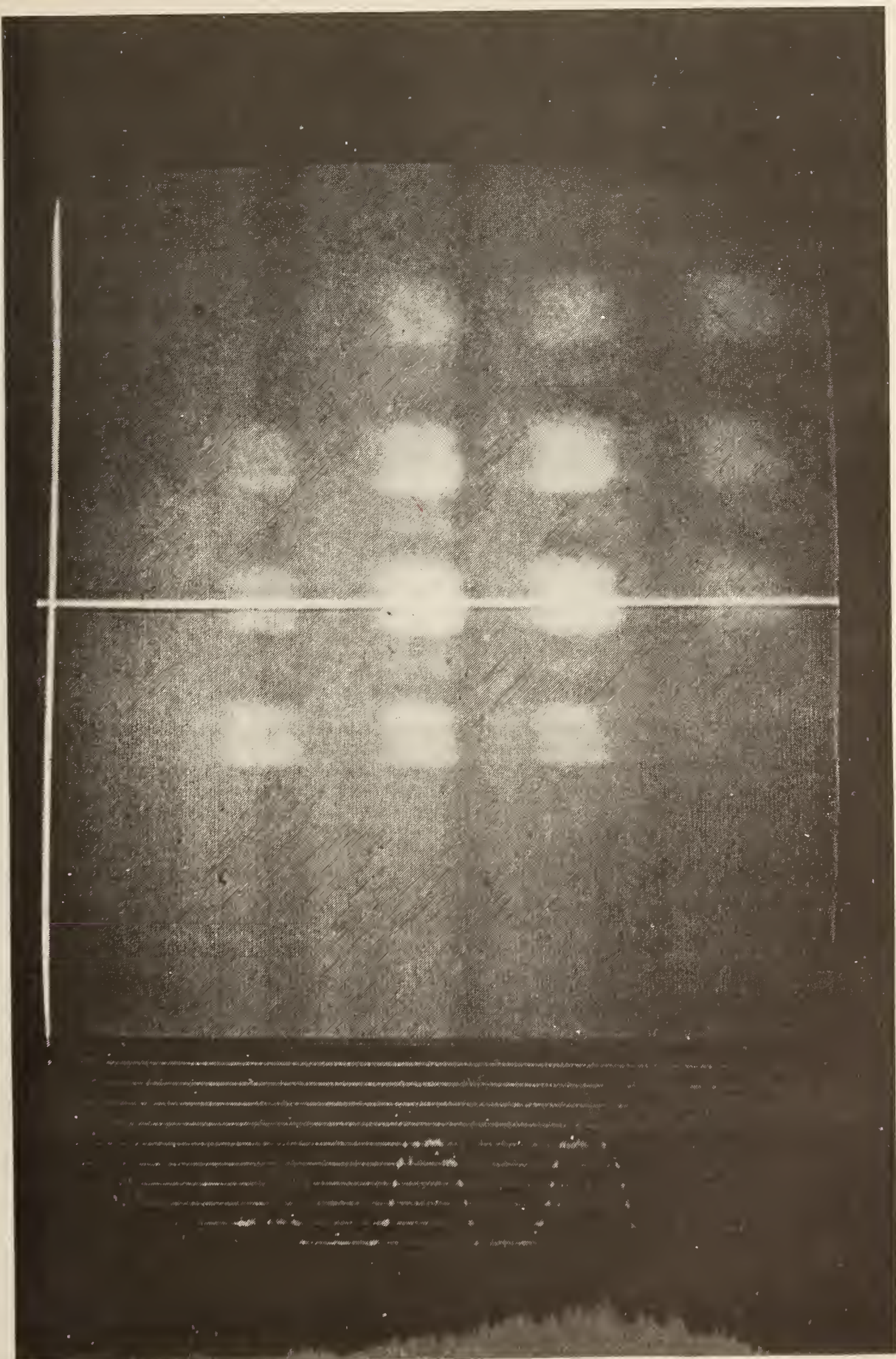
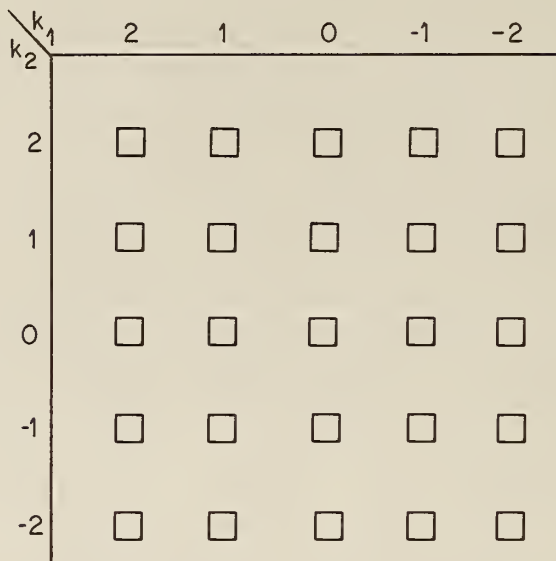


Figure 15. Television picture with $\lambda_1 = -1$, $\lambda_2 = -1$ and $\lambda_1 = 0$, $\lambda_2 = 0$.

Case e : All Beams from prefilter reach the hologram.



Case f : Assume Object Beam, Calibration Beam, and Reference Beam all have uniform intensity and constant phase. In this case the output at the cross-correlation plane is the following intensity pattern.

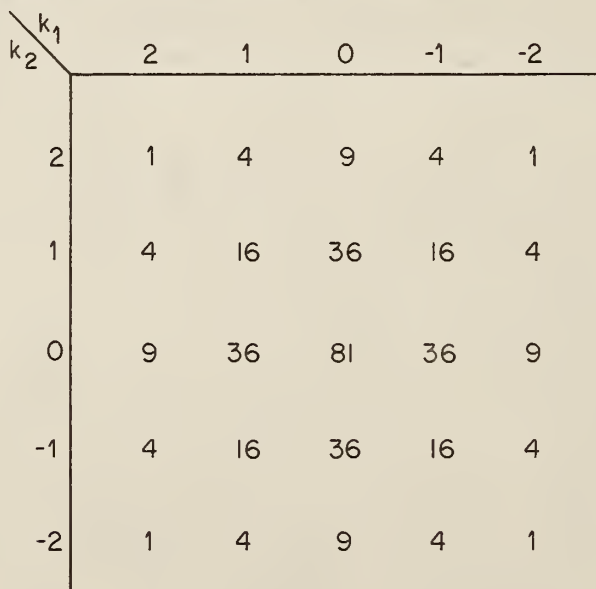


Figure 16. Final examples of output at the cross-correlation plane.

Figures 17, 18, and 19 show the TV pictures of the cross-correlation plane under three conditions. These pictures demonstrate the effects of beam misalignment within the apparatus and of saturation at the vidicon-TV unit.

Figures 20 and 21 show several views of the apparatus. These pictures give scale to the various parts in the apparatus.

Figure 22 shows the intensity distribution of the object and calibration beams at the prefilter. The ring structure arises from the transverse modes in the laser which are not filtered by the pinhole in the beam expander. Figure 4 shows where this laser beam is sampled. The filter was about 3 mm by 3 mm, and the width of the beam was nearly 10 mm in diameter at the half-power points.

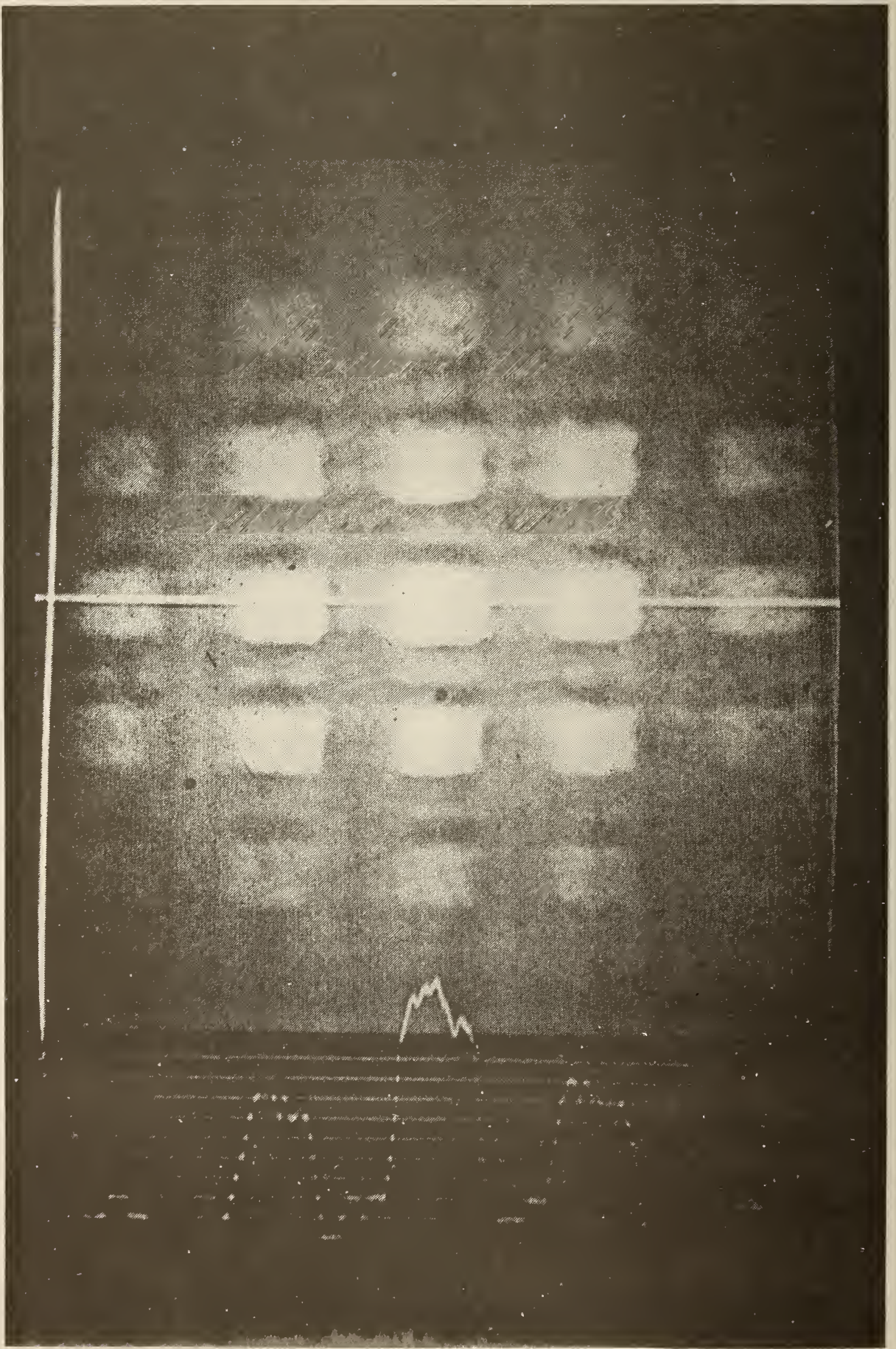


Figure 17. Television picture with all nine holes illuminated and the cross correlation output not saturating the vidicon-TV unit

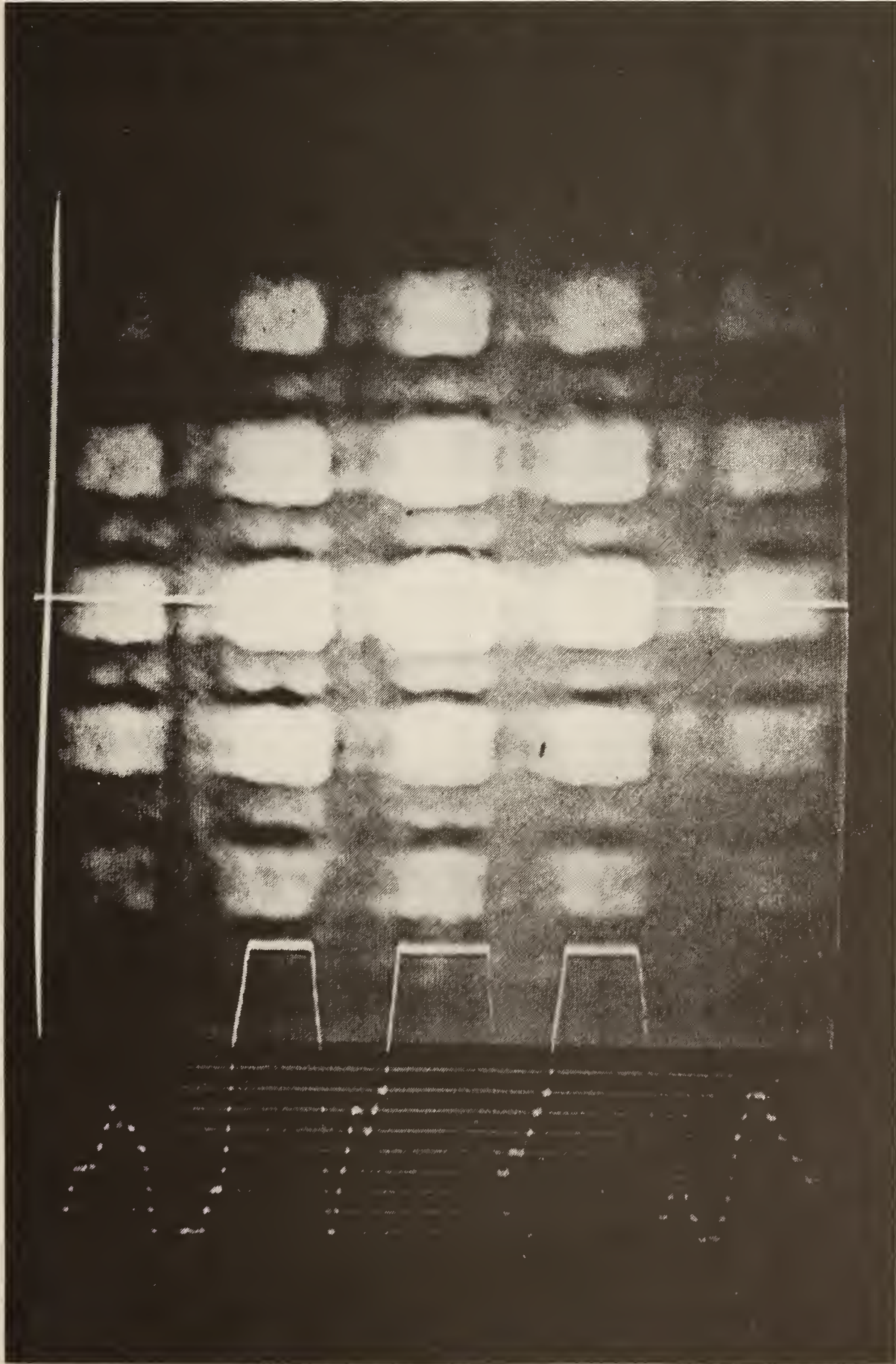


Figure 18. Television picture showing saturation of vidicon-TV unit.

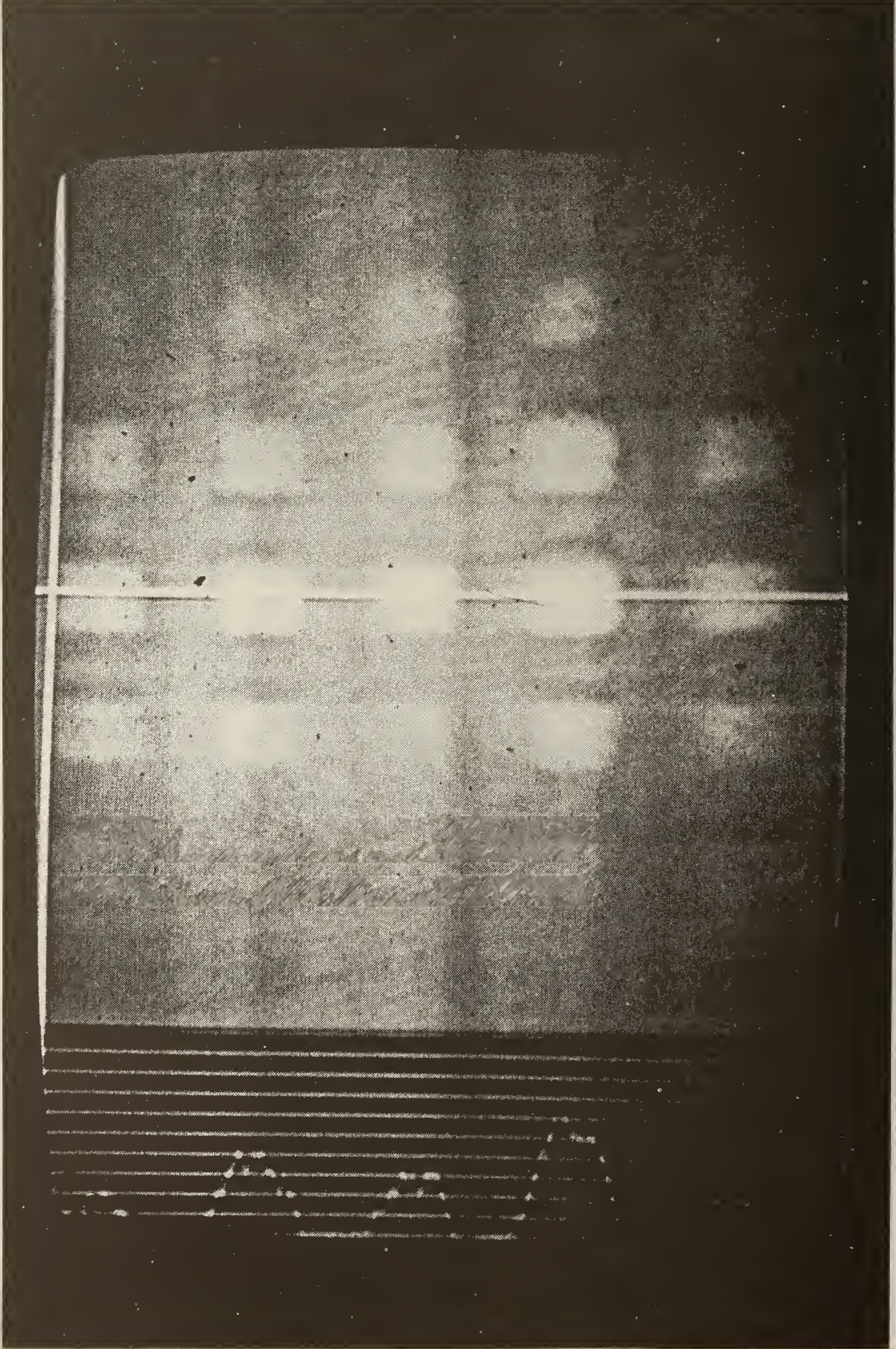


Figure 19. Television picture showing the cross correlation not properly aligned.

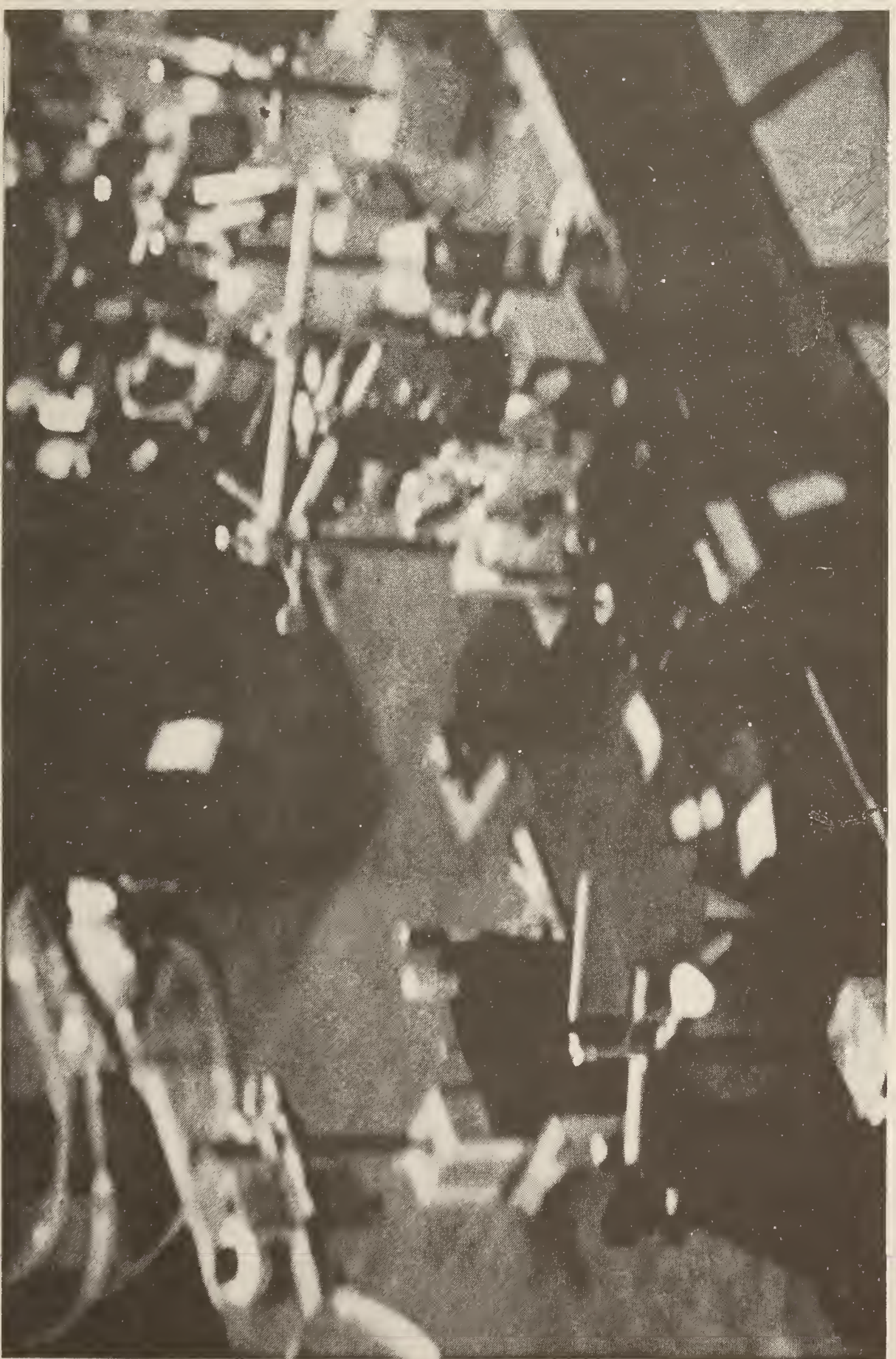


Figure 20. A partial view of the beam profile apparatus.

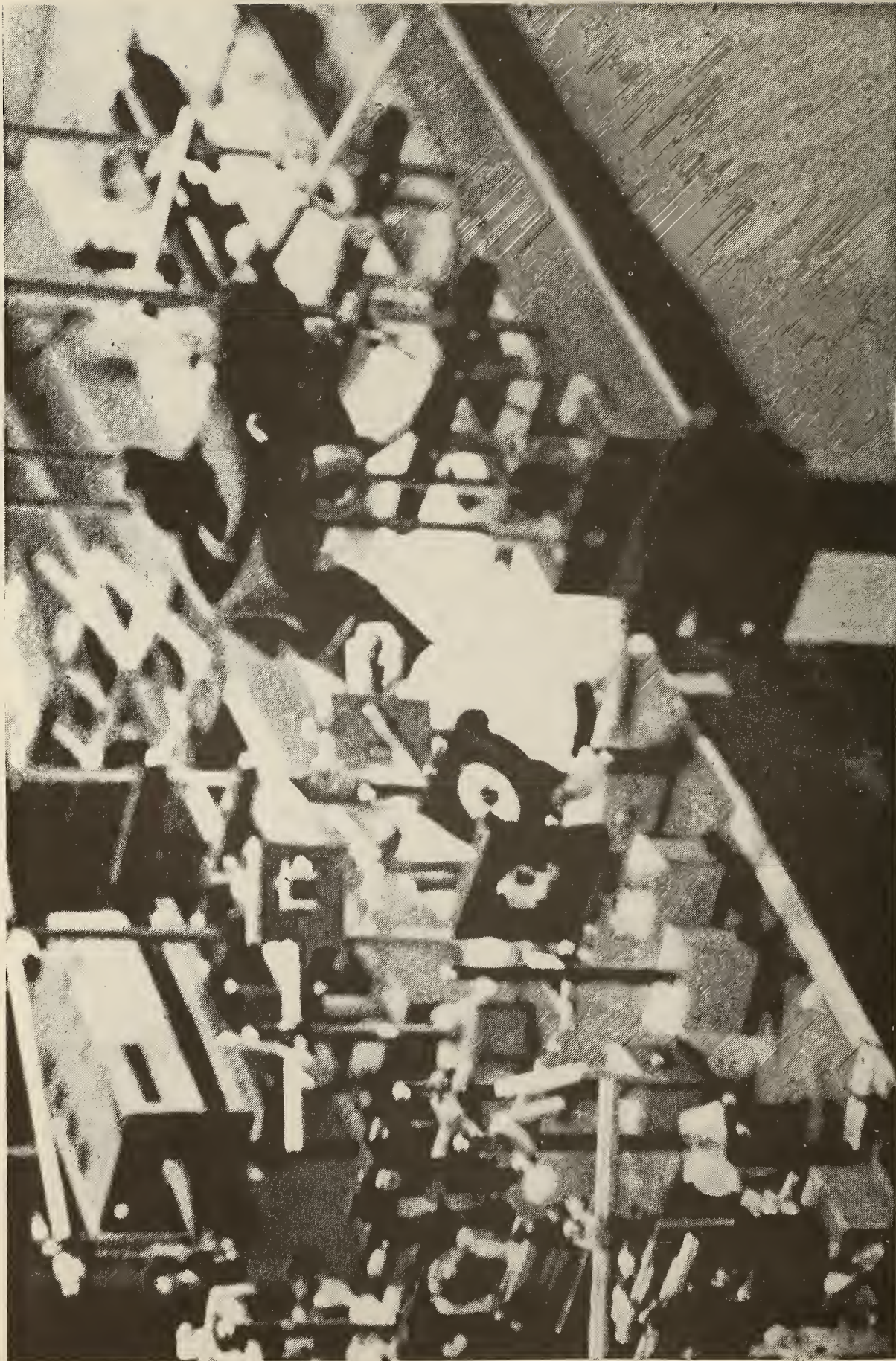


Figure 21. The remaining view of the beam profile apparatus.

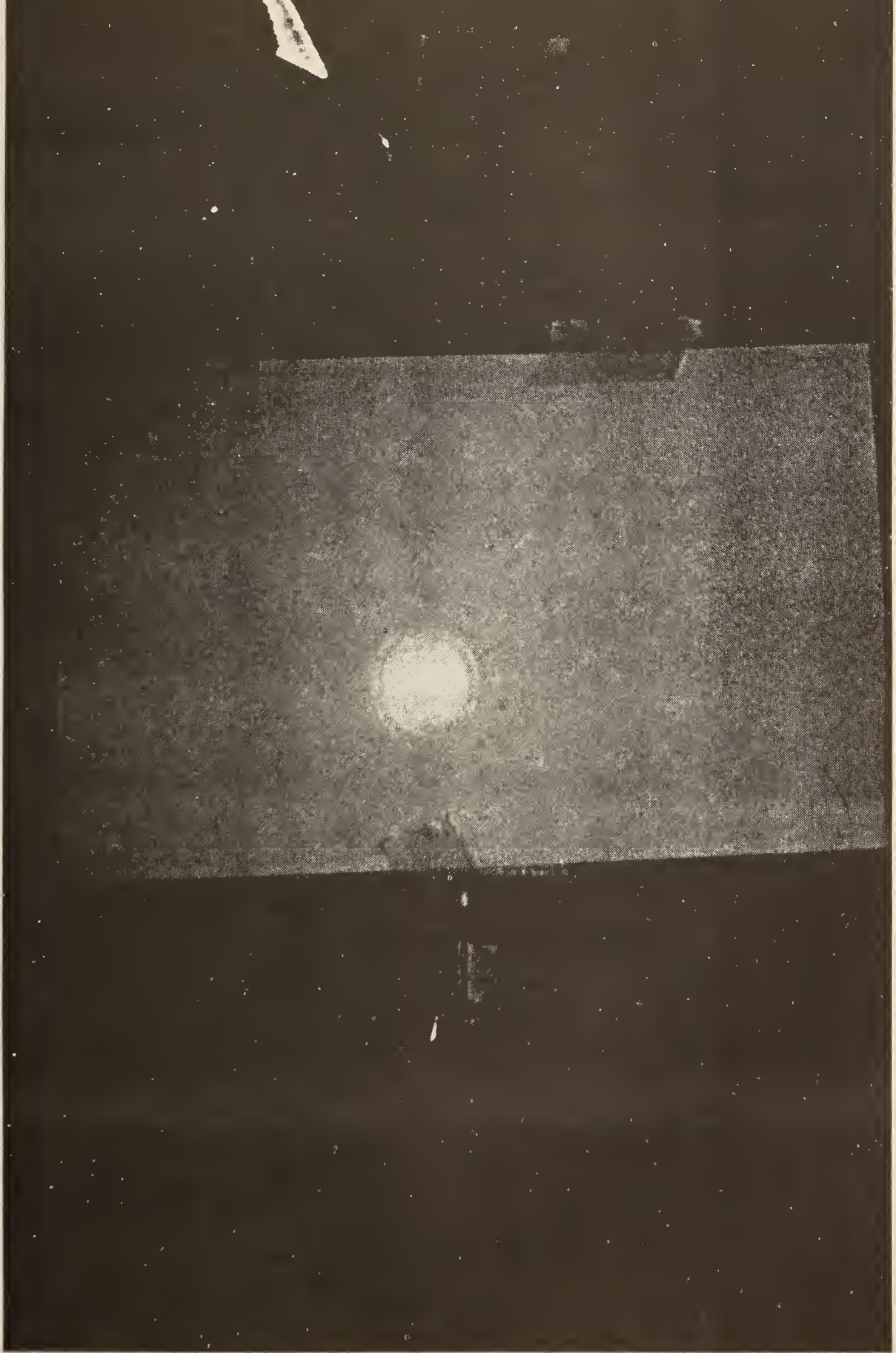


Figure 22. A picture of the object and calibration beam.

5. MODIFYING THE PROTOTYPE APPARATUS TO GENERATE A MORE EFFECTIVE UNIT

This section makes numerous inferences. I discuss new possibilities for beam profile measurements using holography. Each idea addresses a feature that proved to be a problem in the prototype apparatus.

5.1 What this Section Presents

Subsection 5.2 notes that doubling the distance between the apertures in the prefilter permits much simpler measurements. Unlike the prototype where up to nine beams interfere for a single spot, there are cross-correlation spots where only two beams interact; therefore, simple real-time and precision measurements become possible.

Previous discussions on the holographic method have not exhausted its capabilities for beam profile measurements in real time; therefore, subsection 5.3 addresses beam profile analysis by orthogonal cross-correlation structures. We indicate the concept, although an exact technical realization is unknown.

The remaining subsections address briefly two new units, each using the information generated from lessons learned during development of the prototype.

Subsection 5.4 briefly describes the beam profile measuring apparatus [25] that will use reflection concepts. Because design of this system is incomplete, this description addresses only the gross features.

Finally, subsection 5.5 describes how the holographic method can be part of an instrument that makes selected beam profile measurements. This unit, which can be made cheaply [26], should provide the economic means for real-time control of an arbitrary but unknown laser beam.

5.2 A Scale Change between the Original Hologram and a New Sampling Plate Makes a Better Instrument

Figure 16 shows that some spots in the cross-correlation plane have contributions from more than two beams. In fact, the $k_1 = k_2 = 0$ spot involves contributions from all nine beams of the prefilter. This number of beams causes extensive mathematical complexity when unfolding the phases and amplitudes in a test beam.

Figure 23(a) shows separating the sample holes to a new 3×3 beam pattern at the prefilter as indicated by the unblocked beams in the 5×5 prefilter array 23(b) so that one cross-correlation spot has its intensity proportional to the intensity at the prefilter hole (see spot $k_1 = 2$ and $k_2 = 3$). A different spot has information about the relative phase between nearest neighboring holes in the prefilter plane (see spot $k_1 = 1$ and $k_2 = 3$). Briefly, the distance between holes in the new 3×3 prefilter is twice the distance between the holes defining the 3×3 pattern recorded in the hologram. Even this relationship between the prefilter and hologram fails to eliminate all cross-correlation spots with more than two beams contributing. Figure 23(c) shows there are spots with four beams contributing (see spot $k_1 = k_2 = 1$).

Figure 23(a) shows a very limited array at the prefilter. If that array is extended to a large array, say 20×20 , then the cross-correlation plane would expand to 43×43 spots with a change in the pattern shown in figure 23(c). For example, location $k_1 = 3$, $k_2 = 1$ would now have the contribution of two beams, and $k_1 = 3$, $k_2 = 0$ would now have the contribution of two beams, and $k_1 = 4$, $k_2 = 0$ would be a spot where only one beam contributes. Note that the expansion to larger arrays need not be square or rectangular. The hologram pattern could be many other shapes such as crosses or ribbon structures. A cross would eliminate the four-beam contribution in the 7×7 array of the cross-correlation plane.

5.3 Thoughts about a Cross-correlation System
that Can Make Beam Profile Measurements that Are Orthogonal

The original plan in this evaluation program of the holographic technique was to use some form of orthogonal mode analysis using an appropriate hologram to measure beam profile. Unfortunately, there remain extensive technical problems before such holograms are realized. Consequently, we shifted to the digital sampling technique discussed in this paper. We used the resulting hologram to demonstrate feasibility of the beam profile measurements with a hologram as the basic optical processing instrument. In the event the appropriate hologram eventually can be generated either by computer or by known laser beam profiles, an orthogonal mode technique can be used. The literature [15] describes a way to realize orthogonal modes using random phase filters. Unfortunately, this method will produce extreme signal-to-noise problems because too much of the laser power is scattered by the random phase filter. Consequently, it is our opinion that this method is unlikely to be used in a measurement system. To attain an orthogonal mode technique that avoids the unnecessary scattering of the laser power requires a careful restriction of allowed beam shape and a careful choice of the holograms. This discussion indicates very briefly what must be done.

The cross-correlation process is written as:

$$U_5(x_5, y_5) = \iint du dv B(u,v) H^*(u,v) \exp[-i2\pi(uS_1 + vS_2)] , \quad (5.3.1)$$

where we continue to ignore the reference beam in the hologram and where $H^*(u,v)$ represents the spatial structure in the hologram that will generate the desired cross correlations with the incident laser beam, $b(x_1, y_1)$. $B(u,v)$ is the Fourier transform of the incident laser beam. Here u, v, S_1, S_2, x_1, y_1 , etc., are defined in subsection 3.3 and appendix A.

The concept of orthogonal cross correlation can be approached by noting the following:

(1) First, we assume the hologram profile is represented by:

$$H^*(u,v) = \sum_{\ell=0}^N D_{\ell}^* G_{\ell}^*(u,v) e^{-i2\pi\ell au} , \quad (5.3.2)$$

where $G_{\ell}(u,v)$ is a set of complex spatial functions which represent the beam profile; the ℓa factor causes the cross correlation for the ℓ value to be displaced in the x_5 direction by the distance ℓa . The D_{ℓ}^* is a measure of the strength to which the ℓ mode is present in the hologram. N is the total number of such modes used to represent the beam profile.

(2) Second, we assume the beam profile at the hologram is also represented by:

$$B(u,v) = \sum_{\ell=0}^N A_{\ell} G_{\ell}(u,v) , \quad (5.3.3)$$

where A_{ℓ} gives the amount of each mode.

(3) The cross-correlation process thus is understood as the consequence of the interaction between two modes:

$$f_{\ell',\ell}(S_1, S_2) \equiv \iint du dv G_{\ell'}^*(u,v) G_{\ell}(u,v) e^{-i2\pi[u(S_1 + (\ell' - \ell) a) + vS_2]} . \quad (5.3.4)$$

(a) The Fourier transform of the pattern in the hologram filter.

$\ell_2 \backslash \ell_1$	-1	0	1
-1	□	□	□
0	□	□	□
1	□	□	□

(b) The 5×5 array in the prefilter with selected transmission pattern.

$\ell_2 \backslash \ell_1$	-2	-1	0	1	2
-2	⊠	□	⊠	□	⊠
-1	□	□	□	□	□
0	⊠	□	⊠	□	⊠
1	□	□	□	□	□
2	⊠	□	⊠	□	⊠

□ Blocked beams
 ⊠ Unblocked beams

(c) The resulting pattern at the cross-correlation plane.

$k_2 \backslash k_1$	3	2	1	0	-1	-2	-3
3	■	■	□	■	□	■	■
2	■	■	□	■	□	■	■
1	□	□	⊠	□	⊠	□	□
0	■	■	□	■	□	■	■
-1	□	□	⊠	□	⊠	□	□
-2	■	■	□	■	□	■	■
-3	■	■	□	■	□	■	■

■ One beam contributes here
 □ Two beams contribute here
 ⊠ Four beams contribute here

Figure 23. An improved beam profile measurement scheme.

For orthogonal decomposition to work properly, the terms in eq (5.3.4) should correspond to a series of spots in the cross-correlation plane: if $\lambda' \neq \lambda$, there is no well-defined spot; and if $\lambda' = \lambda$, there is a sharp high intensity spot. Under these circumstances, we have a method to get orthogonal decomposition of the beam profile. To realize the above concept requires construction of the appropriate hologram and generation of appropriate calibration beams to confirm that the decomposition via the hologram gives a set of spots with the desired orthogonal decomposition.

5.4 Features of the Proposed Reflection System

Reference [25] will detail the mathematics and many properties of this reflection system. This subsection just briefly indicates the structure of and the expectations for the unit.

A convenient visual summary of the basic holographic technique for a transmission system is shown in figure 24. The two lens elements are symbolic summaries of the more complex optics used in the prototype device and in the proposed reflection system. Figure 25 shows a block diagram of the reflection system. The system uses reflection optics so that it can operate at various wavelengths such as 10.6 and 1.06 μm . This unit has eleven surfaces of interest; each represents a definite stage in Fourier optics. There is one significant correction to the theory defined in appendix A because the beam for each optical component is off axis. This correction implies a corresponding modification of the actual optical components and thereby removes the first-order astigmatism. The low-order aberrations are minimized by using concave mirrors with different, but constant, radii of curvature for the two transverse coordinates. Variable curvature mirrors that could further reduce the aberrations prove to be unnecessary in this unit. This is fortunate because these units can be expensive if we require large aperture optics.

We define each surface and the transfer between surface pairs in the following list.

Surface #	Function
1	Here is the basic prefilter as shown in figure 26.
2	Here is the first Fourier optic transform mirror with both radii of curvature near 2 m. It is used for all wavelengths of interest.
3	Here is the Fourier transform surface of the prefilter plane. It is placed one focal length, f_1 , from the mirror which is one focal length from the prefilter. The radius of curvature is twice f_1 .
4	Here is the first mirror of a magnifying telescope. This mirror is changed to reflect the change in the carrier frequency of the laser pulse. Thus, the 10.6 μm wavelength needs a radius of curvature near 2 m and the 1.06 μm wavelength needs one near 0.2 m. This mirror change permits a proper match of transverse dimension at the Fourier plane of surface 3 to the "hologram" of surface 7.
5	This is a mathematical surface placed one focal length, f_2 , from surface 4 which is one focal length, f_2 , from surface 3. For 1.06 μm , the focal length is about 0.1 m.
6	This mirror, which completes the telescope, has a radius of curvature near 2 m and is unchanged for all wavelengths of interest, namely 1 to 20 μm . This element is placed one focal length, f_3 , from surface 5.
7	This Fourier plane is similar to the mathematical surface 3. Here, a reflection hologram causes the beam from a hole in the prefilter to be diffracted into nine diverging beams. The hologram is structured to generate only these nine beams for each hole. In addition, the hologram causes the beams to generate the desired pattern shown in figure 27. This element is one focal length, f_3 , from surface 6.

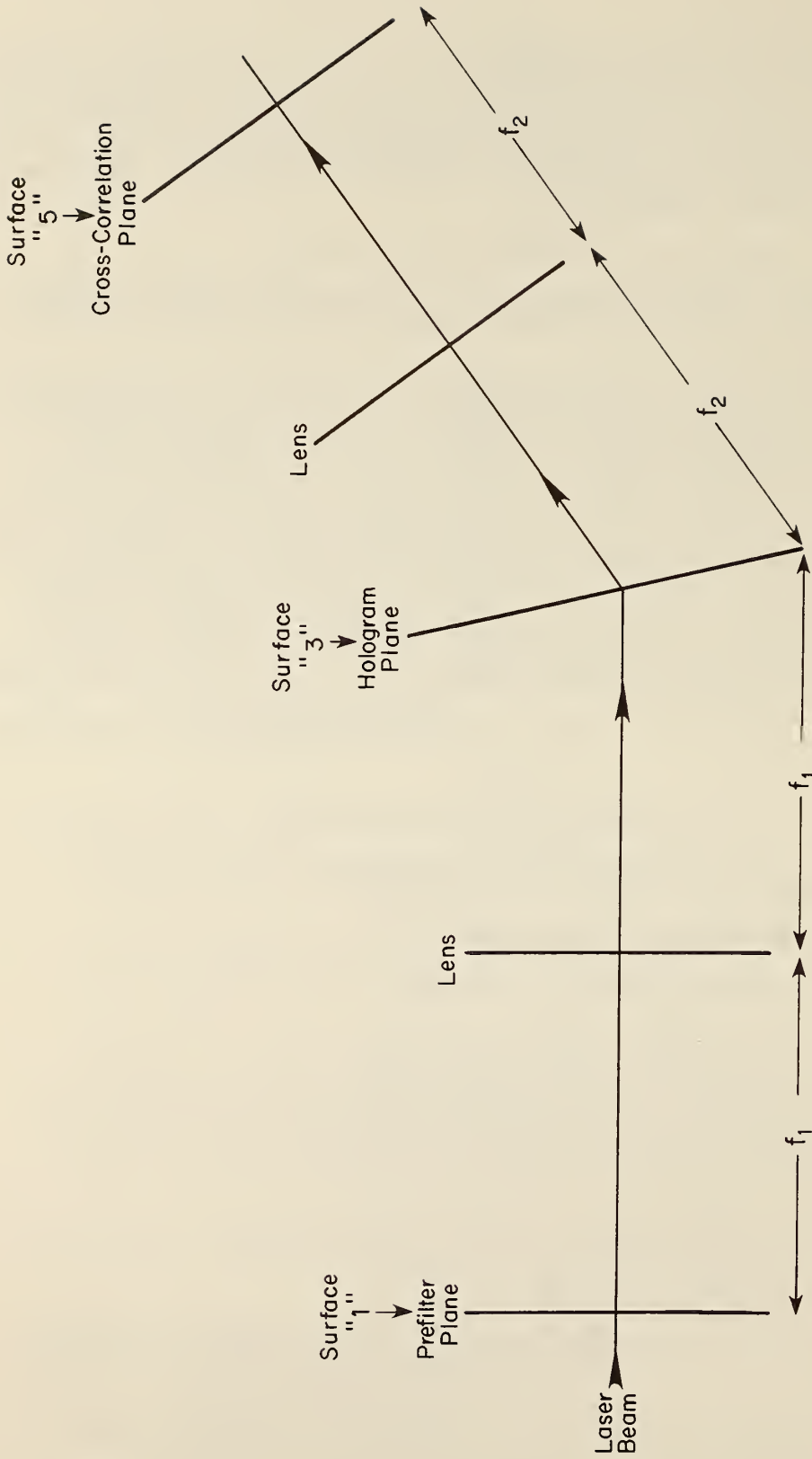


Figure 24. The basic beam profile measurement process.

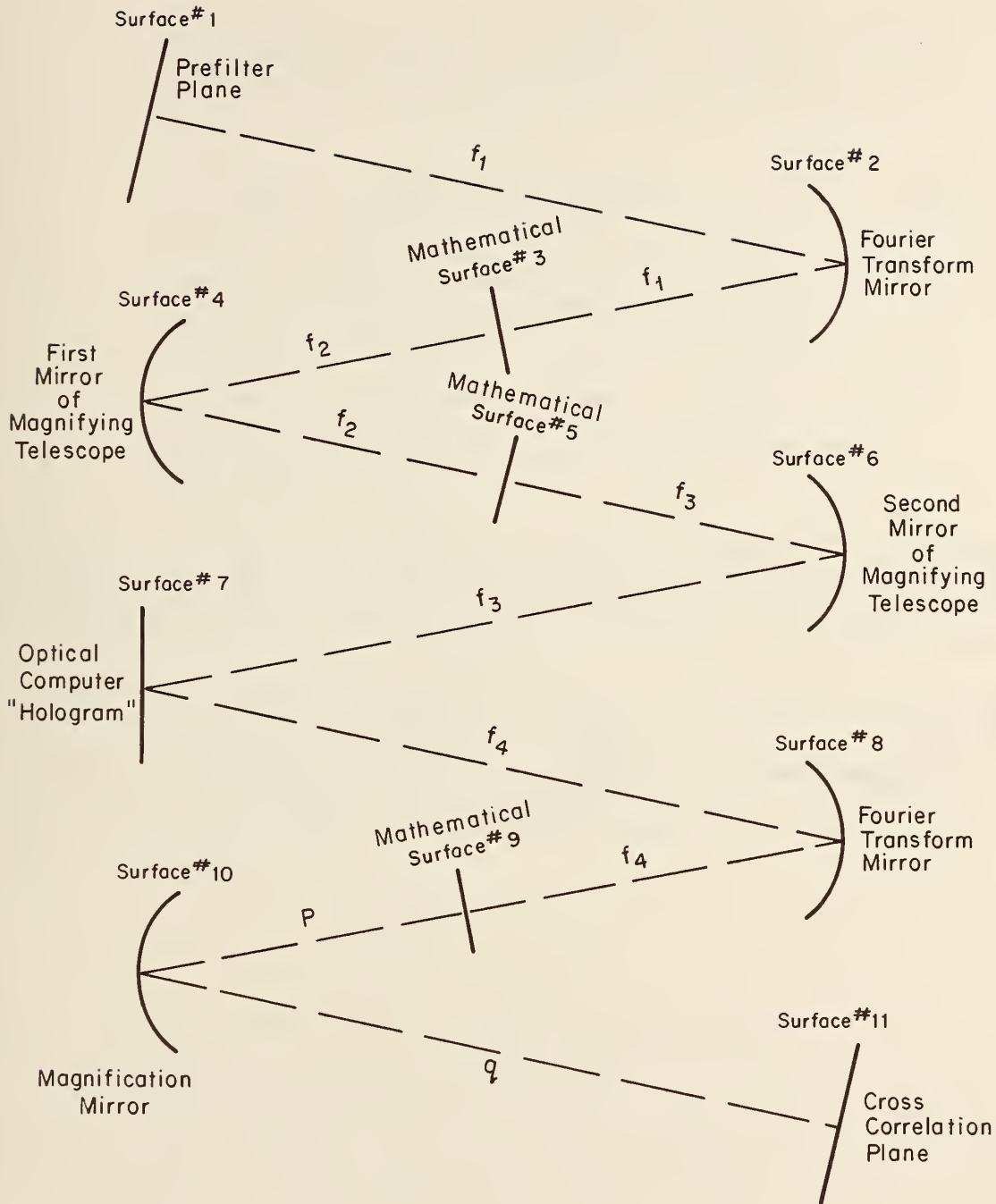


Figure 25. Beam profile measuring apparatus using reflection optics (not to scale).

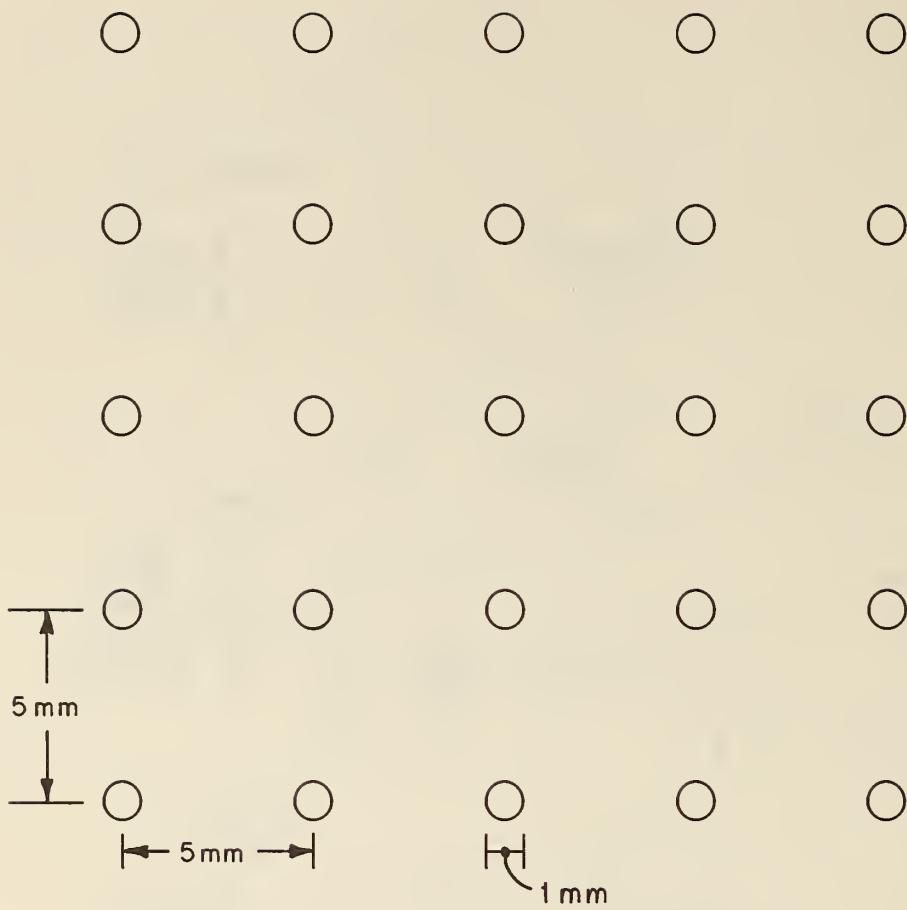


Figure 26. Beam sampling pattern in the prefilter plane.

- 8 This mirror creates the Fourier transform of the beams generated by the hologram pattern at surface 7. It is spaced one focal length, f_4 , from that surface. The radius of curvature of this mirror is about 2 m and is unchanged for those wavelengths of interest.
- 9 This surface is a cross-correlation plane and is located one focal length, f_4 , from the mirror at surface 8.
- 10 Here we have a magnification mirror placed a distance, p , from surface 9. Its radius of curvature is 2 m for 10.6 μm and 0.2 m for 1.06 μm . This mirror allows a match of the pattern in surface 9 to the distribution of the detectors in surface 11. This distance has $p=2$ m for 10.6 μm and 0.11 for 1.06 μm .
- 11 The detector pattern is shown in figure 27. We place detectors at each spot where only one or two beams contribute. The four-beam spots are not used. The distance from the magnification mirror to this array is q . For 1.06 μm , $q=1.1$ m, while for 10.6 μm , $q=2$ m.

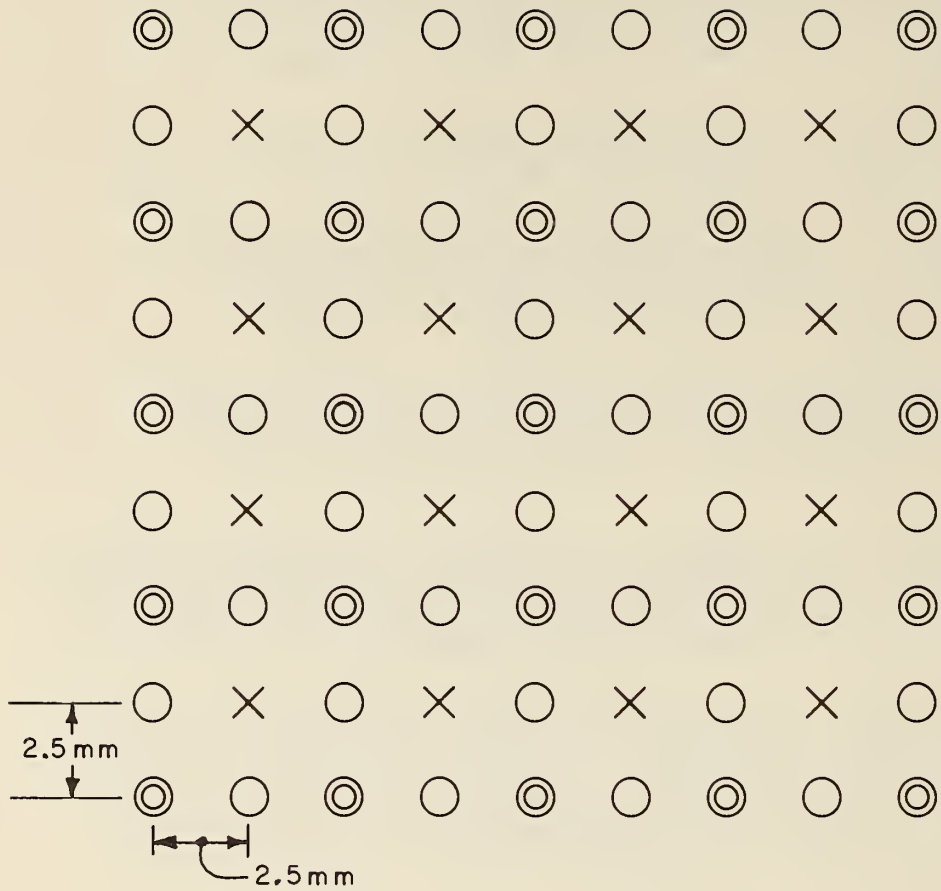
We have seen, briefly, the structure of the reflection unit; therefore, we now can discuss what is expected. There are four key points to note about this device: (1) the peak irradiance for this device for cw use; (2) the range of phase difference between a pair of sampling holes; (3) the particular dimensions (curvatures, focal lengths, etc.); and (4) the dynamic range for the carrier frequency permitted by a given physical setup.

Peak irradiance accepted by this reflection unit is fixed by the allowed peak irradiance for a solid copper surface that is not water cooled and that is required to show no significant change as a beam sampler. This irradiance is less than 100 kW/cm^2 for a cw signal of arbitrary time period. We assume the input beam is a plane wave with uniform irradiance at the prefilter and set the irradiance at each sampling hole at $I_o = 200 \text{ W}/\text{cm}^2$. The peak irradiance at surface 7 for that single hole is related to the incident irradiance as:

$$I_f = I_o \left(\frac{\pi a^2}{4 \lambda f_1 M_1} \right)^2, \quad (5.4.1)$$

where f_1 is the focal length of mirror 1, and $M_1 = f_3/f_2$ is the magnification of the telescope. For the nominal values given previously, the peak irradiance is $I_f = 0.0055 I_o = 1.1 \text{ W}/\text{cm}^2$ for the two setups at either 10.6 or 1.06 μm . If we assume the acceptance diameter for radiation at the prefilter is 10 cm, we find about 300 sampling holes within this diameter. For a plane wave, the peak irradiance at surface 7 can be increased as the square of the number of irradiated holes. Thus we can get $I_p = N^2 I_f = (300)^2 1.1 = 99 \text{ kW}/\text{cm}^2$, which is near the allowed peak irradiance.

If we wish to look at cw power beyond this range, three adjustments to the setup are possible. Make the sampling hole size, a , much smaller; make the effective focal length, Mf_1 , much larger; and make I_o smaller. The first change is controlled by the practical size of the apparatus. The last change is accomplished by using beam splitters in front of and/or behind the prefilter. These beam splitters should be gratings [27], if we want reflection optics. Using a grating between the prefilter and the first mirror allows us to use one of the higher diffraction orders as the collection of sampled beams. The nonideal features of these gratings are accounted for by appropriate calibration as suggested in subsection 4.4. The remaining issues for extremely high power are discussed in reference [25].



- × Four Beams contribute to this intensity
- Two Beams contribute to this intensity pattern. (phase here)
- ⊙ One Beam produces this intensity.

figure 27. Resulting spot pattern in the cross-correlation plane.

Phase Shift

The allowed dynamic range of phase shift between neighboring holes is controlled by the desired accuracy of the phase shift measurement. If we accept the nominal restriction of ± 0.1 wavelengths as chosen in this paper, then we have the following estimates for the dynamic range of the phase shift. With a designated spatial frequency as $b/(2\pi)$, the phase change across a single hole equals ba . The inferred phase shift between holes, assuming a constant gradient, equals cb . Since the hole size is $a = 1$ mm, and the spacing distance is $c = 5$ mm, the latter phase term is 5 times the former. This means a requirement of ± 0.1 wavelengths or less implies a change of ± 0.5 wavelengths or less between neighboring sampling holes. If we accept that the phase front need not exhibit a constant gradient, then the allowed phase change between neighboring holes can be many wavelengths. There is one penalty when this latter condition is present: the actual phase front is undetermined by the 2π modulus of the phase (see the calibration discussion in subsection 4.4 on this point).

Dimensions

The dimensions of this proposed reflection apparatus are somewhat arbitrary. A beam diameter of 10 cm was chosen because it represents a common beam size for many optical setups using laser beams of high power. The sampling frequency represents a compromise between the aperture of a detector versus that in the prefilter. Using a one-meter focal length means that the apparatus can be contained on a 2×4 m² holographic table. This scale is consistent with commercial equipment. The remaining dimensions, not detailed here, minimize the effects of various apertures and allow the mirrors and other units to be as small as possible so that their costs are not extravagant. (For example, a 20 cm (8 inch) mirror with one-meter focal length can cost \$1,000. We need five of these plus other equipment.) Reference [25] details the costs for this proposed system.

Carrier Frequency Range

To show briefly the allowed dynamic range of the carrier frequency (wavelength) for a given physical setup requires some mathematics and skipping of many details. The theory in reference [25] that accounts for the astigmatism and other such details shows the key derivations. We show the final results without the astigmatism using Gaussian beams.

The output electric field at the cross-correlation plane for a single beam from the prefilter and a selected diffraction beam from the hologram is:

$$U(\ell_1, \ell_2, \ell_x, \ell_y) = \frac{A_1(\ell_1, \ell_2)}{M} D(\ell_x, \ell_y) \exp\left\{\frac{ik}{2q} (x^2 + y^2) \left(\frac{1}{M_2} + 1\right)\right\} \\ * \exp\left\{-\frac{1}{M^2 \sigma_1^2} \left[\left[x + Mc\left(\ell_1 - \frac{\ell_x \lambda}{2\lambda_0}\right)\right]^2 + \left[y + Mc\left(\ell_2 - \frac{\ell_y \lambda}{2\lambda_0}\right)\right]^2 \right]\right\}. \quad (5.4.2)$$

The total magnification factor is $M = f_4 f_2 q / (f_3 f_1 p)$; the imaging magnification factor is $M_2 = q/p$; the x coordinate for the ℓ_1 th row of holes in the prefilter is $\ell_1 c$; the y coordinate for the ℓ_2 th row of holes in the prefilter is $\ell_2 c$; and $A_1(\ell_1, \ell_2)$ is the electric field strength at the (ℓ_1, ℓ_2) hole. The order of the diffraction process at the hologram is $\ell_x = \pm 1, 0$ for the x coordinate and $\ell_y = \pm 1, 0$ for the y coordinate. The half-width of the electric field at the prefilter is σ_1 ; the distance between the sampling holes is c ; and λ_0 is the nominal design wavelength for the hologram. The remaining symbols are shown in figure 25. Let $\lambda \equiv \lambda_0 + \Delta$ in the subsequent discussion on the dynamics of the allowed range of carrier frequency.

A detector in the cross-correlation plane at a point where $\ell_x = \ell_y = 0$ has only one beam contributing to its irradiance. In this case, the irradiance is:

$$I(\ell_1, \ell_2) = A_1 A_1^* \frac{D^*(0,0)D(0,0)}{M^2} * \exp \left\{ -\frac{2}{M^2 \sigma_1^2} \left[(x+Mc\ell_1)^2 + (y+Mc\ell_2)^2 \right] \right\} . \quad (5.4.3)$$

If we presume the detector captures all the above irradiance, the power at this detector is:

$$P(\ell_1, \ell_2) = \frac{\pi}{2} \sigma_1^2 [A_1(\ell_1, \ell_2) D(0,0)] [A_1^*(\ell_1, \ell_2) D^*(0,0)] . \quad (5.4.4)$$

A detector at a point where $\ell_2 = \ell_y = 0$ and $\ell_1 = \ell + 1$ with $\ell_x = -1$ has two beams contributing to make up the received power as:

$$P(\ell + \frac{1}{2}, 0) = P(\ell, 0) + P(\ell+1, 0) + 2e^{-F} (P(\ell, 0) * P(\ell+1, 0))^{1/2} \cos Q . \quad (5.4.5)$$

Here Q contains the relative phase. The mismatch from a designed wavelength λ_0 is shown by the F term as:

$$F = \frac{2}{M^2 \sigma_1^2} \left(\frac{Mc\Delta}{2\lambda_0} \right)^2 = \frac{1}{2} \left(\frac{c\Delta}{\sigma_1 \lambda_0} \right)^2 . \quad (5.4.6)$$

If we presume $F \leq 0.1$ for the carrier frequency shift to be insignificant for beam profile measurements of moderate accuracy, we find, given $c = 5$ mm and $\sigma_1 = 1$ mm, that the allowed fractional dynamic range for the carrier frequency is:

$$\left(\frac{\Delta}{\lambda_0} \right) \leq 0.009 . \quad (5.4.7)$$

The above illustrates how a carrier frequency shift affects a single pair of beams. The effect is similar for other pairs of beams. Clearly, for precise measurements, the carrier frequency should be measured simultaneously with the output from all detectors and used to unfold the time dynamics of the relative phase between various sampled beams. The above applies to both the transmission and reflection systems.

5.5 A Beam Profile System that Can Be Mass Produced

Reference [26] will detail this instrument which could be used in a feedback system for real-time control of a laser beam profile. Possible uses of this unit are in conjunction with laser sources in communication, welding, and high energy laser beam units. This subsection indicated the key concepts without the detailed mathematics. To make this unit useful, simplifications of the basic cross-correlation process are made. These changes make this unit both cheaper and more compact than the reflection system described in subsection 5.4 and the transmission unit defined by this paper. Of course, these changes make this unit less accurate and more restrictive in dynamic range for understandable output from the array of detectors at the crosscorrelation plane.

In figure 24, the essential holographic method shows five elements: the prefilter, the first lens or mirror for a Fourier transform, the hologram or filter for cross correlation, the second lens or mirror for Fourier transform, and the array of detectors in the cross-correlation plane. The holographic devices described previously in this paper require a total path length greater than $2 f_1 + 2 f_2$ or about 4 meters with a probable design set where $f_1 = f_2 = 1$ m. Clearly, this length is too large for convenient use in field conditions. Also, the number of distinct elements is significant; therefore, it is important to eliminate those that are unnecessary for the desired field instrument. If we degrade the general flexibility in beam profile measurement, then we can make significant simplifications to the unit shown in figure 24.

First, we eliminate the prefilter and the first lens. We directly illuminate the hologram with the beam. If the beam profile has some appropriate constraints, such as that the center of its peak should overlap the center of the hologram or the gradient of phase and intensity is small compared to the sampling frequency of the hologram, then the output of the detector at the cross-correlation plane may be used for real-time control of the beam profile. The elimination of the first lens reduces the unit's length by two focal lengths or two meters if $f_1 = 1$ m.

Second, we design an appropriate hologram and detector unit to accommodate beam inputs that do not have precise beam centering capability. The details of this hologram are technically complex. I indicate only the concepts. (They may change when the design is developed.)

(1) We subdivide the hologram into squares about 1 mm by 1 mm in size. We presume that the change in the irradiance and phase from square to neighboring squares is less than 5% for irradiance and less than 0.1 rad for the phase.

(2) We make a picket fence grating with 25% modulation and with the base parallel to the x axis in each square. This grating acts as a sampler and multiple beam generator. Each pattern for all squares has the same spatial frequency, perhaps $10^{-2} \text{ (mm)}^{-1}$. Each square has a different position in the y direction where an edge of a modulation peak crosses the square. This shift of location induces an additional phase shift in the beams generated by this grating. Having the same spatial frequency for each square ensures that all beams of a given diffraction order exit parallel to those in the other squares. These beams are deflected in the $\pm y$ direction. This process allows phase analysis of the beam profile.

(3) To get amplitude analysis of the beam profile, we need further filtering of the incident laser beam. To make the construction of a hologram cheap and simple, we may use either a second picket fence or a variable width slit. This pattern is parallel to the y axis and perpendicular to the x axis. Since we are interested only in the zero-order beam of deflection from this grating structure, we can change the spatial frequency, the modulation level, or the slit width of this pattern for each square. These changes accurately control the amount of power in the nondiffracted beam. The diffracted beams are deflected in the $\pm x$ direction.

Third, to minimize the size of the device, we mount the hologram either on a concave mirror for a reflection system or on the front flat surface of a plano-convex lens for the transmission system. This arrangement means that the first focal length distance is eliminated and only the second focal length remains. The choice of appropriate focal length depends critically on the beam profiles being measured and controlled by this unit; therefore, we have a fundamental length limit of f_2 . The lens or mirror causes the beams of a given diffraction order to be focused on a unique spot. This spot has both relative phase and amplitude information on the entire beam profile cross correlated with the hologram. Each spot has a different cross correlation; therefore, it is possible to realize some version of the orthogonal analysis mentioned in subsection 5.2.

Fourth, to complete the unit, a fixed detector at each spot with an appropriate capture cross section generates a voltage or current signal proportional to the laser power

received in the spot. The number of these detectors would be about 10 or less. The object here is to have a minimum number of orthogonal modes in the basic beam profile.

I conclude this subsection by noting that the hologram can be tailored to selected classes of beam profiles and clearly can be generated by using a step and repeat camera. The mass production feature is possible by replicating a master hologram with the above information stored appropriately.

6. CONCLUSIONS DRAWN FROM THE PROTOTYPE APPARATUS

As can be expected in the construction of a prototype device, problems arise such as:

(1) Due to the high absorption in the hologram, the diffraction efficiency as measured by the ratio of irradiance between the incident sampled laser beam and that at the final correlation plane, equals 0.1%.

(2) The mechanical instability of the translation mounts in the beam expander for the object beam destroys calibration stability.

(3) The nonlinearity in response to the irradiance in the vidicon unit even when it is not saturated, destroys linearity.

(4) The fact that the apparatus must be restructured for use at each new laser wavelength implies limited dynamic range of carrier wavelength.

(5) The "spurious" beams from each reflection and refraction reduce the available energy for observing the cross-correlation process.

(6) The optimum hole size in the prefilter and the spacing of these holes are unknown.

This section addresses each problem as numbered and suggests a solution. To prove that each suggestion is adequate requires construction of an appropriate unit incorporating the suggested solution.

(1) This 0.1% conversion efficiency is probably the most serious problem preventing simple application of this hologram technique. To increase this efficiency to 10% and better and to permit the unit to be used at 10.6 μm require construction of reflection holograms. There are three types that can be generated, namely kinoform [11], blazed [11], and binary [28] holograms. The former two have potential of 80-90% efficiencies; however, they require many stages of fabrication to obtain the proper etching of the reflection surface. The binary hologram requires only two stages of fabrication and achieves 10% efficiency. The technical trade-offs here are the number of fabrication steps, the complexity of the computer programs, and the resulting efficiency of the reflection hologram. The description of the reflection unit [25] details this trade-off. If the wavelength of the laser is in the near IR and visible, then phase holograms can permit transmission holographic techniques near 10% efficiency.

(2) The instability of the beam expander can easily be cured by using translation equipment that does not creep and that can be accurately reset; therefore, no further discussion is necessary.

(3) The nonlinearity of the vidicon unit can be cured only by replacing this unit with a different set of detectors. Four types of detectors exist which have sufficient sensitivity and signal-to-noise ratios. These detectors can respond linearly at 1 μW to 1 nW power levels with electronic noise levels less than 1% of the input signal and can be constructed in an array, one detector for each spot. The output signal of each detector filters the spatial dependence within each spot of the cross-correlation plane to give a single output. For visible wavelengths, silicon detectors have sufficient linearity and responsivity. Commercial literature suggests that, for the near infrared (1-3 μm) and for far infrared (3-30 μm), the Lead-Tin-Telluride detectors have sufficient linearity and responsivity. The pyroelectric detector can be used for all laser wavelengths provided that the acoustical noise in the background can be eliminated or made unimportant. Finally, over the UV and visible wavelengths, an array of photomultiplier or silicon

elements can be used for the detectors. Each wavelength range has detectors which do not necessarily exist as arrays; therefore, technical problems must be solved before these detectors are available for use in a hologram unit. Also, reviewing the available commercial units shows that the impulse response for these detectors varies radically from group to group; hence, each must be chosen carefully to provide desired time response. In brief, the choice of detector is sensitive to wavelength, power level, and signal shape of the laser pulse.

Note: The vidicon, as presently constructed, provides convenient qualitative results. This unit allows critical alignment of the elements in the beam profile apparatus. If the nonlinearity, apparently present in the response, could be removed by some appropriate electronics or change in detectors and if the total spatial response at a given spot could be integrated by appropriate electronics or computer analysis, then the vidicon could economically be substituted for the detector array in a beam profile apparatus. If the desired time response for the beam profile apparatus is faster than 1/60 second, then current TV framing will not be adequate and will have to be substantially modified. Parallel processing becomes necessary.

(4) There are two effects in the beam profile unit which modify the precision of the unit as the wavelength of the laser beam changes.

If the beam profile apparatus has refractive optics, then there is a wavelength dependence in the various indices of refraction of the optics. This wavelength dependence can be completely avoided by using reflective optics (see subsection 5.4 for an example).

An effect remains because the transverse dimension of the Fourier transform at the hologram is wavelength dependent. One method to eliminate this effect requires changing either the hologram or the Fourier transform lens to make the appropriate scale change for each wavelength. This approach minimizes the number of reflective surfaces and simplifies the number of optical components. However, a reflection hologram with appropriate hills and valleys in the surface is not commercially available. Development of such a hologram will be expensive. The change in the Fourier transform lens can preserve the convenient dimensions of the apparatus.

A second method to compensate for wavelength dependence would keep the same hologram for some wavelength ranges and would keep the apparatus a fixed size by using appropriate telescopes in front of and behind the holograms to scale the Fourier transform and cross correlation. The curvature of the phase front produced by the telescope in front of the hologram must match the curvature of the phase front recorded in the hologram; otherwise, there will be a significant imprecision at the resulting spots of the cross-correlation plane. The telescope behind the hologram need not match the curvature of the phase front for all wavelengths. To realize these constraints requires appropriate design of the telescopes which correspondingly requires appropriate use of the lens equation as discussed in appendix A.

(5) To minimize the laser power lost from each surface requires using either anti-reflecting coatings on the optics or high quality reflective optics. The former increases the wavelength sensitivity of the device; therefore, coatings should be used only if refractive optics are the most economic for the apparatus and if a single wavelength is appropriate.

(6) The hole size, number, and pattern in the prefilter determine the final precision, the laser power density and heating of the hologram, and the cost of the beam profile apparatus. The larger these holes are, the greater the received power is at the cross-correlation plane and, hence, the simpler the detector units can be. Unfortunately, with increasing hole size the apparatus becomes more sensitive to additional details in the relative position of each hole as well as to the intensity and phase variation across each hole. For example, figure 18 shows the secondary spots generated because the hole size in the prefilter is slightly too large. The more holes in the prefilter apparatus, the greater is the resolution of the beam profile; however, this fact implies a corresponding substantial increase in the size and cost of the detector array. The above effects can complicate the mathematical model needed to deduce the phase and amplitude in the beam profile measurement. There are no simple criteria known that can fix the size, number,

and pattern of the holes; consequently, this report gives no solution to this problem. However, if a measurement problem has a well-defined class of beam profiles, then the choice of sampling size, etc., can be chosen appropriately.

If the problems found in this prototype apparatus can be considered as soluble, then the concepts discussed in this report can be applied to measure, in real time, the amplitude and phase of a laser beam at a prescribed prefilter plane. For those interested in an integrated measurement of a laser pulse, see reference [29].

In conclusion, by proper construction of the hologram and by using appropriate types of prefilters and optics, it appears possible to develop a device that can measure accurately changes in amplitude and phase of a laser beam profile for a particular wavelength in times shorter than 1 ns. The detailed comparison of the relative value of the Hartmann plate versus the holographic method for these speeds is discussed in [25].

7. ACKNOWLEDGMENTS

The author wishes to thank the following persons who provided him with appropriate advice: Mr. Aaron Sanders, Dr. Richard Smith, and Dr. Matt Young at NBS, Boulder. Further, the course on "Coherent Optics" by Professor E. N. Leith and staff at the University of Michigan helped the author develop "hands on" experience in Fourier optics and holography.

The author wishes to thank the following individuals for the fine work on typing and setting up this paper: Sheila R. Aaker, Margaret L. Woolley, and Arlene Miller.

The author also wishes to thank Phyllis O'Rourke for her helpful editorial advice.

8. REFERENCES

- [1] Yoshida, A., and Asakura, T., A simple technique for quickly measuring the spot size of Gaussian laser beams, *Optics and Laser Technology*, 273 (Dec. 1976).
- [2] Saunders, J. B., *J. Res. Nat. Bur. Stand. (U.S.)* 65B, 239 (1961).
- [3] Day, G. W., and Stubenrauch, C. F., The focal plane transform technique for obtaining far-field laser beam profiles, NBS Technical Report #1001 (1977).
- [4] Angelbeck, A. W., and McClug, W. C., Laser wavefront analyzer using sliding reference interferometry, NTIS Code #AD-922 980, Report (1974).
- [5] Skolnick, M. L., and Gowrinathan, S., Laser wavefront analyzer using frequency offset interferometry, NTIS Code #AD-922 980, Report (1974).
- [6] Gillespie, R. W., Wick, R. V., and Saxman, A. C., Laser wavefront profiling technique for pulse radiation, NTIS Code #AD-A011 944/6ST Report (1975).
- [7] Pfeffer, M. K., and Loomis, J. S., Interferometric measurements of windows on an environmental chamber, Third Conference on High Power Infrared Laser Window Material, III: Surface, Coatings, AFCRL-TR-74-0085 (111) Special Report #174, p. 1191 (1973).
- [8] Wick, R. V., Saxman, A. C., and Blankinship, E. A., Real time intensity profiling and beam divergence measurement of a laser beam, Proc. Technical Program Electro-Optical System Design Conference, p. 294, (1973).
- [9] Block, W., Nanosecond response time, room temperature infrared detection with thin film metal, University of Illinois at Urbana, University Microfilms International, Ann Arbor, Michigan (1973).
- [10] Skipper, J. D., Goranson, R. W., and Schaub, C. M., Application manual - Position sensing detector for the far infrared, Dynallectron Corporation, P. O. Box 18068, Kirtland Air Force Base Station, Albuquerque, New Mexico 87115 (1975).
- [11] Cathey, W. T., *Optical Information Processing and Holography* (John Wiley & Sons, New York, 1974).
- [12] Young, M., *Optics and Lasers, An Engineering Physics Approach* (Springer-Verlag, 1977). A useful summary of various aspects of optics and lasers.
- [13] Vander Lugt, Anthony, Coherent optical processing, *Proc. IEEE* 62, 1300 (Oct. 1974).
- [14] Goodman, J. W., *Introduction to Fourier Optics* (McGraw-Hill, New York, 1968).
- [15] Lee, Sing H., Review of coherent optical processing, *Applied Physics* 10, 203 (1976).
- [16] Leith, Emmet N., Quasi-holographic techniques in the microwave region, *Proc. IEEE* 59, 1305 (Sept. 1971).
- [17] Gaskill, J. D., Optics for the electronics engineer, *Electro-Optical System Design*, 22 for part I (Feb. 1977), 28 for part II (June 1977), 43 for part III (June 1977).
- [18] Koglnik, H., and Li, T., Laser beam and resonators, *Proc. IEEE* 54, 1312 (Oct. 1966).
- [19] Ditchburn, R. W., *Light*, Interscience (New York, pp. 371-372, 1958).
- [20] Pennington, K. S., and Harper, J. S., Techniques for producing low-noise, improved efficiency holograms, *Applied Optics* 9, 1643 (July 1970).
- [21] Newport Research Corporation, Short Form Catalog, Film Selection Guide, 29. We arbitrarily chose Holographic plate Type 120-02 by Kodak.

- [22] Kodak Pamphlet No. P-311, Describes how to develop the Type 120 plate for transmission holograms.
- [23] Upatnieks, Juris, Coherent optics laboratory note, Short course at the University of Michigan (1976).
- [24] A private communication with Dr. Stephen Benton of the Polaroid Corporation helped me decide what photographic procedures to follow among the numerous methods in the literature.
- [25] Johnson, E. G., Jr., Design of the reflection apparatus for beam profile measurements (to be published as an NBS Technical Note).
- [26] Johnson, E. G., Jr., Design of a field instrument for beam profile measurements (to be published as a NBSIR).
- [27] O'Neil, R. W., Kleiman, H., Marquet, L. C., Kilcline, C. W., and Northam, D., Beam diagnostics for high energy pulsed CO₂ laser, Applied Optics 13, 314 (Feb. 1974).
- [28] Gallagher, N., Jr., Angus, J. C., Coffield, F. E., Edwards, R. V., and Mann, J. A., Jr., Binary phase digital reflection holograms: Fabrication and potential applications, Applied Optics 16, 413 (Feb. 1977).
- [29] Miyamoto, T. and Yasmura, K., Measurement of the beam parameters of a laser beam and its diffraction field, using a hologram, Applied Optics 10, 161 (Jan. 1971).
- [30] Born, Max and Wolf, Emil, Principles of Optics (Pergamon Press Inc., New York, Third ed., 1965).
- [31] Handbook of Mathematical Functions with Formulas, Graphs, and Mathematical Tables (Edited by Milton Abramowitz and Irene A. Stegun, National Bureau of Standards, Applied Mathematics Series 55, pp. 229-233, for the si(z) and Ci(z) functions).

APPENDIX A. IMPORTANT FORMULAS FOR FOURIER OPTICS

We follow the conventions and definitions given in reference [11] to discuss three formulas of interest: the Fourier transform, the imaging formula, and the effects of displacement formula.

A.1 The Fourier Transform

$U_1(x,y)$ is a scalar of the electric field where all polarization effects are ignored. The fundamental formula using the approximations of Fourier optics for wave propagation over a distance z is:

$$U_2(x_2, y_2) = \frac{e^{ikz}}{i\lambda z} \iint dx_1 dy_1 U_1(x_1, y_1) h(x_2 - x_1, y_2 - y_1; z), \quad (A.1)$$

where

- (a) λ is the wavelength of the radiation;
- (b) x_1, y_1 are the transverse coordinates of a plane for the initial surface "1";
- (c) x_2, y_2 are the transverse coordinates of a second plane for the final surface "2" which is parallel to surface "1";
- (d) $k \equiv \frac{2\pi}{\lambda}$ is the wave number; and
- (e) $h(x,y; z) \equiv \exp \left[\frac{ik}{2z} (x^2 + y^2) \right]$ is the Fourier optics approximation for the transfer function between the surfaces "1" and "2." (A.2)

The first formula of interest using a simple lens arises when surface "3" acts as the Fourier transform of surface "1." A convex lens of focal length f , as shown in figure A.1, generates this transform. The formula, which ignores aperturing by the lens and uses the distances d_1 and d_2 , as shown in figure A.1, is:

$$U_3(x_3, y_3) = \frac{w}{i\lambda d_1 d_2} h[x_3, y_3; d_2/(1-w/d_2)]$$

$$* \iint dx_1 dy_1 U_1(x_1, y_1) h[x_1, y_1; d_1/(1-w/d_1)]$$

$$* \exp \left[-\frac{ikw}{d_1 d_2} (x_1 x_3 + y_1 y_3) \right], \quad (A.3)$$

where $\frac{1}{w} = \frac{1}{d_1} + \frac{1}{d_2} - \frac{1}{f}$ and where the $\exp [i(kz + \phi)]$ factor is suppressed as irrelevant.

The ϕ represents the phase shift due to the presence of a lens. Here $z = d_1 + d_2$.

The simplest Fourier transform case has $d_2 = f$ or $w = d_1$ as well as $d_1 = f$. In this case:

$$U_3(x_3, y_3) = \frac{1}{i\lambda f} A_1(u, v), \quad (A.4)$$

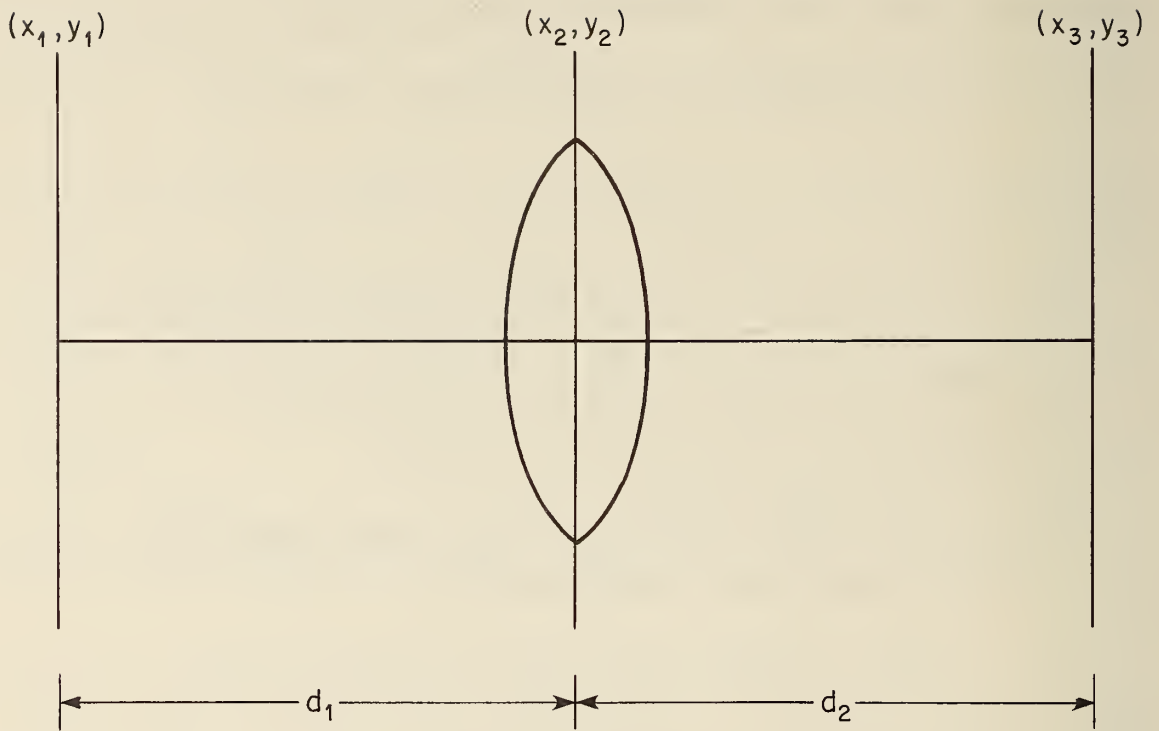


Figure A.1 Relationships between surface "1," "2," and "3" for a simple lens.

where the spatial frequencies u and v are given as:

$$u \equiv \frac{x_3}{\lambda f}, \text{ and } v \equiv \frac{y_3}{\lambda f},$$

and where the Fourier transform is defined as:

$$A_1(u, v) \equiv \iint dx_1 dy_1 U_1(x_1, y_1) \exp[-i2\pi(ux_1 + vy_1)] \quad (A.5)$$

A.2 The Imaging Formula

The second lens formula uses a lens to form a scaled image of the radiation pattern at surface "1." Here the distances between surface "3" and "1" satisfy:

$$\frac{1}{d_1} + \frac{1}{d_2} = \frac{1}{f}. \quad (\text{Figure A. 1 still applies for definitions.}) \quad (A.6)$$

The simplest image formulation assumes no aperturing effects by the lens; therefore, an image law for Fourier optics is:

$$U_3(x_3, y_3) = \frac{1}{M} h[x_3, y_3; d_2/(1+1/M)] U_1\left(-\frac{x_3}{M}, -\frac{y_3}{M}\right)$$

where $M = d_2/d_1$ and again the $\exp [i(kz + \phi)]$ phase factor has been suppressed. M is the magnification of the image at surface "3" relative to surface "1."

Further, note that the radius of curvature of the phase front for the radiation at surface "3" is increased from the radius of curvature for the radiation at surface "1" by the phase factor in $h(x_3, y_3; R)$ where $R \equiv d_2/(1 + 1/M)$ is an effective radius of curvature. This phase curvature has very important consequences in the design of a beam profile apparatus.

A.3 The Displacement Formulas

To identify quantitatively the location of the correct Fourier plane requires knowledge of the behavior of a Fourier transform under transverse displacement of the original radiation pattern at surface "1." We show these effects for the Fourier transform in one dimension, which is:

$$G(u) = \int dx g(x) \exp[-i2\pi xu], \quad (A.8)$$

where $g(x)$ represents the electric field distribution showing one spatial dimension exiting from surface "1." If the radiation pattern moves by a distance a along the x -axis and the phase changes by c , the electric field pattern $g(x)$ becomes $g(x-a) \exp[icx]$. This new form for the field has the following Fourier transform at surface "3":

$$G[u-c/2\pi] \exp [-i2\pi au + iac]. \quad (\text{A.9})$$

This formula demonstrates that a rigid transverse displacement of a spatial field pattern (for example, the two pinholes discussed in the text) shows no change in the position and shape of the intensity distribution of the transform of that field pattern. However, shifting the phase by c causes a corresponding shift in position of the Fourier transform by $c/2\pi$. One can cause this change by bending the angle with which the incident beam illuminates the original pattern, such as the true pinholes at surface "1."

APPENDIX B. THE DIFFRACTION DETAILS OF A SQUARE HOLE

Making proper beam profile measurements by either the mirror scan, the Hartmann plate, or the holographic method depends on understanding and using appropriate diffraction patterns from combinations of selected holes. There are two shapes that demonstrate the necessary details and are easily realizable, namely, the square and circular holes [30]. Appendix C details the key features for the circular hole and this appendix details those for the square hole.

To understand the diffraction pattern in detail for a single square hole, we represent this hole as an electric field $U_s(x_1, y_1)$.

Here:

$$U_s(x_1, y_1) = A_o * \Pi[(x_1 - g_\ell)/a] \Pi[(y_1 - h_\ell)/a] \\ * \exp \left\{ i[b_\ell(x_1 - g_\ell) + c_\ell(y_1 - h_\ell) + d_\ell] \right\}, \quad (\text{B.1})$$

where

- A_o is a convenient reference field (it has the dimensions of $[\text{watts}/(\text{mm})^2]^{1/2}$);
- g_ℓ is the coordinate for the center of the ℓ th hole along the x_1 axis;
- h_ℓ is the coordinate for the center of the ℓ th hole along the y_1 axis;
- ℓ is the label for the ℓ th hole;
- $b_\ell = b_{1\ell} + ib_{2\ell}$ is a complex number characterizing the average gradient of the phase front and intensity profile along the x_1 axis over the ℓ th hole; (here $b_{1\ell}$ is the real part of b_ℓ and $b_{2\ell}$ is the imaginary part);
- $c_\ell = c_{1\ell} + ic_{2\ell}$ is a complex number characterizing the average gradient of the phase front and intensity profile along the y_1 axis over the ℓ th hole;
- $d_\ell = d_{1\ell} + id_{2\ell}$ is a complex number that characterizes the average phase and intensity at the center of the ℓ th hole; and finally, $\Pi[u]$ is defined to be:

$$\begin{aligned}
\Pi[u] &= 1 && \text{if } |u| < 1/2, \\
&= 0 && \text{if } |u| > 1/2, \text{ and} \\
&= 1/2 && \text{if } |u| = 1/2.
\end{aligned}
\tag{B.2}$$

B.1 What this Appendix Presents

For efficient discussion in section 2, the subsection B.2 derives the conditions as well as the form for the far field of an arbitrary square aperture driven by the field pattern in eq (B.1). In addition, the total power received by an adjustable aperture at the far field is detailed here to show the reader how large this aperture must be to capture a significant fraction of the laser power. Because this far-field pattern is used differently by each method for beam profile measurements, corresponding changes in the convenience, precision, and dynamic range for each technique result. Understanding this far-field pattern provides the data base for discussion in section 2 for each of those changes induced by each method.

To utilize correctly the Fourier optics and the aperturing process, the Fourier transform of a given electric field must be known. Therefore, this subsection derives the explicit formulas of this Fourier transform pattern for a square hole aperture with the illumination represented by eq (B.1). The results are almost identical to those obtained in the far-field case.

B.2 The Far-field Diffraction Pattern

Using the assumed form U_s in eq (B.1) for U_1 , eq (A.1) can be rewritten as:

$$\begin{aligned}
U_2(x_2, y_2) &= \frac{e^{ikz}}{i\lambda z} A_0 \int_{-\frac{a}{2} + g_\ell}^{\frac{a}{2} + g_\ell} dx_1 \int_{-\frac{a}{2} + h_\ell}^{\frac{a}{2} + h_\ell} dy_1 e^{i[b_\ell(x_1 - g_\ell) + c_\ell(y_1 - h_\ell) + d_\ell]} \\
&\quad * \left\{ \exp\left[\frac{ik}{2z}(x_2^2 + y_2^2)\right] \exp\left[\frac{-ik}{z}(x_2 x_1 + y_2 y_1)\right] \exp\left[\frac{ik}{2z}(x_1^2 + y_1^2)\right] \right\}.
\end{aligned}
\tag{B.3}$$

If we define $x_1 \equiv u_1 + g_\ell$, $y_1 \equiv v_1 + h_\ell$, $x_2 \equiv u_2 + g_\ell$, and $y_2 \equiv v_2 + h_\ell$, then eq (B.3) can be rewritten as:

$$\begin{aligned}
U_2(u_2, v_2) &= \frac{e^{ikz}}{i\lambda z} \int_{-\frac{a}{2}}^{\frac{a}{2}} du_1 \int_{-\frac{a}{2}}^{\frac{a}{2}} dv_1 e^{i[b_\ell u_1 + c_\ell v_1 + d_\ell]} A_0 \\
&\quad * \left\{ \exp\left[\frac{ik}{2z}(u_2^2 + v_2^2) - \frac{ik}{z}(u_1 u_2 + v_1 v_2)\right] \exp\left[\frac{ik}{2z}(u_1^2 + v_1^2)\right] \right\}.
\end{aligned}
\tag{B.4}$$

The far-field condition for the beam coming out of the ℓ th aperture occurs when the largest $|u_1| = |v_1| = \frac{a}{2}$, and the distance z is such that:

$$\frac{k}{2z} \left[\left(\frac{a}{2}\right)^2 + \left(\frac{a}{2}\right)^2 \right] \leq \frac{\pi}{10} \quad \text{or } z \geq \frac{a^2}{\lambda} 2.5.
\tag{B.5}$$

This approximation presumes we can neglect 1/20th of wavelength changes in the phase front. This is the far-field criterion for this entire paper. If this criterion is satisfied, then eq (B.4) can have the second exp term in the bracket, { }, set equal to one, and the integral becomes:

$$U_2(u_2, v_2) = e^{ikz} \exp\left(\frac{ik}{2z}(u_2^2 + v_2^2)\right) e^{id_{\ell}} a^2 A_0 \\ * \operatorname{sinc}\left[\left(\frac{u_2}{\lambda z} - \frac{b_{\ell}}{2\pi}\right)a\right] \operatorname{sinc}\left[\left(\frac{v_2}{\lambda z} - \frac{c_{\ell}}{2\pi}\right)a\right]. \quad (\text{B.6})$$

Here, the function $\operatorname{sinc}(u) \equiv \frac{\sin(\pi u)}{\pi u} = \operatorname{sinc}(-u)$. (B.7)

If we define

$$\zeta_1 \equiv \left(\frac{x_2 - g_{\ell}}{\lambda z} - \frac{b_{1\ell}}{2\pi}\right)a, \quad \zeta_2 \equiv \left(\frac{b_{2\ell}}{2\pi}\right)a, \\ \eta_1 \equiv \left(\frac{y_2 - h_{\ell}}{\lambda z} - \frac{c_{1\ell}}{2\pi}\right)a, \quad \eta_2 \equiv \left(\frac{c_{2\ell}}{2\pi}\right)a, \text{ and} \\ I_f \equiv A_0^2 \left(\frac{a}{\lambda z}\right)^2 e^{-2d_{2\ell}}; \quad (\text{B.8})$$

then the intensity pattern for the far field can be written as:

$$I[\zeta_1, \eta_1] = I_f \operatorname{sinc}[\zeta_1 + i\zeta_2] \operatorname{sinc}[\zeta_1 - i\zeta_2] * \operatorname{sinc}[\eta_1 + i\eta_2] \operatorname{sinc}[\eta_1 - i\eta_2]. \quad (\text{B.9})$$

From this pattern we can determine the following: (1) The irradiance pattern is symmetric about either inversion $\zeta_1 \rightarrow -\zeta_1$ or $\eta_1 \rightarrow -\eta_1$ or both. (2) The change in either $\zeta_2 \rightarrow -\zeta_2$ or $\eta_2 \rightarrow -\eta_2$ causes no change in the irradiance pattern; therefore, the far field has no information about the sign of the gradient of irradiance at the square hole aperture. (3) The coordinates for peak irradiance have $\zeta_1 = \eta_1 = 0$. If ζ_2 and η_2 are small enough, the peak irradiance is:

$$I(0,0) = I_f \left[1 + \frac{\pi^2}{6} \zeta_2^2\right]^2 \left[1 + \frac{\pi^2}{6} \eta_2^2\right]^2. \quad (\text{B.10})$$

And finally (4) the points of minimum irradiance have $\zeta_1 = n_1$ and $\eta_1 = n_2$, where n_1 and n_2 are nonzero integers. These irradiances are approximately:

$$I(n_1, n_2) = \frac{I_f \zeta_2^2 \eta_2^2}{[n_1^2 + \zeta_2^2][n_2^2 + \eta_2^2]}. \quad (\text{B.11})$$

Note that if ζ_2 and η_2 are both zero, these minimum irradiances are lines defined by $\zeta_1 = n_1$ with η_1 arbitrary and by $\eta_1 = n_2$ with ζ_1 arbitrary. Again n_1 and n_2 are arbitrary nonzero integers.

Knowing the power captured by a finite aperture detector at the far field defines the allowed procedure for measurement of this irradiance pattern. Thus, the power captured by a square aperture detector with edge at $A/2$ and centered at $\zeta_1 = \eta_1 = 0$ for the ℓ aperture is:

$$P_\ell = \int_{-\frac{A}{2}}^{\frac{A}{2}} du_2 \int_{-\frac{A}{2}}^{\frac{A}{2}} dv_2 I(\zeta_1, \eta_1) \quad . \quad (\text{B.12})$$

We define:

$$H(A_1, \zeta_2) \equiv \int_{-A_1}^{A_1} d\zeta_1 \operatorname{sinc}[\zeta_1 + i\zeta_2] \operatorname{sinc}[\zeta_1 - i\zeta_2] \quad , \quad (\text{B.13})$$

with

$$A_1 \equiv \frac{Aa}{2\lambda z} \quad . \quad (\text{B.14})$$

Thus, the power measured is:

$$P_\ell = I_f H[A_1, \zeta_2] H[A_1, \zeta_2] \quad . \quad (\text{B.15})$$

To get a convenient form for H in terms of basic functions that can be generated easily on a computer, we manipulate H . First, we note that $H[A, \zeta] = H[A, -\zeta] = H[A, |\zeta|]$. Hence, with $\zeta > 0$ for the remaining discussion:

$$\begin{aligned} H[A, |\zeta|] &= \int_{-A}^A d\zeta_1 \frac{[\cosh(2\pi\zeta) - \cos(2\pi\zeta_1)]}{2\pi^2 [\zeta_1^2 + \zeta^2]} \\ &= \frac{1}{\pi^2} \cosh(2\pi\zeta) \frac{1}{\zeta} \tan^{-1} \left(\frac{A}{\zeta} \right) - \frac{1}{2\pi^2} \int_{-A}^A d\zeta_1 \frac{\cos(2\pi\zeta_1)}{\zeta_1^2 + \zeta^2} \quad . \quad (\text{B.16}) \end{aligned}$$

H can be further changed by noting the integral in eq (B.16) equals $\frac{\pi}{\zeta} e^{-2\pi\zeta} - 2g(A, \zeta)$.

Here:

$$g(A, \zeta) = \int_A^\infty d\zeta_1 \frac{\cos 2\pi\zeta_1}{\zeta_1^2 + \zeta^2} \quad . \quad (\text{B.17})$$

By shifting the range of integration in g :

$$\begin{aligned} g(A, \zeta) &= \int_0^\infty \frac{dx [\cos 2\pi(x+A)]}{(x+A)^2 + \zeta^2} \\ &= \cos(2\pi A) \int_0^\infty \frac{dx \cos(2\pi x)}{(x+A)^2 + \zeta^2} - \sin(2\pi A) \int_0^\infty \frac{dx \sin(2\pi x)}{(x+A)^2 + \zeta^2} \quad . \quad (\text{B.18}) \end{aligned}$$

These two integrals, which can be found in Fourier transform tables, imply:

$$g(A, \zeta) = \frac{1}{2\zeta} \left(\begin{array}{l} \sinh(2\pi\zeta) [\text{si}(z_1) + \text{si}(z_1^*)] \\ - i \cosh(2\pi\zeta) [\text{Ci}(z_1) - \text{Ci}(z_1^*)] \end{array} \right), \quad (\text{B.19})$$

where:

$$z_1 \equiv (A+i\zeta)2\pi \text{ and } z_1^* = (A-i\zeta)2\pi, \quad ,$$

and where $\text{si}(z)$ and $\text{Ci}(z_1)$ are defined as sin and cos integrals in reference [31].

Therefore, H becomes:

$$\begin{aligned} H[A_1, \zeta_2] &= \frac{1}{\pi^2 \zeta_2} \left\{ \cosh(2\pi\zeta_2) \tan^{-1} \left(\frac{A_1}{\zeta_2} \right) - \frac{\pi}{2} e^{-2\pi\zeta_2} \right\} \\ &+ \frac{1}{\pi^2 2\zeta_2} \left\{ \begin{array}{l} \sinh(2\pi\zeta_2) [\text{si}(z_1) + \text{si}(z_1^*)] \\ - i \cosh(2\pi\zeta_2) [\text{Ci}(z_1) - \text{Ci}(z_1^*)] \end{array} \right\}. \end{aligned} \quad (\text{B.20})$$

If we set $\zeta_2 = 0$, H can be reduced to:

$$H[A_1, 0] = 1 + \frac{2}{\pi} \text{si}(2\pi A_1) + \frac{1}{\pi^2} \frac{(\cos 2\pi A_1 - 1)}{A_1}. \quad (\text{B.21})$$

There are several values of A_1 which are of interest in the design of an arbitrary beam profile apparatus. The first minimum of irradiance has $A_1 = 1$. Here $H[1, 0] = 0.90$. To make $H = 0.98$ requires $A_1 = 5$. Since H appears twice in the captured power eq (B.15), the amount of power captured from the original power, $P_{T\ell}^*$, transmitted through the ℓ th aperture is $P_\ell = 0.96 P_{T\ell}$ for $A_1 = 5$ and $0.8 P_{T\ell}$ for $A_1 = 1$.

In addition to the above effects, there can be significant interference between the far-field patterns from neighboring sampling apertures. For example, for $\eta_1 = 0$ and $\zeta_1 = \pm 5.5$, which locate the first peak just outside the far field apertures for $A_1 = 5$, we find this amplitude is 6% of the amplitude at peak irradiance, $\zeta_1 = \eta_1 = 0$. This fact means this power in the noncaptured part of the far field can interfere with the neighboring far-field pattern from the other apertures. To be sure of complete separation between patterns so that no interference effects are greater than 1% requires $|\zeta_1| \geq 32$. This constraint can be a significant limit on the allowed spatial sampling frequency for the Hartmann plate method.

B.3 The Fourier Transform Pattern

Equation (A.4) shows that the Fourier transform pattern is:

$$U_2(x_2, y_2) = \frac{1}{i\lambda f} \int dx_1 dy_1 U_1(x_1, y_1) e^{-\frac{i2\pi}{\lambda f} (x_1 x_2 + y_1 y_2)}. \quad (\text{B.22})$$

If U_s from eq (B.1) is used for each aperture, and the spherical phase front factor,

$$\exp\left[\frac{ik}{2z}(u_2^2 + v_2^2)\right], \quad (\text{B.23})$$

is dropped from eq (B.4), then eq (B.20) has the same functional form as the far-field form of eq (B.6) except that the focal distance, f , for the mirror or lens replaces the distance, z , from the sampling plate. We write the Fourier transform $U_2(x_2, y_2)$ as:

$$U_2(x_2, y_2) = \frac{A_o e^{i[\phi + d_l + \theta]}}{i\lambda f} a^2 \operatorname{sinc}\left[\left(\frac{x_2}{\lambda f} - \frac{b_l}{2\pi}\right)a\right] \operatorname{sinc}\left[\left(\frac{y_2}{\lambda f} - \frac{c_l}{2\pi}\right)a\right], \quad (\text{B.24})$$

where $\theta = \frac{-k}{f}(x_2 g_l + y_2 h_l)$, and $\phi = 2kf + (n-1)tk$. Here n is the index of refraction for the lens or mirror and t is the thickness of that same lens. We see that most features of the far-field pattern apply equally to the Fourier transform field except for the spherical wave front term (eq (B.2)), the plane wave phase shift defined by θ , and the fact that the x_2 and y_2 are used instead of u_2 and v_2 in the sinc functions (see subsection A.3 about this last point).

*Note: $P_{Tl} = I_f \left(\frac{\lambda z}{a}\right)^2 = A_o^2 e^{d_z} \frac{1}{a^2}$.

APPENDIX C. THE DIFFRACTION DETAILS OF A CIRCULAR HOLE

Many of the details for diffraction pattern from a circular hole are discussed in reference [29]. This appendix extracts these important features and parallels the development of appendix B. Many of the conventions and symbols are the same as in appendix B; therefore, this discussion only shows those new definitions and reduces substantially the details for each derivation.

Here the U_s becomes:

$$U_s(x_1, y_1) = A_o \text{ circ}(r_1/a) \exp \left\{ i[b_\ell(x_1 - g_\ell) + c_\ell(y_1 - h_\ell) + d_\ell] \right\}, \quad (C.1)$$

where a is now the diameter of the aperture and circ is defined as:

$$\begin{aligned} \text{circ}(r/a) &= 1 & \text{if} & \quad r_1 \equiv [(x_1 - g_\ell)^2 + (y_1 - h_\ell)^2]^{1/2} < \frac{a}{2} \\ &= 0 & \text{if} & \quad r_1 > a/2 \\ &= 1/2 & \text{if} & \quad r_1 = a/2. \end{aligned} \quad (C.2)$$

C.1 What this Appendix Presents

Subsections C.2 and C.3 contain brief derivations of the far-field and Fourier transform patterns for the circular aperture and a discussion showing selected features of those patterns.

C.2 The Far-field Diffraction Pattern

Equation (B.4) becomes changed to reflect the far-field condition:

$$z \geq \frac{a^2}{\lambda} \quad (2.5) . \quad (C.3)$$

Using definitions:

$$\begin{aligned} \phi_1 &= kz + \frac{k}{2z} (u_2^2 + v_2^2), \\ \zeta &= \zeta_1 + i\zeta_2 \equiv a \left(\frac{u_2}{z\lambda} - \frac{b_\ell}{2\pi} \right) , \\ \eta &= \eta_1 + i\eta_2 \equiv a \left(\frac{v_2}{z\lambda} - \frac{c_\ell}{2\pi} \right) , \\ r_2^o &= (\zeta_1^2 + \eta_1^2)^{1/2} , \quad r_2 = (\zeta^2 + \eta^2)^{1/2} , \quad \tan \theta_2 = \eta/\zeta , \quad \text{and} \\ \tan \theta_1 &= v_1/u_1 , \end{aligned} \quad (C.4)$$

we rewrite eq (B.4) to reflect the changes in aperture and notation. Further, we use reference [30, page 398] for Bessel function relationships to reduce the two integrals. Thus, we get:

$$U_2(\eta_2) = \frac{A_o e^{i(\phi_1 + d_\ell)}}{i\lambda z} \frac{J_1(\pi r_2) a^2}{r_2} \quad (C.5)$$

By defining:

$$I_f \equiv A_o^2 \left(\frac{\pi a^2}{\lambda z 4} \right)^2 \quad (C.6)$$

with the area, $\left(\frac{\pi a^2}{4} \right)$, for the circular aperture in place of the area, (a^2) , for the square, we can write the irradiance as:

$$I(\zeta_1, \eta_1) = I_f \frac{4}{\pi^2} \frac{J_1(\pi r_2) J_1(\pi r_2^*)}{r_2 r_2^*} \quad (C.7)$$

The r_2 can be written in terms of ζ_1 , ζ_2 , etc., as:

$$r_2 = [(\zeta_1 + i\zeta_2)^2 + (\eta_1 + i\eta_2)^2]^{1/2} \quad (C.8)$$

From this irradiance, eq (C.7), we extract a number of facts: (1) Changing $\zeta_1 \rightarrow -\zeta_1$ and $\eta_1 \rightarrow -\eta_1$ results in no change in the form of the irradiance. (2) Likewise, $\eta_2 \rightarrow -\eta_2$ and $\zeta_2 \rightarrow -\zeta_2$ imply no change in the form of the irradiance; therefore, we cannot deduce the absolute sign of the gradient of the irradiance at the aperture. However, we can deduce the direction of this gradient. This situation means we have less symmetry than with the square hole where we have two possible directions. (3) The coordinates for the peak irradiance are unchanged, $\zeta_1 = \eta_1 = 0$. If ζ_2 and η_2 are small enough, the peak irradiance is:

$$I(0,0) = I_f \left[1 + \frac{\pi^2}{8} (\zeta_2^2 + \eta_2^2) \right]^2 \quad (C.9)$$

(4) Again for small ζ_2 , η_2 , the rings of minimum irradiance in eq (C.7) are the values of r_2^0 where $J_1(\pi r_2^0)$ is zero. The first three values are $r_2^0 = 1.22, 2.23, \text{ and } 3.24$. (5) The asymptotic form of $J_1(\pi r_2)$ is:

$$\sqrt{\left[\frac{2}{\pi r_2} \right]} \cos\left(\pi r_2 - \frac{3}{4} \pi\right).$$

The irradiance function for this region becomes:

$$I(\zeta_1, \eta_1) = \frac{8}{\pi^4 (r_2 r_2^*)^{3/2}} \cos[\pi r_2 - \frac{3}{4}\pi] \cos[\pi r_2^* - \frac{3}{4}\pi]. \quad (C.10)$$

Neglect ζ_2 and η_2 , set $\eta_1 = 0$, and look at local peak values of irradiance.

Then:

$$I(\zeta_1, \eta_1) \sim \frac{8}{\pi^4} \frac{1}{\zeta_1^3} I_f. \quad (C.11)$$

For irradiance in eq (C.11) to be 10^{-4} of eq (C.9), $\zeta_1 = 9.36 \approx 10$. This distance defined by ζ_1 for the circular aperture is about one-third of the same value for the square aperture.

The capture of laser power for a given circular aperture with arbitrary values of ζ_2 and η_2 cannot be determined in terms of known functions. A computer is necessary. For this discussion, we assume that there is no significant gradient at the aperture for the irradiance; thus $\zeta_2 = \eta_2 = 0$. Under these conditions the measured power for a properly centered detector is:

$$P_\ell = P_o [1 - J_0^2(\pi A_1) - J_1^2(\pi A_1)]. \quad (C.12)$$

We set the diameter of the detector equal to A , and the equivalent scale of $A_1 = \frac{a A}{2z\lambda}$. The total power, $P_o \equiv \frac{4}{\pi} \left(\frac{\lambda z}{a}\right)^2 I_f$, is at the original aperture. The power in the first circle is only $0.84 P_o$, in the second circle is $0.91 P_o$, and in the third circle is $0.94 P_o$. Here $A_1 = 1.22, 2.23, \text{ and } 3.24$, respectively, for each of these cases.

C.3 The Fourier Transform Pattern

Equation (C.5) becomes:

$$U_2[r_2^f] = \frac{A_o e^{i[\phi + d_\ell + \theta]}}{i\lambda f} \frac{a^2 J_1(\pi r_2^f)}{r_2^f}, \quad (C.13)$$

where $r_2^f \equiv [(\zeta_f)^2 + (\eta_f)^2]^{1/2}$, $\zeta_f \equiv a[\frac{x_2}{\lambda f} - \frac{b_\ell}{2\pi}]$, and $\eta_f \equiv a[\frac{y_2}{\lambda f} - \frac{c_\ell}{2\pi}]$.

Please note the term $\theta \equiv -\frac{k}{f} (x_2 g_\ell + y_2 f_\ell)$ is exactly the same as for the square hole case and again the Airy disk has no displacement due to g_ℓ and h_ℓ .

This concludes this discussion of the laser beam output produced by a circular aperture in the Hartmann plate.

APPENDIX D. DEPTH OF FIELD ANALYSIS FOR FOURIER OPTICS

The proper assembly of lenses and mirrors to construct a correctly working cross-correlation system requires two distinct analyses for the depth of field of each type of lens [30, page 441]. That is, we must fix the position of the lens used for Fourier transform and the position of the lens for imaging. In both cases, the proper adjustments of a lens require the appropriate $h(x, y; R)$ function to be unity.

In the Fourier transform adjustment, let $x_1 = y_1 = D_1/\sqrt{2}$ where D_1 is the largest radial dimension for interesting detail in surface "1." Further, we make the arbitrary decision that the largest allowed phase shift in the depth of field adjustment which will cause no significant error for design purposes has $h = e^{i\frac{\pi}{10}}$ at this radius. This $\frac{\pi}{10}$ value corresponds to $\frac{1}{20}$ of a wavelength fringe error. That is the level of error we can see in a Michelson interferometer for moderate accuracy phase measurements. Design of a precision system should have this level of sensitivity. This phase shift implies a constraint on d_2 :

$$\left| \frac{kD_1^2}{d_1} \left(1 - \frac{w}{d_1} \right) \right| \leq \frac{\pi}{5}, \quad (D.1)$$

where $R = d_1/(1-w/d_1)$ is the radius of curvature due to improper placement of surface "3" (see figure A.1). Equation D.1 can be rewritten as:

$$\frac{2D_1^2}{d_1 \lambda} \left| \frac{1}{d_2} - \frac{1}{f} \right| \leq \frac{1}{5} \left| \frac{1}{d_1} + \frac{1}{d_2} - \frac{1}{f} \right|. \quad (D.2)$$

Thus, given D_1 , d_1 , λ and f , eq (D.2) fixes the range through which d_2 can be moved and still make a proper Fourier transform of the pattern at surface "1." Equation (D.2) has value for design work; the final adjustment within an actual system uses the insensitivity to displacement discussed in appendix A, to fix accurately the Fourier plane.

Equation (D.2) can be simplified if $d_2 = f + \Delta$, where Δ is a small value. Here, Δ is constrained to be:

$$|\Delta| \leq \frac{\lambda}{10D_1^2} f^2. \quad (D.3)$$

If we define an F number of the image on surface "1" as $F_1^\# = f/(2D_1)$, we get the convenient form for the depth of field at surface "3":

$$|\Delta/\lambda| \leq 0.4(F_1^\#)^2. \quad (D.4)$$

In brief, and $F_1^\#$ less than one implies a very critical adjustment, and an $F_1^\#$ greater than 10 allows ease in this adjustment. Unfortunately, the latter also implies long optical distances. (Incidentally, this same large $F_1^\#$ limit tends to minimize spherical aberration in the lens and permits using a single element lens to make beam profile measurements.)

The following formula fixes the depth of field for image plane placement:

$$\left| \frac{kD_1^2}{w} \right| \leq \frac{\pi}{5} . \quad (D.5)$$

The same arbitrary phase constraint on the h function is used here as was used in the Fourier transform depth of field analysis. If we set $d_2 = d_2^\circ + \Delta$ in the lens formulas, we get $\frac{1}{w} = -\frac{\Delta}{(d_2^\circ)^2}$, where the image equation $\frac{1}{d_2^\circ} + \frac{1}{d_1} = \frac{1}{f}$ applies. The Δ becomes:

$$|\Delta| = \frac{\lambda}{10} \left(\frac{d_2^\circ}{D_1} \right)^2 . \quad (D.6)$$

Here, we define a second number as $F_2^\# = \frac{d_2^\circ}{2D_1}$. The depth of field for surface "3" reduces to:

$$|\Delta/\lambda| \leq 0.4(F_2^\#)^2 ,$$

which is the same form as eq (D.4). Again, long focal length optics and small beam curvature at surface "3" imply large depths of field. On the other hand, short focal length optics and large beam curvature at that same surface imply a small depth of field and corresponding very critical mechanical adjustments. In practice, the adjustments of the image plane are made by observing that the largest off-axis dimension of the image in surface "3" is as visually sharp as possible. One procedure to specify this image plane uses a variable aperture to block a plane wave at surface "1" (note the image of the aperture at surface "3"). The sharpest image corresponds to the best adjustment of the apparatus. The larger this aperture is, the more critical is the depth of field adjustment.

U.S. DEPT. OF COMM. BIBLIOGRAPHIC DATA SHEET	1. PUBLICATION OR REPORT NO. NBS TN-1009	2. Gov't. Accession No.	3. Recipient's Accession No.
4. TITLE AND SUBTITLE Laser Beam Profile Measurements Using Spatial Sampling, Fourier Optics, and Holography		5. Publication Date January 1979	
7. AUTHOR(S) Eric G. Johnson, Jr.		6. Performing Organization Code	
9. PERFORMING ORGANIZATION NAME AND ADDRESS NATIONAL BUREAU OF STANDARDS DEPARTMENT OF COMMERCE WASHINGTON, DC 20234		8. Performing Organ. Report No.	
12. SPONSORING ORGANIZATION NAME AND COMPLETE ADDRESS (Street, City, State, ZIP) Funded in part by: Department of Defense Combined Calibration Group (CCG)		10. Project/Task/Work Unit No.	
15. SUPPLEMENTARY NOTES <input type="checkbox"/> Document describes a computer program; SF-185, FIPS Software Summary, is attached.		11. Contract/Grant No.	
16. ABSTRACT (A 200-word or less factual summary of most significant information. If document includes a significant bibliography or literature survey, mention it here.) Using appropriate holography, lenses, mirrors, and a two-dimensional array of small holes to sample the electric field of a laser pulse, we demonstrate a technique for beam profile measurements at a preselected observation plane. This method can measure the amplitude and phase of a laser pulse at each preselected sampling point on a transverse observation plane. Subject to constraints, these measurements can provide separated visual images of the temporal pulse shapes for the amplitude and phase at each of the sampled electric fields. This paper describes the basic concepts for beam profile measurements via holography and uses pictures generated by a prototype system for illustration. This unit may be calibrated by using a cw laser beam of the same wavelength as the carrier or a Q-switched laser pulse. Therefore, a user can make beam profile measurements of a laser pulse in real time. This technique requires appropriate scaling of the lenses and mirrors, and uses a different hologram to allow the unit to work optimally for each wavelength. We define the potential limits and virtues of the holographic method. In addition, we define limits and virtues of other beam profile techniques such as the two-pinhole scanning method and the Hartmann plate method. Finally, we indicate possible directions for eventual commercial and scientific exploitation of the holographic method. The technique can be used for near- and far-infrared wavelengths and, with appropriate changes in the optics, for visible wavelengths.		13. Type of Report & Period Covered	
17. KEY WORDS (six to twelve entries; alphabetical order; capitalize only the first letter of the first key word unless a proper name; separated by semicolons) Amplitude; beam profile; cross correlation; digital sampling; fourier optics; holography; laser; laser parameters; laser pulse; optical processing; phase; precision measurements; wave front.		14. Sponsoring Agency Code	
18. AVAILABILITY <input checked="" type="checkbox"/> Unlimited <input type="checkbox"/> For Official Distribution. Do Not Release to NTIS <input checked="" type="checkbox"/> Order From Sup. of Doc., U.S. Government Printing Office, Washington, DC 20402, SD Stock No. SN003-003- 02019-2 <input type="checkbox"/> Order From National Technical Information Service (NTIS), Springfield, VA, 22161	19. SECURITY CLASS (THIS REPORT) UNCLASSIFIED	21. NO. OF PRINTED PAGES 96	
	20. SECURITY CLASS (THIS PAGE) UNCLASSIFIED	22. Price \$2.75	

NBS TECHNICAL PUBLICATIONS

PERIODICALS

JOURNAL OF RESEARCH—The Journal of Research of the National Bureau of Standards reports NBS research and development in those disciplines of the physical and engineering sciences in which the Bureau is active. These include physics, chemistry, engineering, mathematics, and computer sciences. Papers cover a broad range of subjects, with major emphasis on measurement methodology, and the basic technology underlying standardization. Also included from time to time are survey articles on topics closely related to the Bureau's technical and scientific programs. As a special service to subscribers each issue contains complete citations to all recent NBS publications in NBS and non-NBS media. Issued six times a year. Annual subscription: domestic \$17.00; foreign \$21.25. Single copy, \$3.00 domestic; \$3.75 foreign.

Note: The Journal was formerly published in two sections: Section A "Physics and Chemistry" and Section B "Mathematical Sciences."

DIMENSIONS/NBS (formerly Technical News Bulletin)—This monthly magazine is published to inform scientists, engineers, businessmen, industry, teachers, students, and consumers of the latest advances in science and technology, with primary emphasis on the work at NBS. The magazine highlights and reviews such issues as energy research, fire protection, building technology, metric conversion, pollution abatement, health and safety, and consumer product performance. In addition, it reports the results of Bureau programs in measurement standards and techniques, properties of matter and materials, engineering standards and services, instrumentation, and automatic data processing.

Annual subscription: Domestic, \$11.00; Foreign \$13.75

NONPERIODICALS

Monographs—Major contributions to the technical literature on various subjects related to the Bureau's scientific and technical activities.

Handbooks—Recommended codes of engineering and industrial practice (including safety codes) developed in cooperation with interested industries, professional organizations, and regulatory bodies.

Special Publications—Include proceedings of conferences sponsored by NBS, NBS annual reports, and other special publications appropriate to this grouping such as wall charts, pocket cards, and bibliographies.

Applied Mathematics Series—Mathematical tables, manuals, and studies of special interest to physicists, engineers, chemists, biologists, mathematicians, computer programmers, and others engaged in scientific and technical work.

National Standard Reference Data Series—Provides quantitative data on the physical and chemical properties of materials, compiled from the world's literature and critically evaluated. Developed under a world-wide program coordinated by NBS. Program under authority of National Standard Data Act (Public Law 90-396).

NOTE: At present the principal publication outlet for these data is the Journal of Physical and Chemical Reference Data (JPCRD) published quarterly for NBS by the American Chemical Society (ACS) and the American Institute of Physics (AIP). Subscriptions, reprints, and supplements available from ACS, 1155 Sixteenth St. N.W., Wash., D.C. 20056.

Building Science Series—Disseminates technical information developed at the Bureau on building materials, components, systems, and whole structures. The series presents research results, test methods, and performance criteria related to the structural and environmental functions and the durability and safety characteristics of building elements and systems.

Technical Notes—Studies or reports which are complete in themselves but restrictive in their treatment of a subject. Analogous to monographs but not so comprehensive in scope or definitive in treatment of the subject area. Often serve as a vehicle for final reports of work performed at NBS under the sponsorship of other government agencies.

Voluntary Product Standards—Developed under procedures published by the Department of Commerce in Part 10, Title 15, of the Code of Federal Regulations. The purpose of the standards is to establish nationally recognized requirements for products, and to provide all concerned interests with a basis for common understanding of the characteristics of the products. NBS administers this program as a supplement to the activities of the private sector standardizing organizations.

Consumer Information Series—Practical information, based on NBS research and experience, covering areas of interest to the consumer. Easily understandable language and illustrations provide useful background knowledge for shopping in today's technological marketplace.

Order above NBS publications from: Superintendent of Documents, Government Printing Office, Washington, D.C. 20402.

Order following NBS publications—NBSIR's and FIPS from the National Technical Information Services, Springfield, Va. 22161.

Federal Information Processing Standards Publications (FIPS PUB)—Publications in this series collectively constitute the Federal Information Processing Standards Register. Register serves as the official source of information in the Federal Government regarding standards issued by NBS pursuant to the Federal Property and Administrative Services Act of 1949 as amended, Public Law 89-306 (79 Stat. 1127), and as implemented by Executive Order 11717 (38 FR 12315, dated May 11, 1973) and Part 6 of Title 15 CFR (Code of Federal Regulations).

NBS Interagency Reports (NBSIR)—A special series of interim or final reports on work performed by NBS for outside sponsors (both government and non-government). In general, initial distribution is handled by the sponsor; public distribution is by the National Technical Information Services (Springfield, Va. 22161) in paper copy or microfiche form.

BIBLIOGRAPHIC SUBSCRIPTION SERVICES

The following current-awareness and literature-survey bibliographies are issued periodically by the Bureau:

Cryogenic Data Center Current Awareness Service. A literature survey issued biweekly. Annual subscription: Domestic, \$25.00; Foreign, \$30.00.

Liquified Natural Gas. A literature survey issued quarterly. Annual subscription: \$20.00.

Superconducting Devices and Materials. A literature survey issued quarterly. Annual subscription: \$30.00. Send subscription orders and remittances for the preceding bibliographic services to National Bureau of Standards, Cryogenic Data Center (275.02) Boulder, Colorado 80302.

U.S. DEPARTMENT OF COMMERCE
National Bureau of Standards
Washington, D.C. 20234

OFFICIAL BUSINESS

Penalty for Private Use, \$300

POSTAGE AND FEES PAID
U.S. DEPARTMENT OF COMMERCE
COM-215



SPECIAL FOURTH-CLASS RATE .
BOOK